Clouds and the Earth's Radiant Energy System (CERES)

Algorithm Theoretical Basis Document

Instrument Geolocate and Calibrate Earth Radiances

(Subsystem 1.0)

CERES Science Team Instrument Working Group

Robert B. Lee III/Group Leader[1]
Bruce R. Barkstrom/P.I.[1]
Dominique A. Crommelynck[2]
G. Louis Smith[1]

Count Conversion

William C. Bolden[3]
Jack Paden[3]
Dhirendra K. Pandey[3]
Susan Thomas[3]
Lee Thornhill[3]
Robert S. Wilson[3]

Telemetry and Geolocation

Kathy A. Bush[3]
Phillip C. Hess[3]
William L. Weaver[3]

[1]NASA Langley Research Center, Hampton, Virginia 23681-0001
[2]Belgium Royal Meteorological Institute, Avenue Circulaire 3, B-1180 Brussels, Belgium
[3]Science Applications International Corporation (SAIC), Hampton, Virginia 23666

June 2, 1997

CERES Top Level Data Flow Diagram

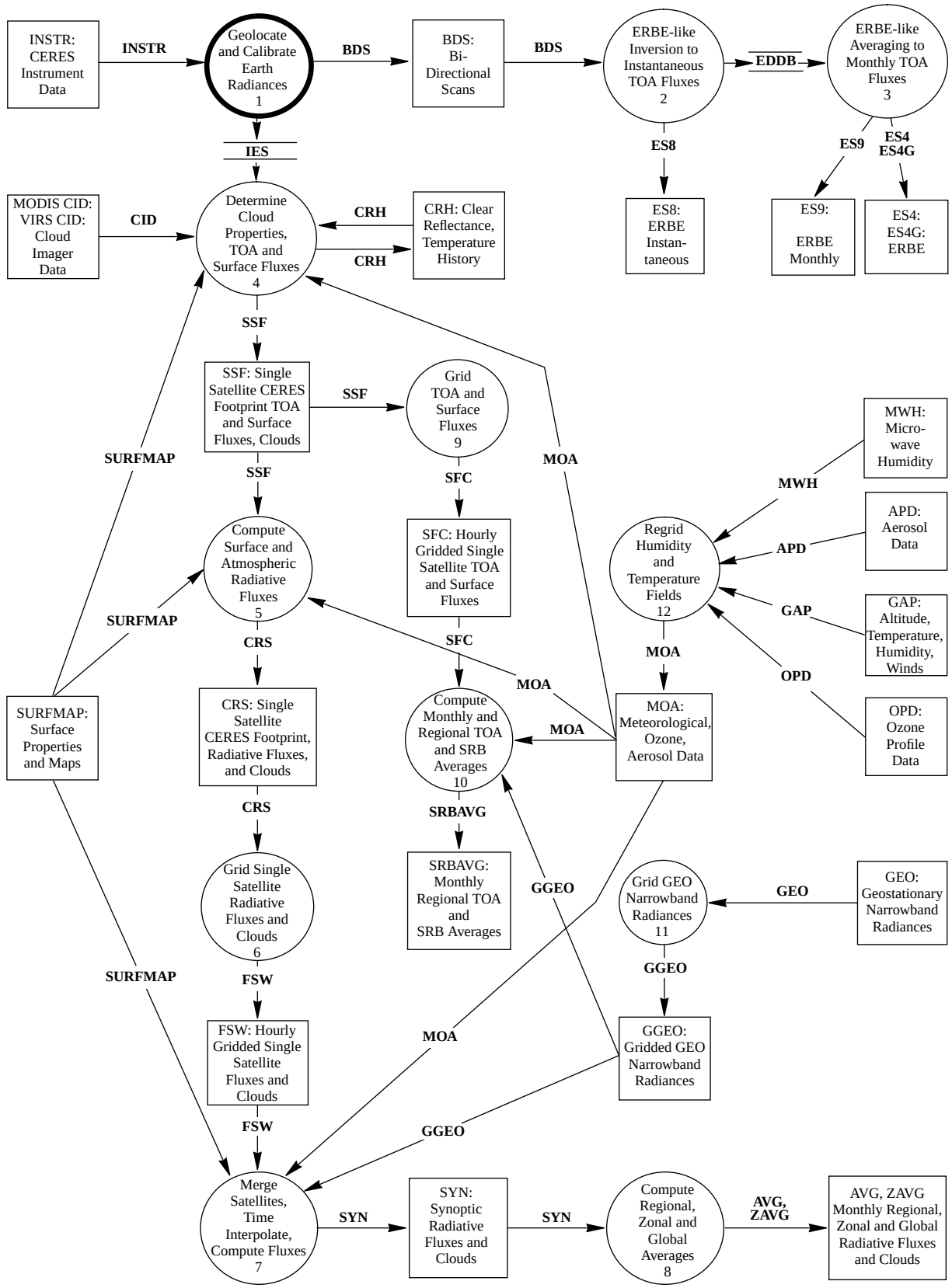

Subsystem 1.0 Top Level Data Flow Diagram

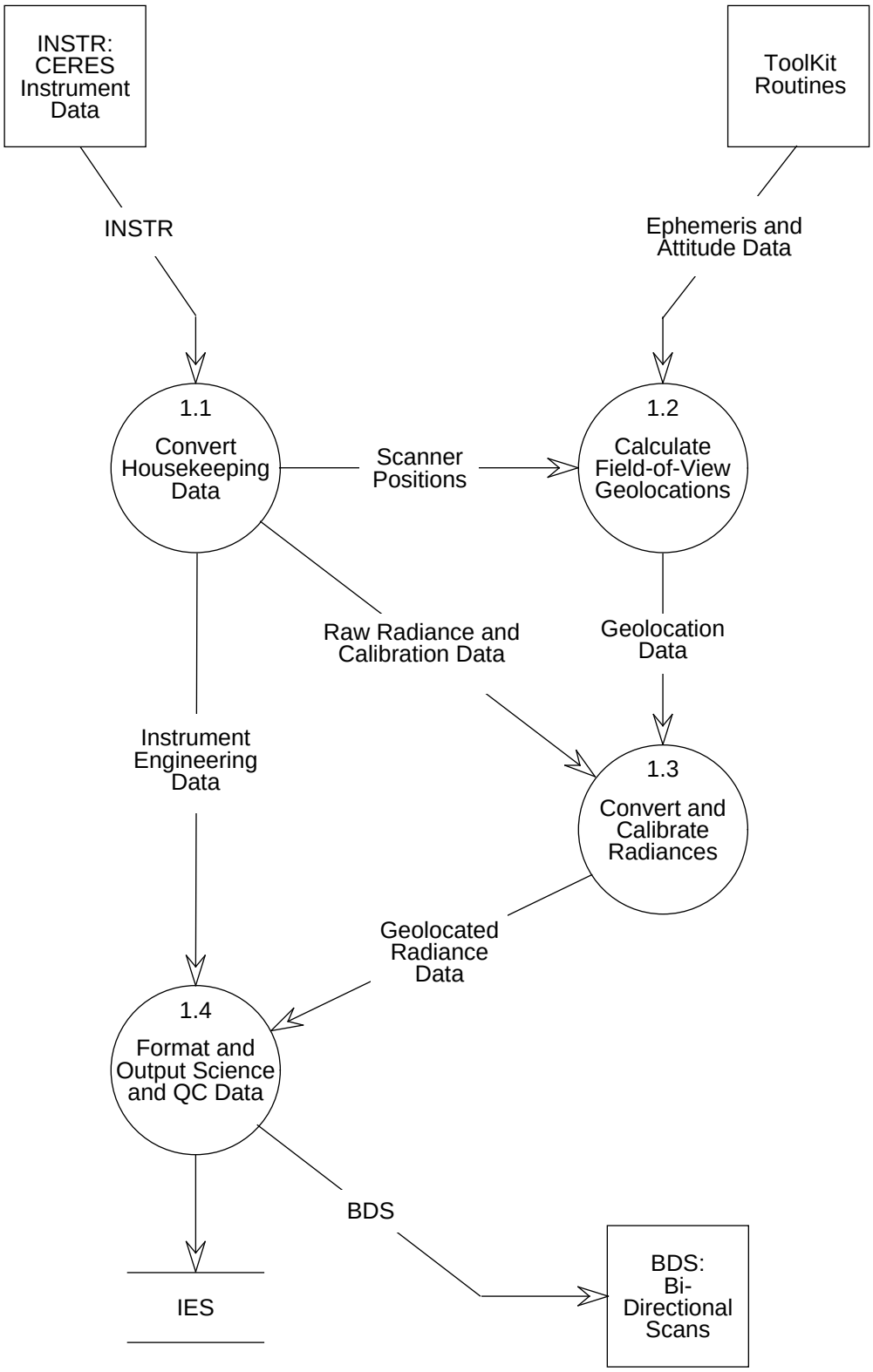

Abstract

The instrument geolocate and calibrate Earth radiance subsystem is the front end of the Clouds and the Earth's Radiant Energy System (CERES) data management system. The spacecraft ephemeris and sensor telemetry are inputs to this subsystem which uses instrument calibration coefficients to convert the spacecraft telemetry inputs into geolocated filtered radiances and housekeeping data into engineering units. These level-1b, chronologically organized standard data products are called the bidirectional scan (BDS) radiances. The BDS product package contains the full set of raw telemetry data along with the converted engineering values. The BDS filtered radiances are converted by the Earth Radiation Budget Experiment (ERBE)-like inversion subsystem into the standard product of unfiltered fluxes at the top of the atmosphere. The instrument subsystem produces nonstandard/internal radiance products, identified as instrument Earth scan (IES). The IES spatially organized products are inputs to the cloud processing subsystem.

1.0. Instrument Geolocate and Calibrate Earth Radiances

Acronyms

ACA	Azimuth Control Assembly
ADC	Analog-to-Digital Conversion
ADM	Angular Distribution Model
APID	Application Process Identifier
BB	Blackbody
BDS	Bidirectional Scan
CAM	Calibration Attitude Maneuver
CCSDS	Consultative Committee for Space Data Systems, based on octets
CERES	Clouds and Earth's Radiant Energy System
CPU	Central Processing Unit
CRR	Constant Radiance Reference
CSR	Cold Space Reference
DAA	Data Acquisition Assembly
DAAC	Distributed Active Archive Center
DAC	Digital-to-Analog Converter
DAP	Data Acquisition Processor
DMS	Data Management System
ECA	Elevation Control Assembly
ECS	EOSDIS Core System
EOS	Earth Observing System
EOSDIS	EOS Data and Information System

ERBE	Earth Radiation Budget Experiment
FM1	Flight Model 1
FM2	Flight Model 2
FM3	Flight Model 3
FM4	Flight Model 4
FOV	Field of View
FTM	Functional Test Model
FTS	Fourier Transform Spectrometer
ICA	Instrument Control Assembly
ICM	Internal Calibration Module
ICP	Instrument Control Processor
ICS	Instrument Coordinate System
ICSBB	Internal Calibration Source Blackbody
IES	Instrument Earth Scan
IPTS-68	International Practical Temperature Scale of 1968
ITS-90	International Temperature Scale of 1990
LaRC	NASA Langley Research Center
LW	Longwave
MAM	Mirror Attenuator Mosaic
MEA	Main Electronics Assembly
MODIS	Moderate-Resolution Imaging Spectrometer
NFBB	Narrow Field-of-View Blackbody
PCA	Power Converter Assembly
PFM	Protoflight Model
PRFS	Point Response Function Source
PROM	Programmable Read Only Memory
PRT	Platinum Resistance Thermometer
RAM	Random Access Memory
RAPS	Rotating Azimuth Plane Scan
RCF	Radiometric Calibration Facility
RTM	Radiometric Test Module
S/C	Spacecraft
SEA	Sensor Electronics Assembly
SPS	Solar Presence Sensor
SDP	Science Data Processing
SSA	Sensor Scan Assembly
SW	Shortwave
SWICS	Shortwave Internal Calibration Source
SWRS	Shortwave Reference Source

TACR	Transfer Active Cavity Radiometer
TBD	To Be Defined
TC	Total Channel
TOA	Top of the atmosphere, defined 30 km above the surface of the Earth
TRMM	Tropical Rainfall Measuring Mission
VIRS	Visible Imaging Radiometer Sounder
WFBB	Wide Field-of-View Blackbody

Symbols

A_B	Detector bias voltage constant defined by equation (1-21)
A_D	Detector DAC constant defined by equation (1-20)
A_H	Detector heat-sink constant defined by equation (1-19)
A_S	Space observation constant defined by equation (1-18)
A_V	Detector gain expression, defined by equation (1-17)
AB	Detector bias voltage calibration constant
AD	Detector DAC voltage calibration constant
AHA	Detector heat-sink calibration constant
AV	Detector calibration gain
AVA	Detector space observation calibration constant
B	Temperature coefficient of bolometer material, 3400 K
C	Digital-to-analog conversion factor of 409.5 counts per volt
C_1	1.1909×10^8 W-μm^4-m^{-2}
C_2	14388 μm-K
h	Height of spacecraft above the surface of the Earth
K_{fo}	Post amplification gain
K_T	Housekeeping temperature thermistor coefficient, defined by equation (1-25)
K_1, K_2, K_f, K_{on}, K_{p1}, K_{p2}, K	Housekeeping temperature coefficients defined in table 1-2
$\tilde{L}$	Filtered radiance
$L(\lambda)$	Unfiltered spectral radiance
m	Detector output signal at time *t*
m_s	Detector output signal, observing cold space
o(t)	Detector offset dependent upon scan geometry (elevation angle)
P	Point spread function
p	Roll angle around the spacecraft *X*-axis
Q	Heat transfer
q	Pitch angle about spacecraft *Y*-axis
R	Bolometer resistivity at temperature *T*
R_e	Earth radius at the equator

R_0	Bolometer resistivity at reference temperature T_0, 250 ohm-cm
R_p	Earth radius at either pole
r	Yaw angle about spacecraft Z-axis
S	Detector response
$S(\lambda)$	Spectral response
$S(\theta,\phi,x,y)$	Detector angular and spatial response
T	Temperature
T_H	Detector heat-sink temperature
T_m	Thermistor temperature
T_0	Reference temperature of thermistor bolometer electrical resistance measurement
T_{PRT}	Detector temperature
T_s	Sensor heater control temperature, defined by equation (1-23)
t	Time
t_k	Time of the reference space observations
t_{ki}	$t_k + i$ (10 msec)
t_0	Time of space observation
V_{bias}	Bolometer bias and bridge voltage
V_D	Detector DAC drift voltage
$V(t)$	Detector output signal voltage at time t
$V(t_k)$	Detector output signal voltage at time t_k space observation
X_S	Spacecraft fixed X-axis, figure 1-21
X_β	Detector X-axis, perpendicular to elevation plane
Y_S	Spacecraft fixed Y-axis, figure 1-21
Y_β	Detector Y-axis, in elevation plane and perpendicular to detector optical axis
Z_S	Spacecraft fixed Z-axis, figure 1-21
Z_β	Detector Z-axis, aligned with the detector optical axis
α	Azimuthal angle of rotation, between Y_β and Y_α axes
α_b	Absorptance of bolometer black paint layer
β	Elevation angle of rotation
γ	Average time lag between the instantaneous detector optical field of view and point spread function centroid
Δ_t	6.6-sec total scan period
δ_k	Estimate of unaccounted detector drift during the kth scan period
ε	Emittance
η	Heading angle defined between north and the projection of the spacecraft velocity vector in the local horizon plane
θ	Polar angle aligned with optical axis of telescope
Λ	Geodetic longitude of detector measurement
λ	Wavelength, μm

ρ_m	Reflectance of telescope silvered mirrors
σ_k	Noise variance estimate during space measurements
τ	Filter transmission
Φ_G	Geodetic latitude of the detector measurement
ϕ	Azimuthal angle aligned with the scan direction
Ω	FOV solid angle

1.1. Introduction

Subsystem 1.0 generates geolocated broadband shortwave and total (shortwave and longwave) filtered radiances as well as narrowband filtered radiances in the 8 to 12 μm water vapor window region. The Clouds and the Earth's Radiant Energy System (CERES) thermistor bolometers sense radiances in the broadband shortwave and total spectral regions. Daytime longwave radiances are derived from the differences of the total and shortwave bolometer measurements while the nighttime longwave radiances are derived from the total bolometer measurements, with the nighttime shortwave radiances equal to zero. The broadband shortwave and longwave filtered radiance accuracy requirements are 0.8 $Wm^{-2}sr^{-1}$ and 0.6 $Wm^{-2}sr^{-1}$, respectively. The accuracy requirement for radiances in the narrowband 8 to 12 μm water vapor window region is 0.3 $Wm^{-2}sr^{-1}$. The CERES instrument pointing knowledge requirement for the geolocated measurements is 0.1 angular degree per 10 msec, at the spacecraft.

This report outlines the pre-flight calibration plan (Lee *et al*. 1996a, Lee *et al*. 1997) as well as the on-line and off-line processing of the CERES filtered radiance data products. The in-flight calibration and validation plans are outlined by Lee *et al*. (1996b) and are summarized in sections 1.4.4. and 1.8., respectively. Validation summary charts are found after the appendices.

1.1.1. Algorithm Purpose

Geolocate algorithms identify the geographic scenes emitting the measured filtered radiances and define the solar and observational geometries of the radiances. The identification of the geographical scenes allows the radiances to be correlated with the cloud coverage of the scene. Scene cloud coverage and solar/observational geometries are vital in the inversion processes in which the filtered radiances are converted into unfiltered fluxes.

In order to determine accurately the scene radiances, the radiometric count conversion algorithms must be adjusted for changes in specific detector housekeeping temperatures and voltages. These specific housekeeping parameters are used as inputs into the radiometric algorithms and calibration processes.

The detectors output signals are fed into the telemetry stream as digital counts, which are converted into voltages. The radiometric count conversion algorithms convert the detector voltages into the level-1 product of radiances, using calibration (count conversion) coefficients (Lee *et al*. 1997) which are derived in ground laboratory measurements. The detector radiance conversion algorithms are represented by equations (1-15) through (1-21), while the detector housekeeping algorithms are outlined by equations (1-22) through (1-25). The Pixel-FOV toolkit geolocate algorithms, summarized by equation (1-26), calculate geodetic latitudes and longitudes of the radiance measurements while the CERES processing systems convert the coordinates into a geocentric system.

The "Geolocate and Calibrate Earth Radiances" processing bubble on the Clouds and the Earth's Radiant Energy System (CERES) Top Level Data Flow Diagram, found on page 2, is outlined on page 3. As illustrated in the Geolocate and Calibrate Earth Radiances processing level flow diagram, this instrument subsystem (1) converts the raw housekeeping telemetry into engineering units (temperatures, voltages, etc.), (2) calculates the geographical location of the CERES footprints, (3) merges the raw spacecraft ephemeris and detector point knowledge telemetry, converted housekeeping data, and raw radiometric detector telemetry, (4) off-line, revises the radiometric detector count conversion coefficients when required (Lee et al. 1996b), (5) converts the detector radiometric signals into filtered radiances, and (6) archives the bidirectional (BDS) standard products and generates the nonstandard/internal instrument Earth scan (IES) products.

1.1.2. Historical Perspective

The basic geolocate and calibrate algorithm schemes were developed in the Earth Radiation Budget Experiment (Barkstrom *et al*. 1990) and the Nimbus-7 (Kyle *et al*. 1993) spacecraft missions. The specific algorithms for the Earth Radiation Budget Experiment (ERBE) thermistor bolometers are outlined by

Halyo *et al.* (1987) and Lee *et al.* (1989), while the validation geolocate algorithms are summarized by Hoffmann *et al.* (1987). The geolocate, housekeeping, and radiometric count conversion algorithms are discussed briefly in the sections to follow.

To provide a better understanding of the physical and operational processes vital to these algorithms, the CERES detector characteristics and measurement operational modes are discussed before the algorithms are presented. The input and output products of the instrument subsystem are listed in Appendixes A and B, respectively.

1.2. Instrument Description

1.2.1. General Description

Table 1-1. CERES Instrument Accuracy Requirements (1 sigma)

Detector	Shortwave		Total		Window
Spectral Region	0.3 → < 5.0 μm		0.3 → < 100 μm		8 → < 12 μm
Scene Levels	< 100 W-m^{-2}sr^{-1}	> 100 W-m^{-2}sr^{-1}	< 100 W-m^{-2}sr^{-1}	> 100 W-m^{-2}sr^{-1}	All levels
Accuracy Requirements	0.8 W-m^{-2}sr^{-1}	1.0%	0.6 W-m^{-2}sr^{-1}	0.5%	0.3 W-m^{-2}sr^{-1}

The CERES experiment concepts are built upon the successful legacy of the Earth Radiation Budget Experiment (ERBE) spacecraft mission (Barkstrom et al. 1990). The CERES experiment has challenging goals of defining Earth-emitted longwave and Earth-reflected solar radiances, with precisions (1σ) approaching 0.5 percent and 1.0 percent, respectively, at the instrument level, and measuring narrowband longwave (8-μm to 12-μm) radiances. In table 1-1, the CERES instrument accuracy requirements are listed. The ground calibrations of the CERES sensors are described by Lee *et al.* (1996a, 1997).

In addition, the CERES spacecraft investigation is designed to define the physical properties of clouds, define the surface radiation budget, and determine the divergence of energy throughout the atmosphere (Barkstrom 1990, Wielicki and Barkstrom 1991, Wielicki *et al.* 1996). The CERES proto-flight model (PFM) instrument package is scheduled for launch on the NASA Tropical Rainfall Measuring Mission (TRMM) spacecraft in 1997. The TRMM spacecraft will be launched into a low-inclination 35°, 350-km altitude orbit by a National Space Development Agency (Japan) launch vehicle. The flight model 1 (FM1) and flight model 2 (FM2) instruments are scheduled for launch on the Earth Observing System (EOS) morning (AM-1) spacecraft platforms in 1998. The EOS AM-1 spacecraft platform will be launched into a 10:30 a.m. Sun-synchronous polar, 705-km orbit using NASA Atlas IIC launch vehicles. In 2000, the flight model 3 and 4 (FM3 and FM4) instruments will be launched on the EOS afternoon (PM-1) spacecraft mission into a 1:30 p.m. Sun-synchronous polar, 705-km orbit. Flight model 5 (FM5) is tentatively scheduled for launch on a follow-on TRMM spacecraft in 2004.

CERES will focus upon cloud studies and initiate new studies on the surface radiation budget. The work of Ramanathan *et al.* (1989), based on ERBE detector measurements, has demonstrated that clouds serve to cool the Earth's climate. The higher spatial and spectral resolution cloud pixel measurements from instruments such as the Moderate-Resolution Imaging Spectrometer (MODIS) will be merged with the CERES footprint radiance measurements to provide the best identification of the cloud properties. Along with the continuation of the ERBE-like measurements of reflected solar fluxes and emitted terrestrial fluxes, the CERES instruments will provide angular radiance measurements which will be used to build better Angular Distribution Models (ADM).

The CERES instrument package, as shown in figure 1-1, contains total, window, and shortwave scanning thermistor bolometer detector units (Lee *et al.* 1993a). The detectors measure the radiation in the

near-visible through far-infrared spectral region. The main electronics assembly (MEA) access connector is shown in the upper portion of the figure, while the mirror attenuator mosaic (MAM) baffles are shown to the right. The CERES detectors are designed, manufactured, and tested by TRW's Space and Electronics Group, Spacecraft and Technology Division (Redondo Beach, CA) under NASA contract number NAS1-19039. The shortwave detector measures Earth-reflected solar radiation in the wavelength region of 0.3 μm to 5.0 μm; the window detector measures Earth-emitted longwave radiation in the water vapor window wavelength region of 8 μm to 12 μm; and the total detector measures radiation in the range of 0.2 μm to <100 μm. The spectral responses of the TRMM CERES detectors are shown in figure 1-2. The responses represent the spectral throughput of the individual detector optical elements, illustrated in figure 1-3, and described in section 1.31. The three detectors are coaligned and mounted on a spindle that rotates about the elevation axis. The detectors fields of view overlap about 98 percent.

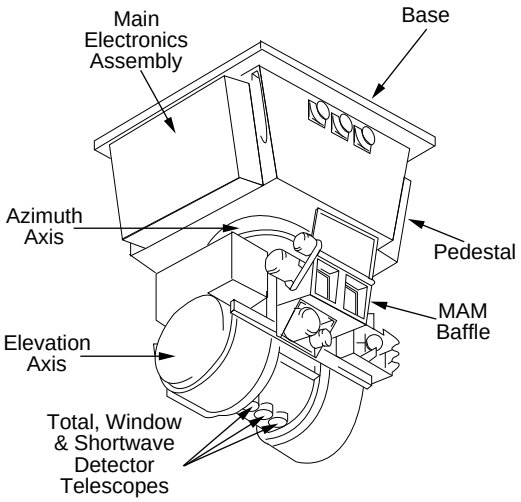

Figure 1-1. CERES instrument.

1.2.2. Detector Element

Each CERES detector unit consists of telescope baffle, telescope, and thermistor bolometer detector modules as shown in figure 1-3. The detector module consists of an active and a reference thermistor bolometer flake with time constants less than 9 and 12 milliseconds, respectively. Telescope baffle prevents radiation from striking the active bolometer flake at angles greater than 16° off the telescope optical axis. The f/1.8 Cassegrainian telescope module has a silvered secondary mirror and an 18-mm diameter silvered primary mirror. In the shortwave and window detectors, the filters are located before the secondary mirror spider and in front of the active bolometer flake. The shortwave detector has a filter made of Dynasil, fused, waterless quartz. The 8 μm–12 μm window detector has 1-mm-thick zinc sulfide and 0.5-mm-thick cadmium telluride filter elements. The total detector does not have an optical filter. The active and the reference flakes are arranged on a heat sink, which is maintained at a constant temperature of 38°C using 1.9-watt electrical heaters. Surfaces of both the active flake and the reference bolometers are covered with a 12-μm-thick absorptive black paint layer of Aeroglaze Z-306 that is doped with 10-percent carbon black. The absorptance of the paint layer is greater than 85 percent out to 100 μm (Jarecke *et al*. 1991). The cross-sectional view of a bolometer detector element assembly is given in figure 1-4.

The black paint layer on the active flake absorbs and converts the target scene energy into heat, which causes a measurable change in the bolometer electrical resistance. The bolometer consists of a sintered

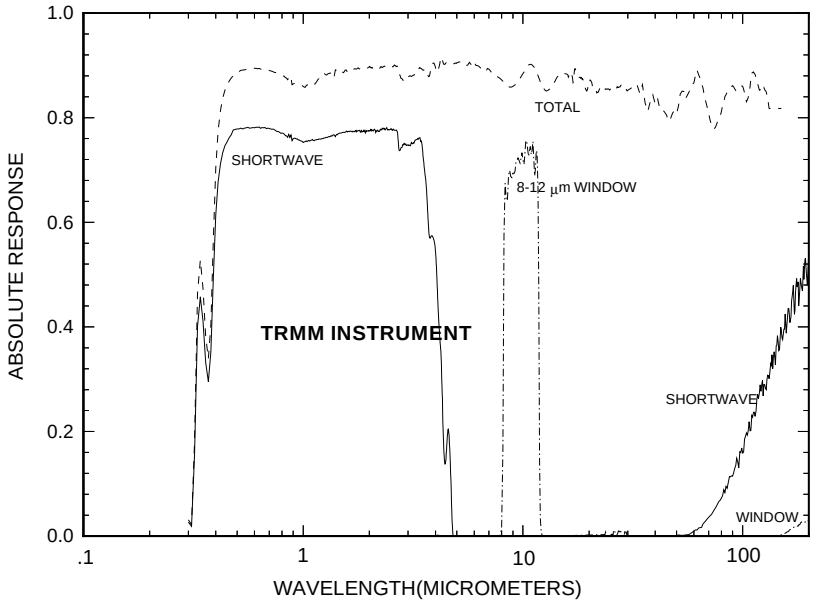

Figure 1-2. Spectral responsivity of CERES TRMM spacecraft detectors.

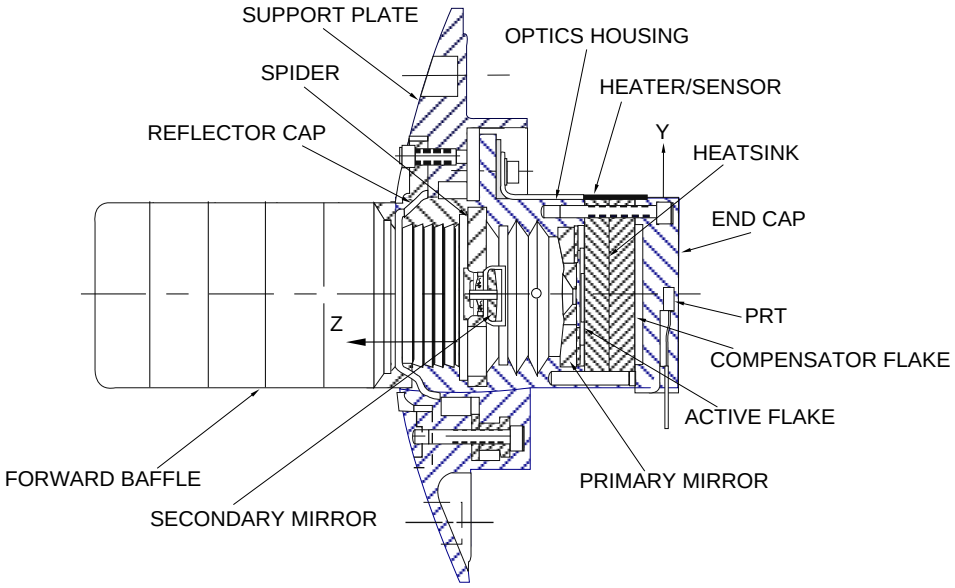

Figure 1-3. CERES baffle, telescope, and detection modules.

semiconductor material with a high negative coefficient of resistance. The bolometer electrical resistivity, *R*, can be represented as a function of the temperature, *T*, by the following equation (Astheimer 1983)

$$R = R_0 \exp\left[B\left(\frac{1}{T} - \frac{1}{T_0}\right)\right] \tag{1-1}$$

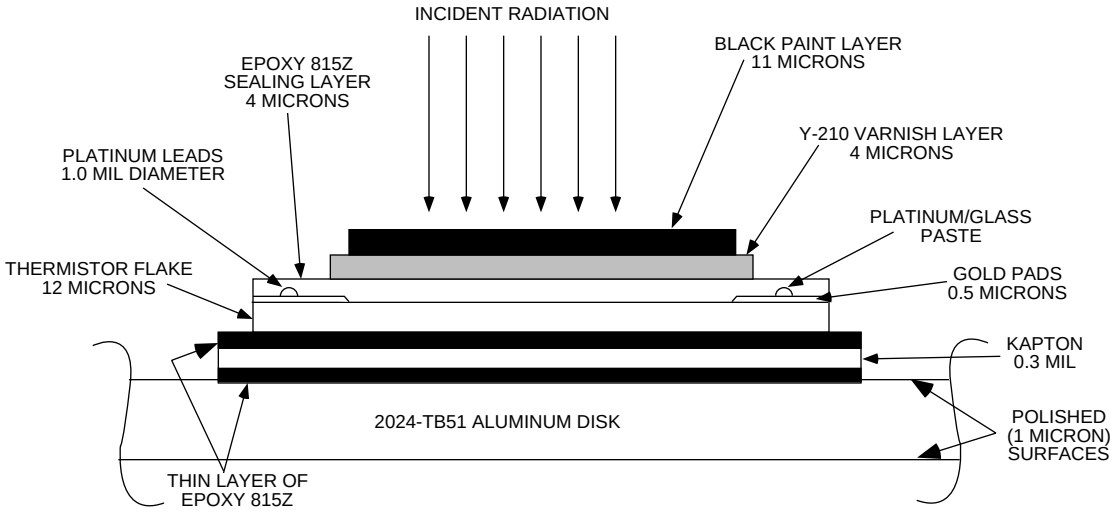

Figure 1-4. Detector element assembly cross-section.

where R_o is the resistance at the reference temperature T_0 (293 K), and B (3400 K) is the temperature

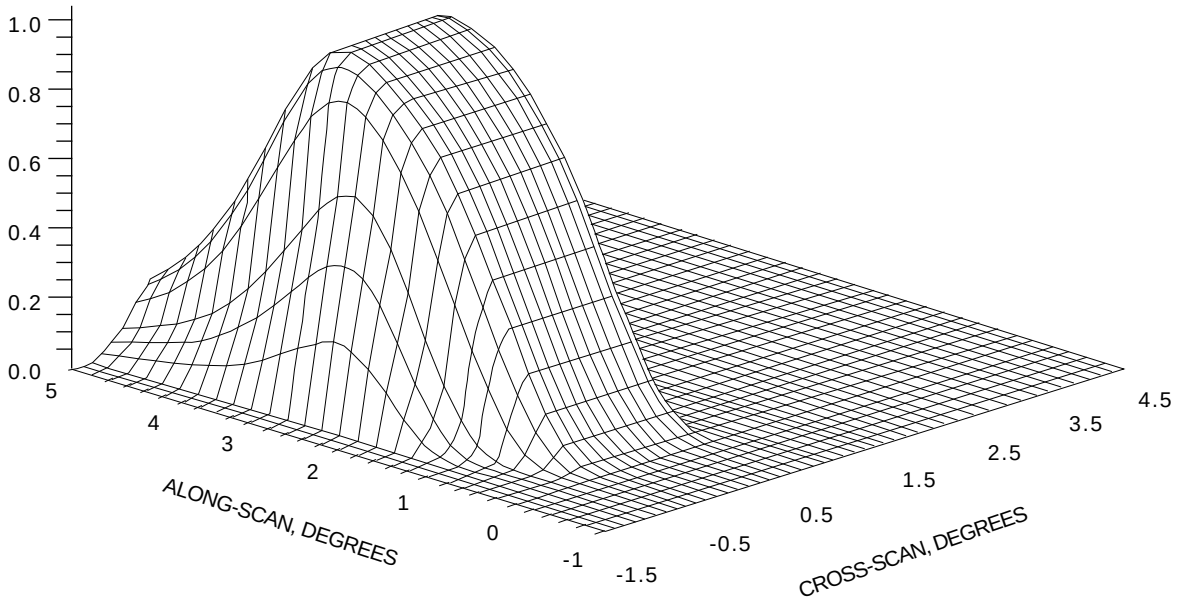

Figure 1-5. Illustration of point spread function.

coefficient of the bolometer material. The sintered semiconductor bolometer material is a mixture of manganese, nickel, and cobalt oxides having a resistivity, R_0, of approximately 250 ohm-cm at 25°C. Note that Astheimer's equation and equation (1-1) are equivalent except for a geometric constant factor associated with the thermistor that relates resistivity and resistance. Because the temperature of the bolometer responses to both incoming radiation and heat conducted from the heat sink, we used a compensator bolometer flake to follow thermal changes in the heat sink. The active and compensator bolometer flakes are elements of a Wheatstone bridge. Thus, the bridge output is determined by the scene dependent energy

that is absorbed and sensed by the active flake. The bridge signal is passed through a noise filter and a four-pole Bessel filter. The electronic filtering delays and smooths the analog signal before sampling. Using a 0.514 μm laser, the TRMM shortwave and total-wave sensor responses were measured at 65.4 and 62.9 volts/W. At 10.6 μm, the TRMM total-wave and 8-12 μm window sensors had 61.5 and 52.1 volts/W responses.

The radiometric measurements are sampled from the detectors every 10 milliseconds. The radiation being sampled enters the telescope and strikes the 0.75-mm by 1.50-mm hexagonal precision field stop. The field stop aperture restricts the detector field of view to 1.3° by 2.6°; the small angular dimension is in the elevation plane and the larger dimension is perpendicular to the elevation plane. The bolometer signal is then passed through a noise filter and a 4-pole Bessel filter. The filter further delays and smooths the analog signal before the electronics sample it. The footprints of the CERES detectors are approximately 10- and 20-km squares at nadir for the instruments on the TRMM and EOS spacecraft, respectively. Portions of the Earth near the center of the optical axis will contribute more strongly to the measurements than those off center. Quantitatively, each part of the field of view contributes according to the point spread function (*P*) as shown in figure 1-5 (Smith 1994); the normalized detector response is plotted as functions of along-scan and cross-scan angles, which are found perpendicular to and in the elevation plane, respectively. If the half power point is considered to be the footprint, the CERES footprint measured in Earth central angle is about 4 degrees along track and 2.6 degrees cross track. The point spread function is used in the data reduction algorithms, as described later in sections 1.3.2, Algorithms/Theoretical Basis and 1.3.3, Flight Algorithms/Practical Basis. The TRMM and EOS detector pointing requirements are presented in tables 1-2 and 1-3.

Table 1-2. CERES Instrument-TRMM Pointing Requirements

Science requirement	Mission requirement	Boresight requirement	CERES instrument capability	TRMM capability	CERES/TRMM capability
Sensor coalignment	98 percent common FOV	98 percent common FOV	>98 percent common FOV	N/A	N/A
Pointing knowledge	10 percent effective FOV	9.8 arc-min	3 arc-min (0.05°)	12 arc-min	12.4 arc-min
Pointing accuracy	Earth/Sun knowledge	<30 arc-min	3 arc-min (0.05°)	24 arc-min	24.2 arc-min
Coregistration	0.75 km	7.4 arc-min	3 arc-min (0.05°)	6 arc-min	6.7 arc-min
Jitter	2 percent of FOV	2.0 arc-min/Earth Scan	0.6 arc-min (0.01°)	6 arc-min/ 1 sec	6 arc-min/ 1 sec

Table 1-3. CERES Instrument-EOS AM-1 and PM-1 Pointing Requirements

Science requirement	Mission requirement	Boresight requirement	CERES instrument capability	EOS-AM capability	CERES/EOS-AM capability
Sensor coalignment	98 percent common FOV	98 percent common FOV	>98 percent common FOV	N/A	N/A
Pointing knowledge	10 percent effective FOV	588 arc-sec	180 arc-sec (0.05°)	114 arc-sec	215 arc-sec
Pointing accuracy	Earth/Sun knowledge	<1800 arc-sec	180 arc-sec (0.05°)	312 arc-sec	360 arc-sec
Coregistration	0.75 km	215 arc-sec	180 arc-sec (0.05°)	215 arc-sec	215 arc-sec
Jitter	2 percent of FOV	120 arc-sec/Earth Scan	36 arc-sec (0.01°)	36 arc-sec/ 6.6 sec	79 arc-sec/ 6.6 sec

1.2.3. Instrument Operations

1.2.3.1. General. The CERES instrument has an operational cycle of 6.6 seconds and several different operational modes, shown in table 1-4. The outputs of the detectors are sampled every 10 milliseconds in all operational modes. While the detectors rotate in the vertical (elevation scan) and horizontal (azimuth rotation) planes, the instrument makes Earth science measurements. The scanning geometry for the TRMM CERES detectors is illustrated in figure 1-6. The instrument has built-in calibration sources, for performing flight calibrations, and can be calibrated by measuring solar radiances reflected by a solar diffuser plate into the instrument field of view.

The normal Earth and the short Earth scans are the two basic elevation scan profiles associated with the fixed-azimuth and biaxial/rotating azimuth plane scan (RAPS) modes. Figure 1-6 identifies scenes observed at some specific elevation angles, and figure 1-7 shows the elevation angle with time during a 6.6 second scan period for the normal and short scan profiles of the instrument on the TRMM spacecraft. Figure 1-7 illustrates the uniform motion of the detectors across the Earth and the time spent at several of the fixed scan positions illustrated in figure 1-6. The built-in internal calibration sources are not active (turned on) during normal science operations. The short scan profile restricts the detectors to elevation angles below the Earth limb and is used primarily during rotating azimuth plane scan operation to prevent the detectors from scanning the Sun.)

Table 1-4. Operational Modes and Configurations of CERES Instruments

	Fixed azimuth scan mode	Rotating azimuth plane scan mode	Solar calibration mode	Standby mode	Diagnostic mode	Safe mode
Nominal profile	Normal Earth scan	Normal Earth scan	MAM scan	Scan head stowed	Scan head stowed	Scan head stowed
Secondary profile	N/A	Short scan	N/A	N/A	N/A	N/A
Azimuth angle	Crosstrack (180°)	Uprange-downrange (90°–270°)	At predicted Sun angle	Braked at arbitrary angle	TBD	Braked at arbitrary angle
Inflight calibration sources	OFF or alternate: ON and OFF for internal vals	OFF or alternate: ON and OFF for internal cals	OFF	OFF	OFF	OFF
Data type	Science	Science	Calibration	Diagnostic	Diagnostic	Diagnostic
Data output format	Science	Science	Science	Science	Diagnostic	Science or diagnostic

1.2.3.2. Science operations. The most important science operational configuration is crosstrack, fixed-azimuth scan mode and the normal Earth scan profile. In this configuration, the detectors scan perpendicular to the spacecraft orbit plane in a whiskbroom fashion. Data collected and archived chronologically are referred to as bidirectional scan (BDS) measurements. Data internally stored spatially, in one hour time blocks, is referred to as instrument Earth scan (IES) measurements. The crosstrack, fixed-azimuth measurements will be the primary data used by the CERES science team for performing Earth radiation budget studies.

The biaxial/rotating azimuth plane scan operation also includes the normal Earth scan profile. In this configuration, the detector elevation scan plane normally oscillates through an azimuth angle of 180° with the end points being uprange and downrange. At the nominal azimuthal rotation rate of 6° per second, a complete azimuth scan cycle is completed in 1 minute. During rotating azimuth operations, the detectors measure radiances from all geographical scenes with varying incident solar radiation and observing geometry. The resulting angular radiance measurements will be used to compute new angular distribution models for use in converting radiances to radiant fluxes.

The alternate configuration during rotating azimuth plane scan includes the short Earth scan profile, which is used to prevent the detectors from scanning the Sun during sunrise and sunset. The scan operation is changed to the short scan profile at the beginning of sunrise and sunset events, and is changed back to the normal scan profile at the end of these events. Changes between scan profiles will be made via stored commands whose times of execution are based on ephemeris predictions. The instrument will perform normal and short scan profiles about 75 and 25 percent of the time, respectively, during RAPS operation.

1.2.3.3. Calibrations. The instrument can perform flight calibrations while operating in the fixed-azimuth (cross track) or rotating azimuth plane scan mode. During flight calibrations, the internal calibration sources are cycled on and off via a programmed sequence of commands while the instrument continues to perform a normal Earth scan profile. Earth measurement data taken during internal calibrations are also included in the archival science data.

Two different in-flight calibration systems are built into the CERES instrument package. They will be used to define shifts or drifts in the sensor responses. The in-flight calibration systems are shown in figure 1-6. At the elevation angle of 194 degrees, the primary in-flight calibration system is called the internal calibration module (ICM). The ICM and the sensors will carry the ground calibration radiometric scale into orbit. The ICM consists of 2.75-cm diameter, concentric grooved, anodized black aluminum blackbody sources for the total and window sensors, and an evacuated tungsten lamp source, known as the shortwave internal calibration source (SWICS), for the shortwave sensor. The blackbodies can be operated at any temperature between ambient and 320 K range. Imbedded in the blackbodies, platinum resistance thermometers (PRT) indicate the temperatures of the blackbodies' emitting surfaces. Before the PRT's are placed in the ICM blackbody structure, the PRT's are calibrated in a temperature controlled bath to verify that the correct coefficients are used in the PRT temperature equation at 273.16 K. After the PRT's are placed into the blackbody structure, the blackbodies are immersed in a temperature controlled bath in order to verify that the PRT's are indicating the same temperature as the controlled bath. If the PRT derived temperatures are not consistent with the bath temperature within 0.05 K, the coefficients in the temperature equation are evaluated empirically using the bath measurements.

At an elevation angle of 236 degrees, the second system is called the mirror attenuator mosaic (MAM), a solar diffuser plate. The shortwave and total-wave channels will be calibrated using the solar radiances reflected from the MAM's. Each MAM consists of baffle-solar diffuser plate systems which guide incoming solar radiances into the instrument fields of view of the shortwave and total wave sensor units. The MAM baffle, solar view cover, and MAM are labeled in figure 1-1. The MAM diffuser plate consists of an array of spherical aluminum mirror segments which are separated by a black paint reflecting surface. Thermistors are located in each MAM plate and in each MAM baffle.

The MAM calibration procedure includes measurements of the MAM before the Sun drifts into the MAM baffle field of view, of the MAM when the Sun is in the field of view, and after the Sun has drifted out of the view. During the MAM scan cycle of 6.6 seconds, the sensors make staring radiance measurements of first the MAM, second the ICM, and then cold space at the elevation angle of 169 degrees. The ICM is not activated during the MAM calibrations.

The solar calibration mode incorporates a special scan profile in which solar radiances, reflected by the mirror attenuator mosaic (MAM), are measured by the detectors. In this profile, the CERES TRMM detectors alternate between making measurements at space (169°), the internal calibration sources, and the MAM. The solar calibration procedure requires that the instrument be rotated to the predicted azimuth angle at which the Sun drifts through the MAM field of view.

1.2.3.4. Other operational modes. The diagnostic mode will be used primarily for handling microprocessor memory loads. The safe mode is incorporated to protect the instrument during emergencies or high-risk situations. The safe mode can be entered at any time from any operational mode via a command from either the instrument or the spacecraft. It can be exited only by a real-time ground command. The standby mode is essentially the same as the safe mode, except that it can be entered only

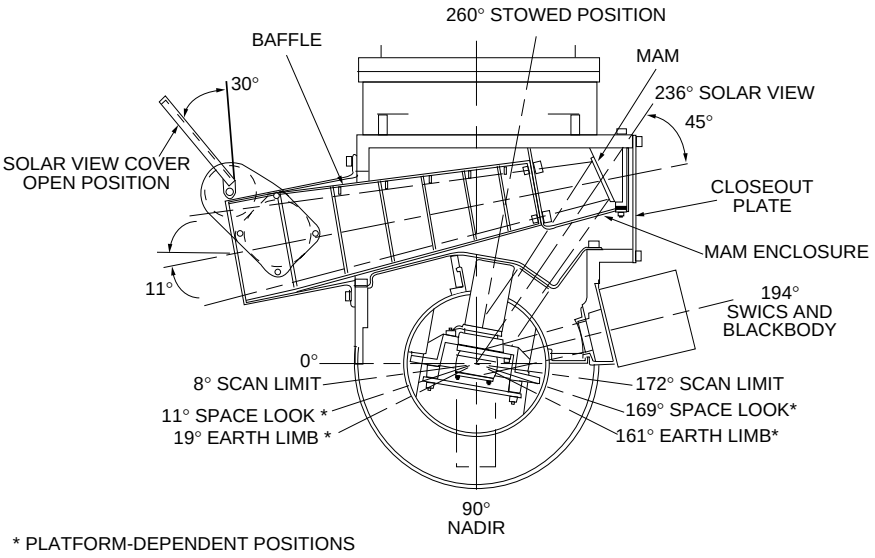

Figure 1-6. Elevation scan positions for instrument on TRMM platform.

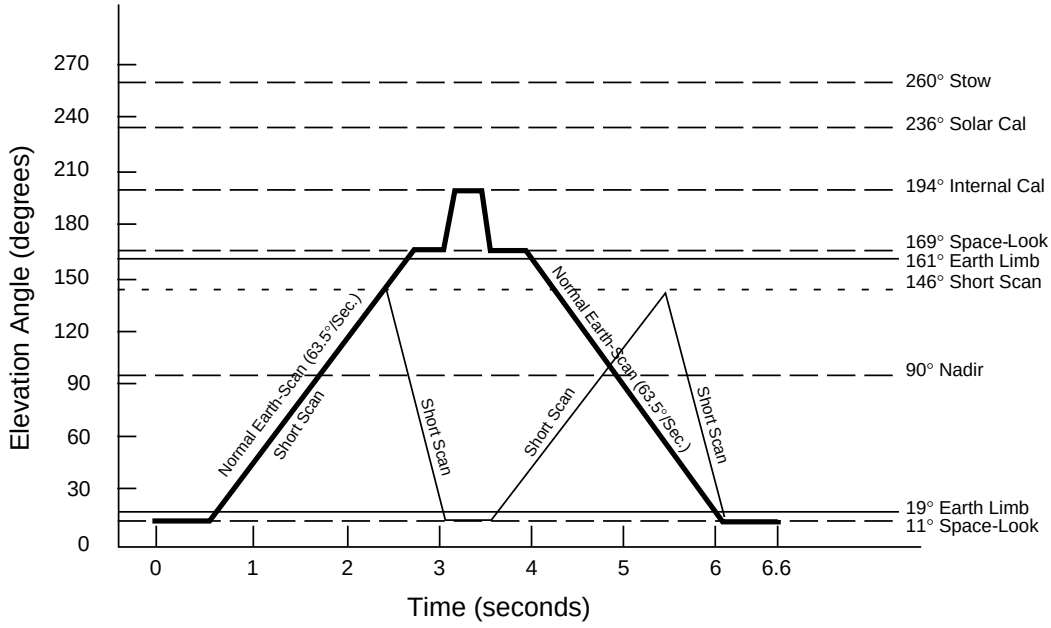

Figure 1-7. Normal and short Earth scan profiles for instrument on TRMM platform.

via a few operational commands, but the instrument will respond to most operational commands during the standby mode. Diagnostic instrument parameters are listed in table A-4.

1.2.3.5. Operational plans. The TRMM spacecraft will have a single CERES instrument. The current plan is to operate the instrument in the cross track/normal Earth scan configuration for 2 days and in the rotating azimuth plane mode for 1 day out of every 3 days. The internal flight and solar calibrations are performed on each instrument during the same orbit about every 2 weeks. There will be two CERES

instruments aboard the EOS AM-1 (morning) and PM-1 (afternoon) spacecraft. The current plan is to operate one instrument in the cross-track/normal Earth scan configuration and the other instrument in the rotating azimuth plane mode with the instrument switching between the normal and short scan profiles as described above in paragraph 1.2.3.2.

1.3. Earth Radiance Count Conversion Algorithms

1.3.1. Math Model

In figure 1-3, the silvered primary and secondary telescope mirrors, the filters, and the black paint layer on the active bolometer flake represent the sensor optical elements that reflect, absorb, or transmit scene energy. The spectral response or sensitivity, *S*, of these sensor elements can be represented as

$$S(\lambda) = \tau_f(\lambda)\rho_m^2(\lambda)\alpha_b(\lambda) \tag{1-2}$$

where τ_f represents the combined transmittance of the filters, ρ_m represents the reflectance of the telescope secondary or primary mirrors, and α_b is the effective absorptance of the black paint layer on the bolometer. In the 0.3 to 2.1 μm wavelength region, the reflectances of the silvered telescope mirrors were derived using the TRW Absolute Reflectance Measurement Station (ARMS) while in the 0.3 to 15 μm wavelength region, Cary spectrometers defined the transmittances of the filters. In the 0.3 to 2.5 μm wavelength region, the absorptance of the black paint was equated to 95% while beyond 2.5 μm, Fourier transform spectrometer (FTS) measurements defined the absorptance between 2.5 to 200 μm. In the 1 to >100 μm wavelength region, end-to-end sensor spectral responses were defined using the TRW Bio-Rad Fourier transform spectrometer and a pyroelectric reference detector (Frink *et al*. 1993). In figure 1-2, for the 0.3 to 2.1 μm wavelength region, the absolute detector spectral responses are derived using equation (1-2), the spectral characterizations of the optical component elements, and the narrowband shortwave calibration results which are outlined in section 1.4.2. For the 2 to >100 μm wavelength region, the responses are derived from end-to-end spectral characterizations (Jarecke *et al.* 1994) of each detector using a Fourier transform spectrometer. In the 1 μm to 3 μm spectral region, the end-to-end FTS spectral characterizations are tied to the absolute shortwave characterizations. In figure 1-2, the spectral responses for the CERES TRMM proto-flight model detectors are presented. Note that the shortwave detectors have longwave out of band sensitivities at wavelengths beyond 60 μm and that window detectors have slight out of band leaks beyond 100 μm. The filtered radiance sensed at the bolometer surface can be represented as

$$\tilde{L} = \int_0^\infty L(\lambda)S(\lambda)\,d\lambda \tag{1-3}$$

where $L(\lambda)$ is the unfiltered radiance from a target scene before the radiance enters the telescope. During ground or flight calibrations, the unfiltered spectral radiance $L(\lambda)$ from a blackbody target (Siegel and Howell 1981) is calculated as a function of the temperature *T* and is expressed as

$$L(\lambda) = \frac{C_1}{\lambda^5(e^{C_2/\lambda T} - 1)} \tag{1-4}$$

where C_1 (1.1909×10^8 W-μm^4-m^{-2}) and C_2 (14388 μm-K) are the constants. The filtered radiance $\tilde{L}$ can be described as the average filtered radiance over the point spread function (*P*). Thus, $\tilde{L}$ is expressed as

$$\tilde{L} = \int d\Omega P(\Omega) \int_0^\infty d\lambda S(\lambda)L(\lambda\Omega) \tag{1-5}$$

where $d\Omega$ is the increment of solid angle and is given as

$$d\Omega = d\phi\, d\theta \sin(\theta) \tag{1-6}$$

where θ is the polar angle aligned with the optical axis and ϕ is the azimuthal angle aligned with the scan direction. The symbols θ and ϕ define the right-handed, spherical polar coordinate system. Using the shortwave detector spectral response (Fig. 1-2) and integrating equation 1-5 between 5 and 200μm, the magnitude of the longwave leak in the shortwave filter is approximately 0.2 $Wm^{-2}sr^{-1}$ for the typical Earth-emitted top-of-the-atmosphere longwave radiance level of 77 $Wm^{-2}sr^{-1}$. The longwave leak in the window filter is less than 0.01 $Wm^{-2}sr^{-1}$.

A simplified version of the basic sensor data reduction equation for filtered radiance is

$$\tilde{L} = \frac{AV[m(t) - m_s(t_0)]}{CV_{\text{bias}}} \tag{1-7}$$

where AV is the detector gain, V_{bias} represents the bias voltage in applied to the bolometers at time t, $m(t)$ is the detector output voltage signal, in counts, at time t, m_s (t_0) is the detector output voltage signal, in counts, when exposed to cold space (3 K radiance source) at time t_0, and C is the digital-to-analog conversion factor of 409.5 counts/volt. Thus, the gain can be expressed as

$$AV = \frac{CV_{\text{bias}}(\tilde{L} - \tilde{L}_{\text{cold dark source}})}{m - m_{\text{cold dark source}}} \tag{1-8}$$

where gain is a function of the bias voltage. For the ERBE thermistor bolometer detectors, equations (1-7) and (1-8) are described by Halyo *et al*. (1987, 1989). The CERES sensor gains are derived from observations of the standard radiometric sources, described in section 1.4.

1.3.2. Algorithms/Theoretical Basis

As shown in figure 1-3, the radiation from the target scenes passes through the filters (except for the total channel) and falls on the 18-mm diameter primary telescope mirror and is then reflected to the secondary mirror, which reflects the radiation through the primary insert, the precision field stop (aperture), and through the corresponding filters. Finally, the radiation is absorbed by the active flake paint layer. The absorbed target radiation causes a change in temperature between active and reference flakes that is detected by a balanced bridge. Figure 1-8 shows the block diagram for the detector electronics. The difference in active and reference flake resistances produces a signal that is amplified in the preamp and processed through a low pass filter. The filtered output is sampled, digitized into counts, and telemetered to Earth as the radiometric output of the detector.

The detector output, illustrated in figure 1-9 and resulting from the combined interaction of the incoming radiation, conduction, and electrical modes of heat transfer, Q, can be written under steady state conditions as

$$Q_{\text{conduction}} + Q_{\text{radiation}} + Q_{\text{electrical}} = 0 \tag{1-9}$$

The CERES estimation equation for filtered radiance is of the same form as that for the ERBE thermistor bolometers, described by Halyo *et al.* (1987, 1989). The radiance estimation equation for the CERES sensors can be expressed as

$$\tilde{L}(t-\gamma) = A_V[m(t) - m(t_k)] + A_H[T_H(t) - T_H(t_k)] + A_\delta \delta_k \frac{t - t_k}{\Delta t} \tag{1-10}$$

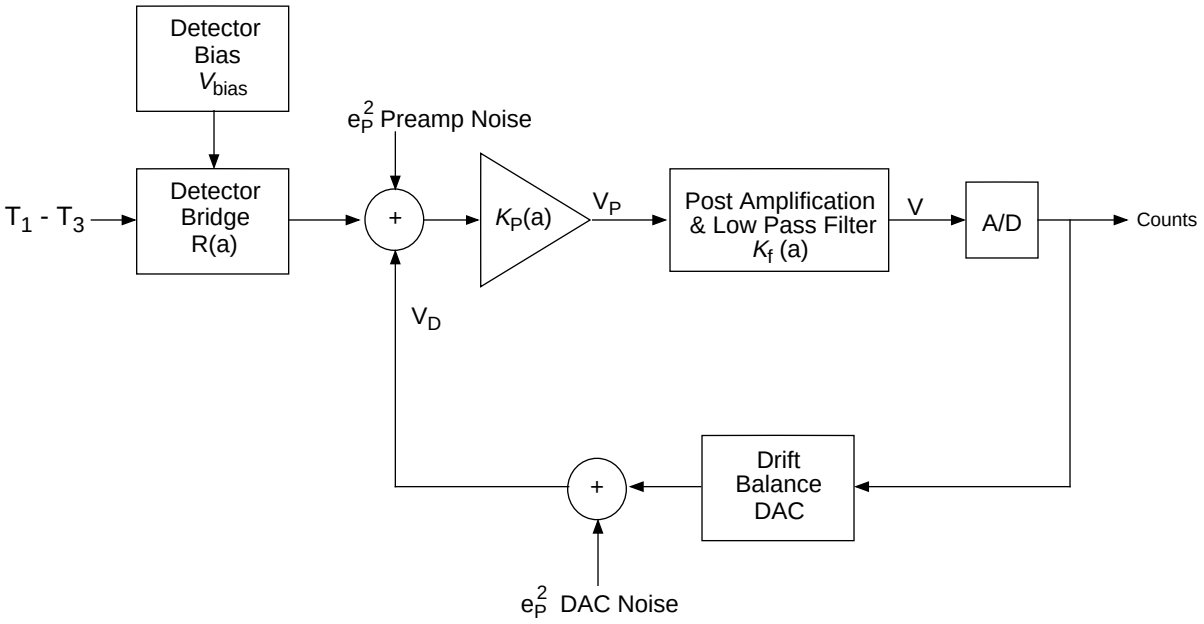

Figure 1-8. Scanner electronics block diagram.

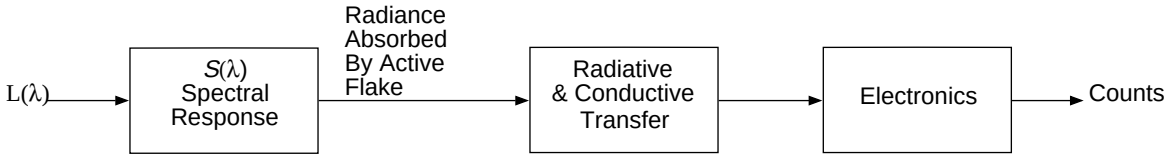

Figure 1-9. Detector output.

for

$$t_{k-1} \le t \le t_k$$

The coefficient gain terms A_V and A_H are determined using the detector voltage and heatsink temperature measurements, respectively. The coefficient A_V is the gain expression. The term A_δ can be given as

$$A_\delta = CK_{f_o} A_V \tag{1-11}$$

The time t_k is given as

$$t_k = t_{k-1} + \Delta t \tag{1-12}$$

The average of the scan points during space clamp is given as

$$\bar{m}(t_k) = \frac{1}{n} \sum_{i=1}^{n} m(t_{ki}) \text{ where } n = 12 \tag{1-13}$$

The mean variance of the counts compared with the space clamp during a scan cycle is obtained by the equation

$$\sigma_k^2 = \frac{1}{n}\sum_{i=1}^{n}[m(t_k) - \bar{m}(t_k)]^2 \tag{1-14}$$

The constants in the above equations are defined as

$\bar{m}(t_k)$ = detector signal, in digital counts, corresponding to space measurement at time t_k

$m(t_{ki})$ = detector signal, in digital counts, when viewing space at time $t_{ki} = t_k + i$ (10 *ms*)

σ_k^2 = noise variance estimate during space look

$m(t)$ = detector output signal, in counts, at time t

$T_H(t)$ = heat sink temperature measurement at t or most recent value (K)

Δt = total scan period (6.6 sec)

t_k = time of space measurement (sec)

t = time of detector measurement (sec)

$V_{\text{bias}}(t)$ = detector bridge bias voltage, in digital counts, measurement at time t

$V_D(t_k)$ = drift balance digital to analog conversion (DAC) voltage, in counts, measurement at time t_k

δ_k = estimate of unaccounted drift during t_kth scan period (v)

γ = average time lag between the instantaneous detector optical field of view and point spread function centroid (sec)

K_{f_o} = post amplification gain

C = digital to analog conversion factor, 409.5 digital counts/volt

1.3.3. Flight Algorithms/Practical Basis

From the standpoint of computational time, it is desirable to have as simple an algorithm as possible. Based on equation (1-10), the following algorithm (Lee et al. 1989) has been selected to interpret the CERES detector's radiometric output voltage, $m(t)$, in digital counts at time t:

$$\begin{aligned}\tilde{L}(t-\gamma) = {} & A_V[m(t) - \bar{m}(t_k) - o(t)] + \frac{t-t_k}{\Delta t}[A_S(\bar{m}(t_{k+1}) - \bar{m}(t_k)) \\ & + A_H(T_H(t_{k+1}) - T_H(t_k)) + A_D(V_D(t_{k+1}) - V_D(t_k)) \\ & + A_B(V_{\text{bias}}(t_{k+1}) - V_{\text{bias}}(t_k))]\end{aligned} \tag{1-15}$$

where

$$t_k = t_{k+1} - \Delta t \tag{1-16}$$

and $\bar{m}(t_k)$ is the average detector output signal during the reference space measurements at the beginning of the scan and at time t_k, Δt is the scan duration of 6.6 sec, $o(t)$ is an offset dependent on the scan geometry during the scan. The housekeeping data $T_H(t_k)$ and $V_D(t_k)$ are transmitted to Earth once every scan and are not available during the scan. The symbol $T_H(t)$ is the heatsink temperature used to drive the heatsink controller, and $V_D(t)$ is the digital to analog conversion drift voltage. The symbol $V_{\text{bias}}(t)$ is the detector bridge bias voltage.

The coefficients A_V, A_S, A_H, A_D, and A_B are defined as

$$A_V = \frac{AV}{CV_{\text{bias}}(t)} \tag{1-17}$$

$$A_S = \frac{AVA}{CV_{\text{bias}}(t)} \tag{1-18}$$

$$A_H = \frac{AHA}{CV_{\text{bias}}(t)} \tag{1-19}$$

$$A_D = \frac{AD}{CV_{\text{bias}}(t)} \tag{1-20}$$

$$A_B = \frac{AB}{CV_{\text{bias}}(t)} \tag{1-21}$$

where *AV*, *AVA*, *AHA*, *AD*, and *AB* are constants determined using the ground calibration data (Lee *et al.* 1989, Halyo *et al.* 1989, and Jarecke *et a*l. 1993), and *C* is the digital-to-analog conversion factor and is equal to 409.5 digital counts/volt.

The first term, A_V, in equation (1-15) is the most important term, while the remaining terms are relatively small. A_S is equal in magnitude to A_V but opposite in sign. When there are changes in the bias voltages$_B$, heat sink temperature, T_H, or in the analog-to-digital voltage, V_D, during a 6.6-second scan cycle, the corresponding filtered radiometric radiances are flagged as bad from equation (1-15). It is important to point out that the A_B term in ERBE ground calibration data analysis was found to be negligible. The ground calibrations of the detectors are outlined in the following section, along with descriptions of the in-flight calibrations.

1.4. Ground and Flight Calibrations

The ground calibrations are designed to define the sensor gain and offset terms which are presented in equation (1-15). In order to define these terms with the highest accuracies, the CERES pre-flight calibration plans include characterizing temporal, spatial, and spectral variations in the calibration sources and CERES sensors. The TRW radiometric calibration facility (RCF) is used to define the gain terms using the spectral characterizations of the calibration sources and sensors and using the sensor offset determinations. In the facility, the sensor in field of view and out of field of view responses are considered in the gain determinations.

Using equation (1-15), the basic calibration procedure consists of (1) defining the filtered radiances reaching the sensor active bolometer flake, (2) correcting for variations in the sensor zero-radiance offset with elevation angle, (3) staring and measuring alternately the radiances from a reference calibration source and a cold space reference [near zero-radiance, blackbody], and (4) performing least squares analyses of the filtered calibration radiances and the independent variables equation 1-15. The in and out fields of view calibration filtered radiances can be described by the following relation:

$$\tilde{L} = \int_{in} L(\lambda, T)\, P(\Omega)\, S(\lambda)\, d\Omega\, d\lambda + \int_{out} L(\lambda, T) P(\Omega)\, S(\lambda)\, d\Omega\, d\lambda + \text{OFFSET(FUNCTION OF SCAN ANGLE)}$$

where

$L(\lambda, T)$ - Plank's relationship, equation (1-4)

$P(\Omega)$ - point spread function

$S(\lambda)$ - spectral response, equation (1-2)

IN - response within field of view

OUT - response outside of field of view

Using the TRW 137-cm diameter vacuum chamber or the radiometric calibration facility, in a vacuum environment of approximately 10-6 torr, the sensors' output signals are sampled as a function of elevation scan angle/geometry with low-emittance caps on the telescope module, in place of the telescope baffles. These samplings are used to determine the variation of the detector zero-radiance offset signal with elevation angle. The observed systematic offset variations are used to adjust the near zero-radiance measurement of the cold space reference source as a function of scan position.

In ground laboratories, it has been noted that the sensor output signals are affected by gravitational forces (due to gravity-induced strain coupling) during the offset determination processes. To account for gravitational effects, the sensors' offsets are determined with the instrument elevation plane aligned perpendicular to the gravitational force and in the same orientation in which the calibration gain terms are derived. In this orientation, the gravitational force is constant on the sensors at all elevation angles. The sensors' offsets are determined again with the instrument elevation plane rotated 180^{o}. If both orientations produce the same offset variations, then the flight (gravity-free) offset variations should be equal to the measured offset as a function of elevation angle.The electronic offsets variations are caused by strain induced in the bolometer flakes by the scanning elevation torques.

The CERES radiometric test model (RTM), functional test model (FTM), TRMM S/C proto-flight model (PFM), flight model 1 (FM1), and flight model 2 (FM2) detectors were calibrated in the TRW radiometric calibration facility (RCF), which is illustrated in figure 1-10. In 1998, flight models 3 and 4 are scheduled for calibrations in the RCF. The radiometric calibration facility is 2.44 meters in diameter and 3.66 meters in length. In the early 1980's, the facility was used to calibrate the Earth Radiation Budget Experiment (ERBE) scanning thermistor bolometer detectors (Lee *et al.* 1989). During the ERBE detector calibrations, the wide field of view blackbody (WFBB) was the primary calibration standard for the TRW facility. The blackbody was formerly called the master reference blackbody (Carman 1983) and the WFBB was based on the International Practical Temperature Scale of 1968 (IPTS'68). The blackbody consists of a 12.7-cm-diameter, concentric-groove, anodized black aluminum blackbody. Presently, its emitted radiances are based upon the international temperature scale of 1990 (ITS-90) using six platinum resistance thermometers (PRT), and it is operated over the 200 K and 370 K temperature range. One of its six thermometers is used for temperature control, while the remaining five PRT's are used for temperature knowledge with measurement precisions of the order of ±0.1 K. During the ERBE calibrations, the TRW radiometric calibration facility employed cold space reference (CSR) blackbodies, a solar simulator, a 50.8-cm-diameter integrating sphere with associated optics (Hesser and Carman 1983), liquid nitrogen cooled shroud walls, and Earth visible and infrared albedo radiation simulators.

Since the 1980's, TRW has expanded the facility to include a very accurate reference narrow field of view blackbody (NFBB), an accurate shortwave reference source (SWRS) with minimum longwave variations and better spectral characterizations, a point response function source (PRFS), a blackbody mask for the narrow field of view blackbody that is used as an out of field response mechanism, a constant radiance reference (CRR), curved strip blackbody that is an offset variation measuring instrument, an improved solar simulator, and a cryogenically cooled transfer active cavity radiometer (TACR). The TACR is identical to the reference active-cavity radiometer used by the National Institute of Standards and Technology (NIST). Detailed descriptions of the radiometric calibration facility are given by Folkman *et al.* (1991), Jarecke *et al*. (1991), and Lee *et al*. (1993a). The May 1992 longwave calibration results and equations for the CERES radiometric test model total detectors are presented by Jarecke *et al.* (1993). The

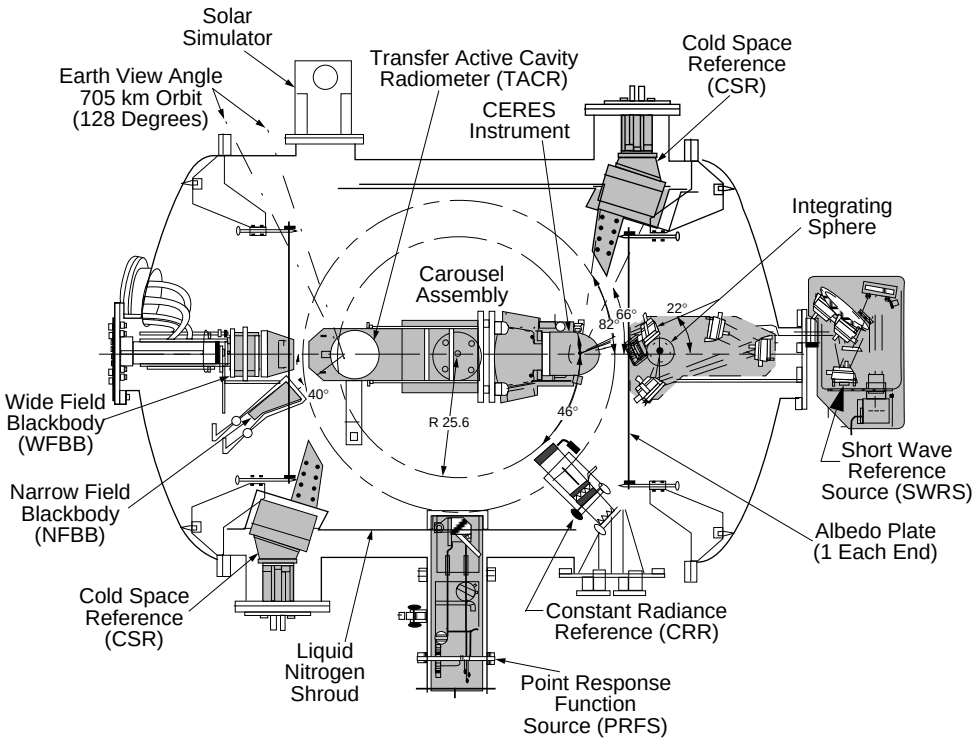

Figure 1-10. Radiometric calibration facility (RCF).

CERES functional test model shortwave, window, and total detectors were calibrated during December 1993. The TRMM protoflight model (PFM) detectors were calibrated in the July-September 1995 time frame while the EOS AM-1 flight model 1 and 2 detectors calibrations were completed October 1996 and February 1997, respectively. Flight models 3 and 4 are scheduled for calibrations in 1998.

1.4.1. Longwave Calibrations

The narrow field of view blackbody (NFBB) is the reference source for the CERES longwave and shortwave calibrations (detector gain determinations). The narrow field of view blackbody (NFBB) is the CERES reference standard because its spectral radiances are characterized more accurately than those for the wide field of view blackbody. The NFBB has an aperture opening that is 3.8 cm by 4.7 cm. Using the NFBB, the CERES detectors are calibrated in the staring configuration and not in the scanning configuration since the NFBB aperture opening and the CERES detector field-of-view are of the same size. The aperture is shown in the front view of figure 1-11. The narrow field of view blackbody has copper walls that are coated with an Aeroglaze Z-302 specular black paint. The paint spectral absorptance was characterized beyond 100 um and its vectorial reflectance field was determined. The blackbody is approximately 21.45 cm deep with an estimated emittance of 0.999952 (Jarecke *et al.* 1993). It has seven platinum resistance thermometers that are used for temperature knowledge, and it has one thermometer that is used for temperature control. The PRT's exhibit less than ±0.033 K uncertainty in temperature knowledge. The aperture of the blackbody is covered by a thermally controlled, diffused black mask. The mask permits the CERES detector out of field response to be determined and the longwave out of field radiances to be known and held constant during longwave calibrations. The mask covers the detector out of field view between the telescope module field of view and the location of the telescope detector baffle, 16° off the detector optical axis. The blackbody temperature is varied at different levels between 200 K and 320 K, while the blackbody aperture mask temperature is typically maintained at 170 K. The mask temperature is operated in the 170 K to 380 K range during the detectors out of field response determination tests.

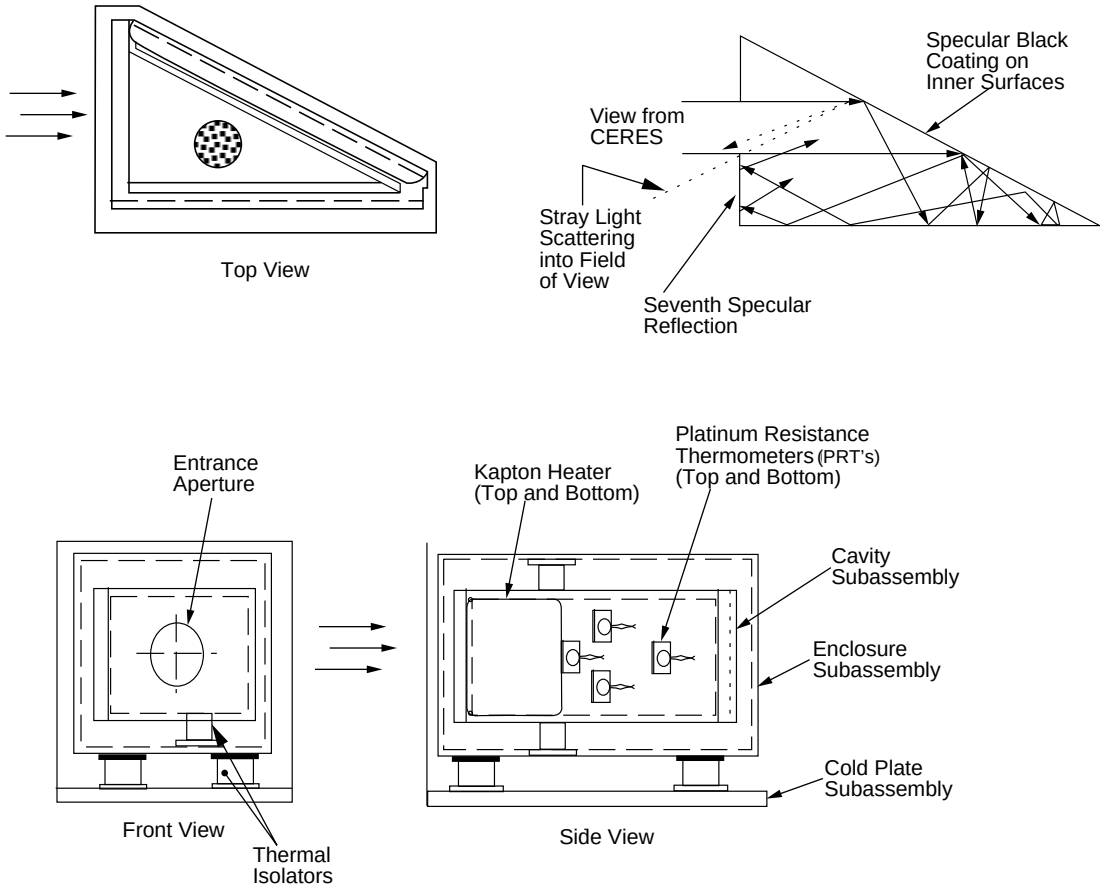

Figure 1-11. Schematic of narrow field of view blackbody (NFBB).

The longwave gain determination of CERES detectors consists of alternating staring observations at the narrow field of view blackbody and staring observations at the cold space reference blackbody identified in figure 1-10. The cold space reference blackbody is a 12.7-cm-diameter, concentric groove, anodized black aluminum emitting surface. It has two platinum resistance thermometers, which can be used for either temperature control or knowledge. It is cooled by liquid nitrogen to a constant temperature near 85 K. The narrow field of view blackbody radiances are calculated using a temperature-based model. The model is tied to the international temperature scale of 1990 using platinum resistance thermometers. The blackbody radiances are measured by CERES detectors when the NFBB is operated at different temperature levels in the 200 K to 330 K range. Using a form of equation (1-8), the detector gains are determined from regression analyses of the differences in the filtered radiances emitted from the NFBB and the CSR, and of the differences in the detectors output signals corresponding to measurements of the NFBB and CSR radiances. Since the detectors are sensitive to the out of field radiances as well as in field radiances, the detector out of field response is considered in the gain determinations. The out of field response is determined from observations of the narrow field of view blackbody with the NFBB temperature held constant near 200 K, while the NFBB aperture mask temperature is varied between 170 K and 380 K. For the FTM, PFM, FM1, and FM2 detectors, regression analyses of the mask data indicate out-of view responses less than 1.4% of the in-field responses.

The detector zero-radiance offset signal varies as a function of scan elevation angle position. Using low emittance polished aluminum end-caps on the telescope module in place of the telescope baffles, the detector output signal is sampled as a function of elevation angle. The end-caps emit low constant radiances. Therefore, variations in the signal are used to characterize variations in the near zero-radiance measurements of the cold space reference source as a function of scan elevation angle position. The

detectors are sensitive to gravity forces during the offset determination processes. Consequently, the offset variation determinations are determined with the elevation plane perpendicular to the gravitational force. The detector gains are determined in the same gravitational configuration. Observations of the constant radiance reference (CRR) yield offsets which are affected by gravity. However, the CRR derived offsets can be vectorially added to characterize the offset variations with reduced precision. The CRR measurements over a period time were used to demonstrate that the PFM detector offset variability did not change with time.

In figure 1-12, the uncertainty allocations in percent for the NFBB radiances are presented (Jarecke *et al.* 1993). In late 1999, after the CERES flight model 5 detectors are calibrated, the NFBB irradiances will be compared with those from the cryogenically cooled transfer active cavity radiometer (TACR), shown in figure 1-10. Presently, the TACR is operated only in the radiance measuring configuration. In the comparisons, the TACR baffle will be replaced with precision primary and secondary apertures which are required to make absolute irradiance measurements at the 0.1% accuracy level.

The wide field of view blackbody (WFBB) is observed in the staring and operational scanning cycle modes to define calibration differences that may be caused by observational geometry and scan rate.

In figure 1-13, the longwave uncertainty allocations in percent are presented for the total detector ground and flight calibrations (Jarecke *et al*. 1993). In the upper panel of figure 1-13, the ground longwave percent uncertainty allocations are presented for the total detector. The delta from ground block represents the uncertainty error due to differences in the radiant and thermal environments between the ground calibration in the radiometric calibration facility and flight in space, which result in an offset error in the internal calibration source blackbodies (ICSBB). The symbol $\Delta S(\lambda)$ represents the longwave percent uncertainty in characterizing the spectral throughput of each detector. The symbol $S(\theta,\phi,x,y)$ represents the angular and spatial detector response. The point response function source (PRFS) device is used to define the spatial response function $S(x,y)$ and the point spread function. The internal calibration source blackbody uncertainty is represented by the transfer uncertainty block, and RANDOM is the random error. In the lower panel, the flight longwave percent uncertainty requirements are presented for the total detector.

1.4.2. Shortwave Calibrations

The ERBE total-wave and longwave bolometer sensors were used to transfer the WFBB international practical temperature scale of 1968 (IPTS’68) temperature-based radiometric scale to the calibration facility integrating sphere. The ERBE longwave sensor unit had a diamond substrate filter system which transmitted radiances in the 5 to 20 mm broadband spectral region. Initially, the ERBE total-wave and longwave sensor gains were derived from observation of the wide field of view and the cold space reference blackbodies. Then, the total-wave sensor was used to measure the longwave and shortwave radiances from the integrating sphere while the longwave sensor was used to measure longwave radiances from the integrating sphere. The differences between the total and longwave sensor measurements were used to characterize the shortwave radiances from the integrating sphere. The spectral responses of the total-wave, longwave, and shortwave sensors were used to transform the total-wave minus longwave radiance differences into the shortwave sensor spectral region.

During shortwave calibrations, the ERBE integrating sphere emitted significant longwave radiances to the sensors because its lamps were located within the sphere. For the CERES calibrations, the new shortwave reference source (SWRS) system was developed which minimizes the longwave heating effects of the integrating sphere and which uses an electrical substitution radiometer to transfer the NFBB temperature-based radiometric scale to the new shortwave reference source system.

The radiometer is called the transfer active-cavity radiometer (TACR), identified in figure 1-14. The radiometer (Foukal *et al.* 1990), which operates near 4 K, is equipped with the same telescope and field stop aperture design geometries as those for the CERES sensors, in order to duplicate the CERES sensor

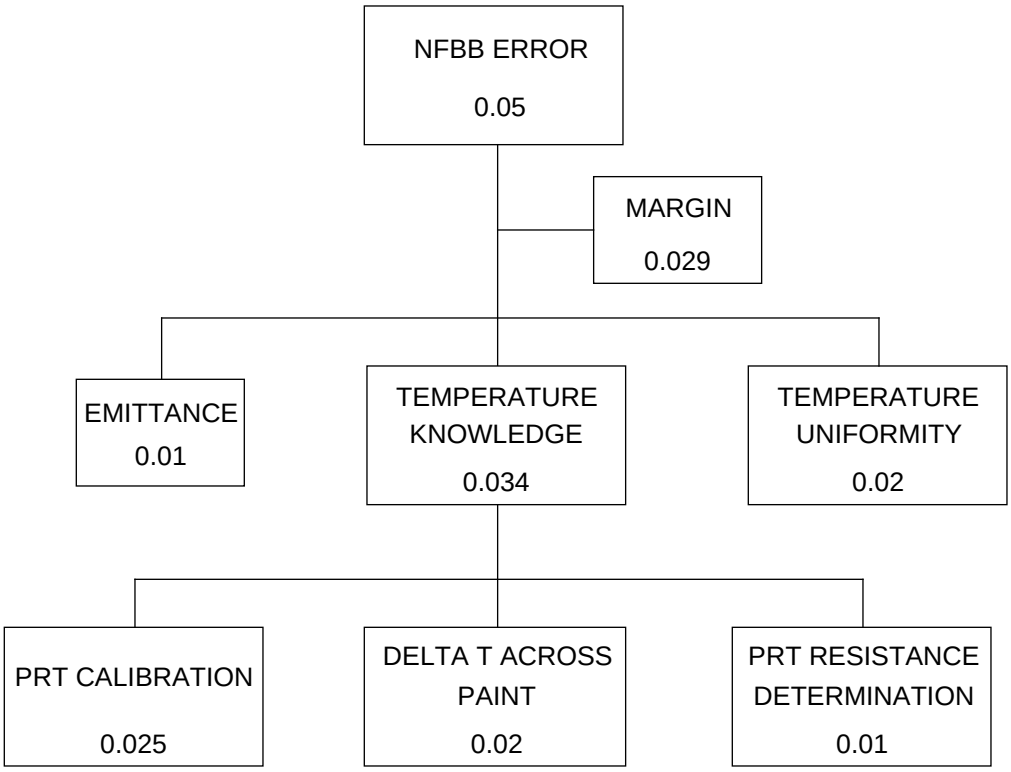

Figure 1-12. Narrow field of view blackbody (NFBB) percent uncertainty allocations.

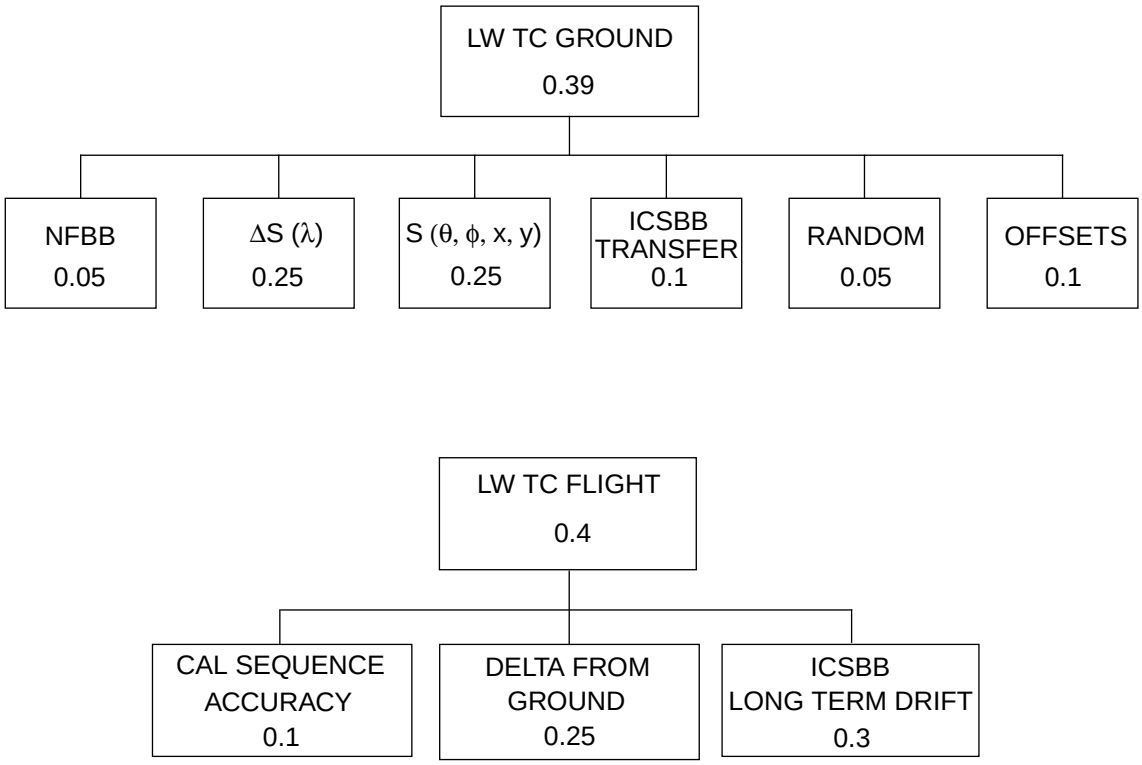

Figure 1-13. Longwave (LW) ground and flight calibration percent uncertainty allocations.

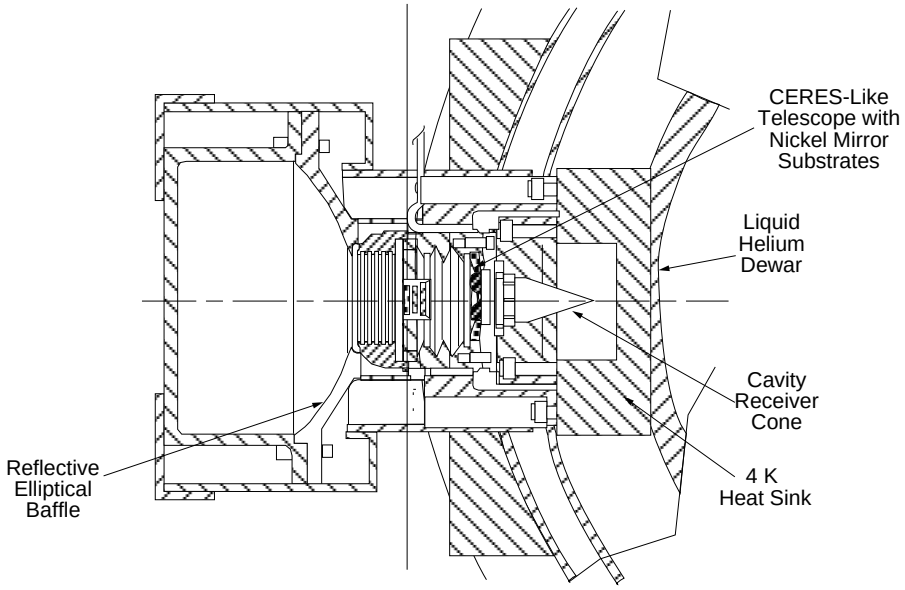

Figure 1-14. Transfer active cavity radiometer (TACR).

field of view and aperture area. The TACR makes power measurements at an accuracy of $\pm$ 0.05% with an NEP of 2 nW and has a 1-second time constant. The product of the TACR aperture area and field of view is calculated from the TACR power measurements of the NFBB divided by the modeled NFBB source radiances. Folkman *et al.* (1994) describe the calibration of the SWRS using the TACR. During the calibration of the TACR, the TACR measures longwave radiances from the NFBB. The resultant TACR signals are regressed against the corresponding NFBB radiances in order to determine the TACR gain and offsets which are required to place the TACR on the NFBB radiometric scale. The uncertainty allocations in percents for the radiometer are presented in figure 1-15.

The shortwave reference source is used to determine the shortwave sensor and shortwave portion of the total-wave sensor gains. The SWRS consists of a 250-Watt quartz tungsten halogen source lamp, a variable area aperture, 17 narrowband optical filters, a broadband Potassium Di-Phosphate (KDP) filter, relay reflective optics, an 11-cm diameter Spectralon integrating sphere, and associated optics (Folkman *et al.* 1991). The sphere exit port is 3.6 angular degrees in the along track direction and 7.5 degrees in the cross track direction as measured from the scanning sensors (See Fig. 7 for the illustration of cross track direction). The SWRS lamp output is maintained at the 0.1% stability level over as many as 14 hours. The radiant exitance from the sphere has been mapped at the 0.3% uniformity level over the exit port.

For shortwave calibrations, narrow band filters are used to define the spectral shape of the integrating sphere radiances. The narrow band filters are centered at 0.38, 0.40, 0.45, 0.50, 0.60, 0.70, 0.80, 0.90, 1.00, 1.15, 1.25, 1.35, 1.47, 1.64, 1.94, 2.24, and 3.25 μm with corresponding sphere radiance levels of 0.9, 22, 86, 105, 142, 160, 196, 182, 132, 230, 256, 103, 90, 139, 41, 49, and 27 $Wm^{-2}sr^{-1}$, respectively. During the calibrations of the CERES functional test model sensors, the TACR was used to measure the above narrow band radiances. Using the narrow band filters, the SWRS radiances are not high enough to calibrate, at the 0.1% accuracy level, the shortwave and total-wave sensors gains. With the variable aperture opened at the maximum setting and using the KDP filter, the SWRS provides radiances over 500 $Wm^{-2}sr^{-1}$ between 0.3 and 1.6 μm with peak radiances occurring at 1.29 μm. Therefore, the broadband KDP filter is used to define the sensors' shortwave region filtered gains. The shortwave radiances are chopped. A variable area aperture is used to regulate the amount of shortwave radiances which are transmitted through the KDP filter to the SWRS integrating sphere. During the calibration of each flight sensor set, the SWRS is calibrated using the TACR. The window sensors are calibrated with

shortwave radiances to determined the impact of shortwave leaks or shortwave heating of the window filter system upon its output signal. Figure 1-2 shows that the window sensors are sensitive to radiances beyond 100 mm.

In the upper portion of figure 1-16, the shortwave calibration percent uncertainty allocations are presented. The uncertainty in the shortwave internal calibration source (SWICS) is considered in the error budget.

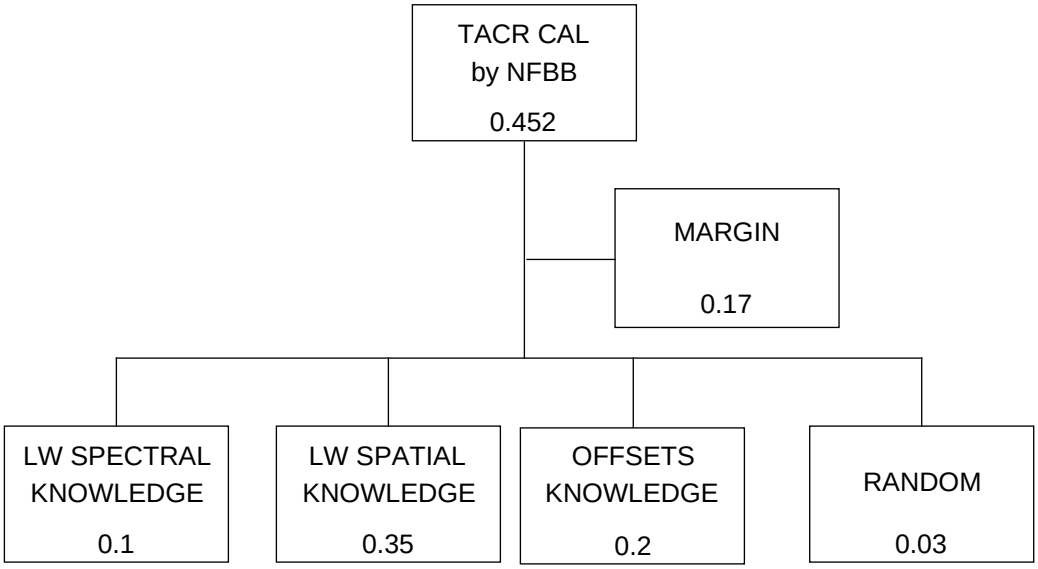

Figure 1-15. Transfer active cavity radiometer (TACR) percent uncertainty allocations.

In figure 1-17, the uncertainty allocations for the total detector are presented. The numbers in italics represent the predicted performance levels.

1.4.3. Point Response Function

As shown in figure 1-10, the RCF has a point response function source (PRFS). Paden *et al*. (1997) describe the point response measurement procedures and present comparisons of the CERES detector PRFS measurements with the theoretical models of the detectors point spread function (Smith 1994). The point response function source (PRFS) has a Nernst glower source whose angular subtense is slightly less than 0.17 degree. The glower is operated at 2400 K and has an emittance of 0.7. In 3.3 seconds, the target sensor scans through the collimated PRFS beam $\pm$ 17 degrees relative to the beam. The sensor's output signal is sampled every 0.6 degrees. In order to fill in data gaps, a PRFS steering mirror introduces $\pm$ 0.2 degree phase shifts into the scan. Therefore, there are three sets of measurements for each sensor cross track scan position. The scan positions in the field of view are spaced every 0.2 degrees. Thirteen cross track scans are required to cover the sensor's 2.6 degree field of view. The CERES sensors will scan across the PRFS imaged at infinity.

1.4.4. In-Flight Calibrations

In-flight calibration systems are built into the CERES instrument. The three detectors are calibrated using the internal calibration module (ICM), shown in figure 1-18. The module consists of concentric grooved, anodized aluminum blackbody sources for the total and longwave detectors and an evaluated tungsten lamp source system, known as the shortwave internal calibration source (SWICS), for the shortwave detector. The basic SWICS design is described by Lee *et al.* (1993b). The ICM was used to

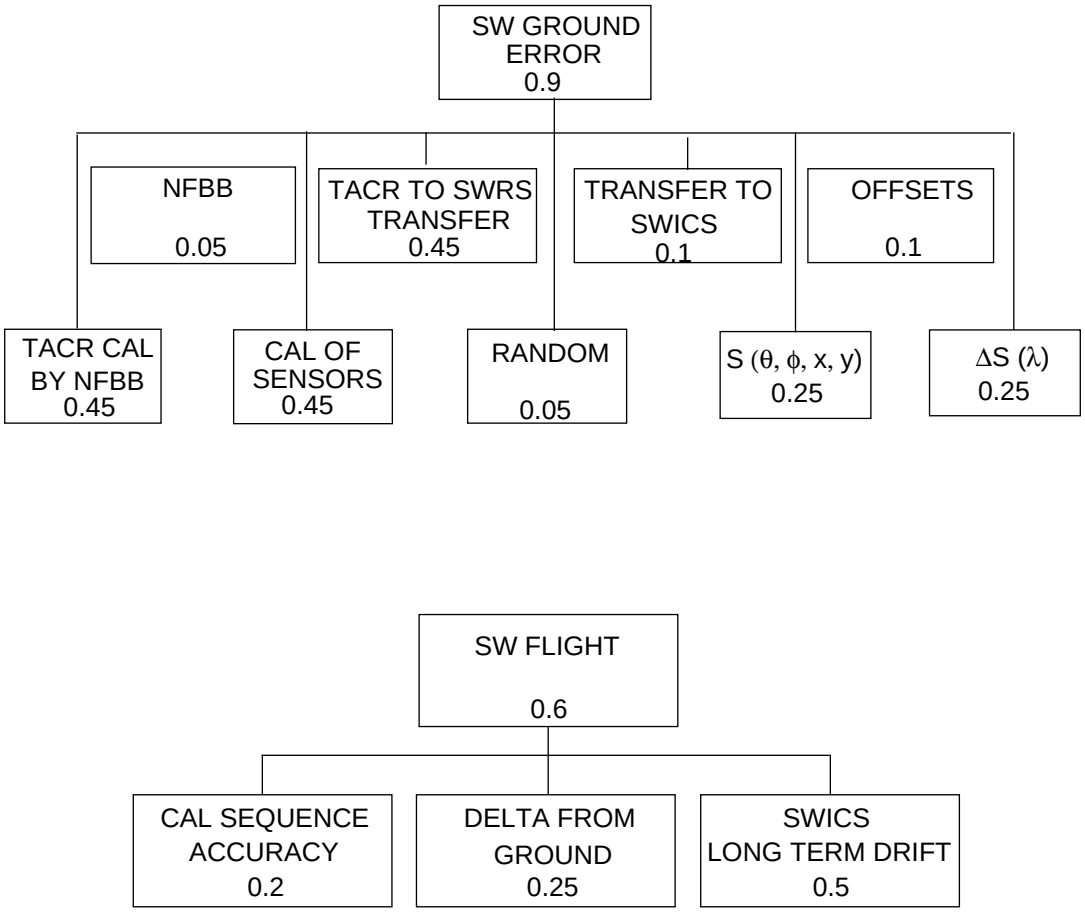

Figure 1-16. Shortwave ground and flight percent uncertainty allocations.

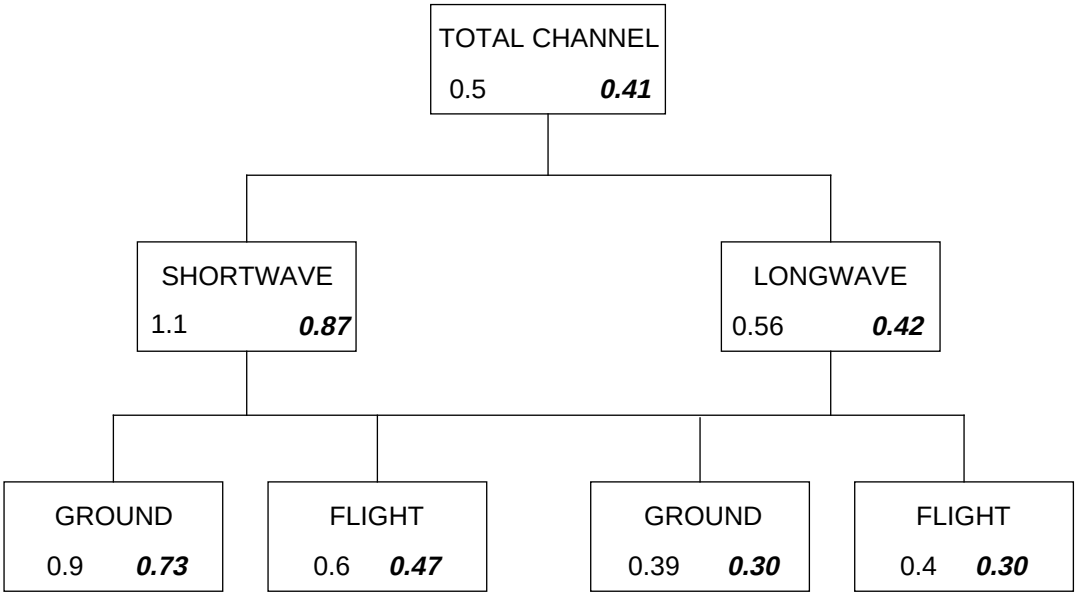

Figure 1-17. Total detector ground and flight percent uncertainty allocations.

calibrate thermistor bolometers and active-cavity radiometers aboard the Earth Radiation Budget Satellite (ERBS), NOAA-9, and NOAA-10 spacecraft platforms. In figure 1-19, ERBS thermistor bolometer flight calibration measurements demonstrate the maturity of the CERES ICM design. The measurements represent raw output signals from the shortwave, longwave, and total thermistor bolometers. The dropouts in the measurements were caused by misalignments between the bolometers and the calibration sources. The misalignments occurred when the sensor scanning mechanism became sluggish (Kopia and Lee 1992). The measurements show that the bolometers and flight calibration sources (evacuate tungsten lamp and blackbodies) were stable to approximately 0.3 percent (Lee and Barkstrom 1991, Lee *et al.* 1993b). The shortwave and total channels are calibrated using the solar radiances reflected from a solar diffuser plate, referred to as the mirror attenuator mosaic (MAM). The locations of the MAM baffle and reflecting surface are identified in figure 1-6. The MAM solar radiance reflecting surface consists of an array of spherical aluminum mirror segments that are separated by a black painted reflecting surface. The CERES MAM design should yield calibration precisions approaching 1 percent for the total and shortwave detectors (Folkman *et al.* 1993). The CERES basic solar calibration approach and flight data reduction algorithms are similar to those for ERBE, described by Lee *et al*. (1992). The ERBE MAM calibration approach,

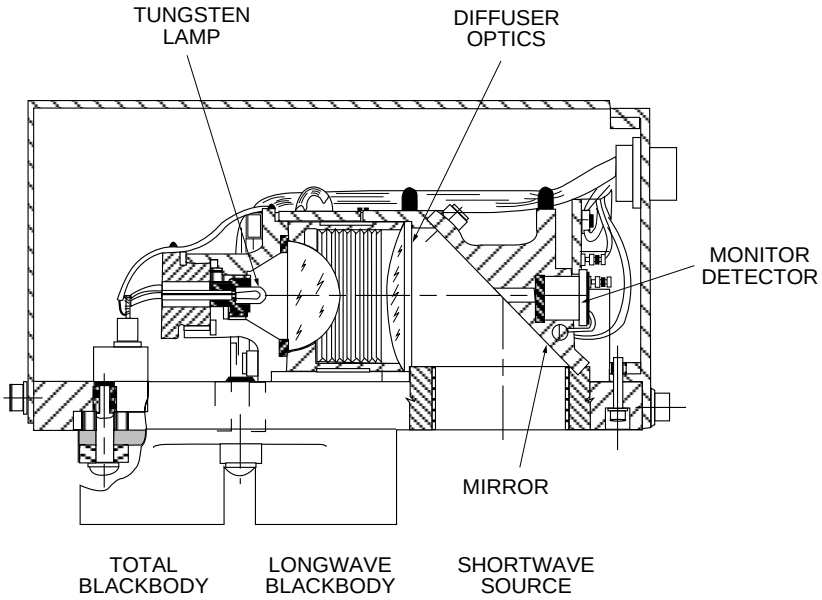

Figure 1-18. Internal calibration module (ICM).

flight data reduction algorithms, and in-flight performances yielded measurement precisions at the 3-percent level (Lee *et al.* 1992) as shown in figure 1-20. Using the ICM, the CERES total, window, and shortwave detectors will be calibrated to define revisions in the count conversion coefficients, used in equations 1-17 to 1-21, and to monitor the gain stability of these detectors (Lee *et al.* 1990, Gibson *et al.* 1992). The nighttime radiance time series for each shortwave detector will be produced on a daily basis to modify the detector offset. By definition, the nighttime shortwave radiance should be zero.

During the ICM calibration process, the blackbodies are operated and maintained at several temperatures between ambient and 320 K. Using equation 1-15, the total-wave and window sensors measurements of the in-flight blackbodies are converted into filtered radiances. The blackbody radiances are calculated from the Stefan-Boltzman relationship using the PRT temperatures and the effective blackbody emittances. The calculated sensor and the calculated blackbody radiances are compared using regression analyses to verify that the blackbodies are on the same radiometric scale as the sensors.

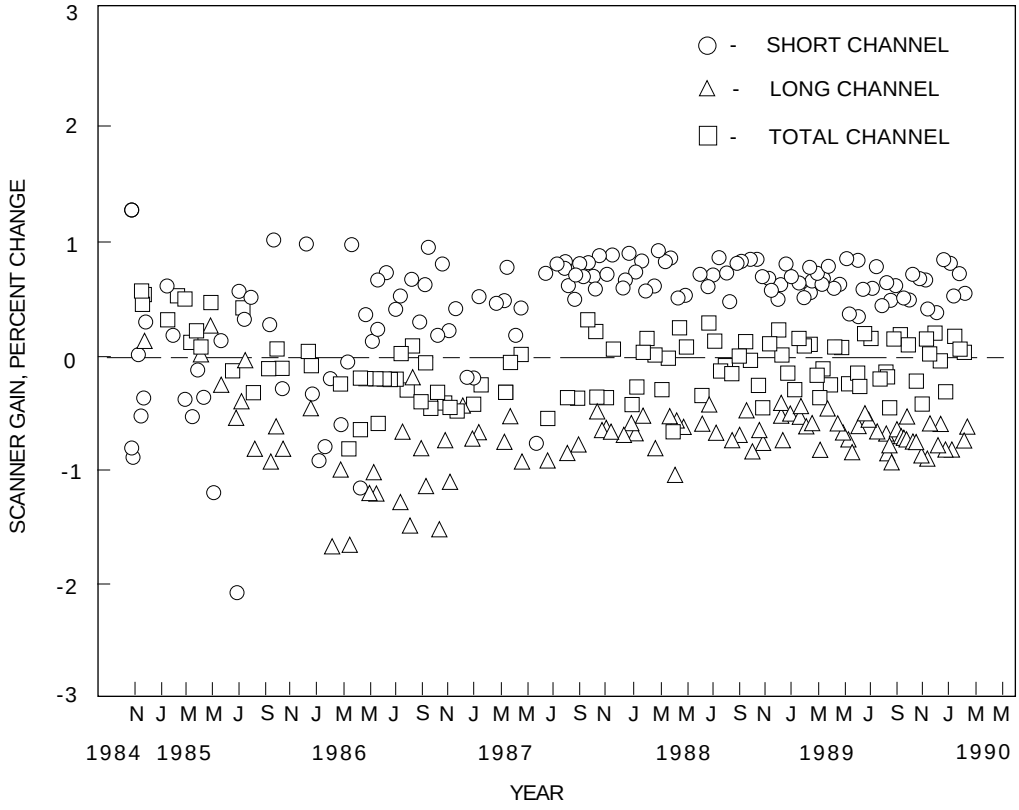

Figure 1-19. ERBS scanner calibration.

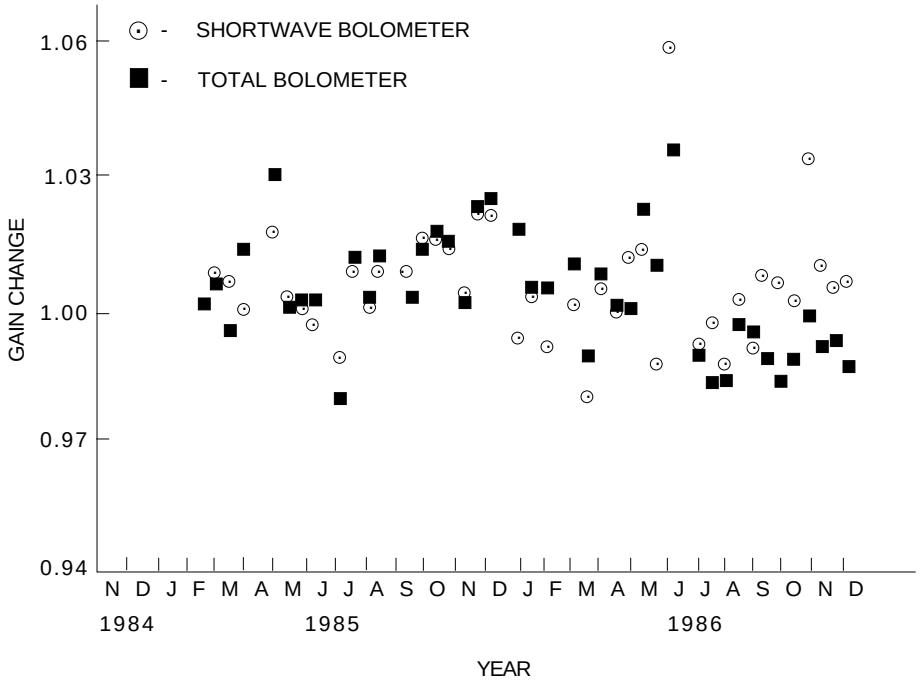

Figure 1-20. NOAA-9 thermistor bolometer solar calibrations.

The SWICS radiances are calibrated using the shortwave sensor. The sensor measures the SWICS radiances at 3 different constant non-zero radiance levels between 0 and 400 $Wm^{-2}sr^{-1}$. Using equation 1-15, the sensor output signals are converted into radiances. The calculated radiances are then assigned to the four SWICS levels. The first non-zero level of SWICS tungsten lamp has peak radiances near 1.7 μm, since it operates at temperatures near 1700 K.

The MAM reflectance uniformity is determined using the total-wave and shortwave sensors and using the solar simulator, illustrated in figure 1-10. The simulator is a 5 KW Xenon arc lamp which is typically operated at the one Sun level of 434.5 $Wm^{-2}sr^{-1}$. The lamp beam is 15.2 cm which is large enough to cover the total-wave and shortwave MAM baffles. In the elevation plane, the incident angle, between the optical axes of the solar simulator beam and the MAM baffle, is varied in 0.1 angular degree steps in the $\pm$ 5.0 degree range relative to the MAM baffle optical axis. The total-wave and shortwave sensors are used to measure the MAM-reflected shortwave and longwave radiances as well as MAM emitted longwave radiances. For the shortwave sensor, the MAM-reflected shortwave radiances are equal to the differences between the MAM and cold space reference radiances. In the case of the total-wave sensor, the MAM radiances consist of both shortwave and longwave components. For the total-wave sensor calibrations, the MAM-emitted and -reflected longwave radiances must be regressed against the MAM baffle and MAM structure temperatures in order to derive an empirical relation for the longwave radiances as a function of MAM temperatures. The empirical relationship is needed to define the longwave component of the mixed shortwave and longwave radiances from the MAM during flight calibrations.

The MAM is a relative calibration system. Its vectorial reflectances are not defined absolutely. Calibrations of the CERES functional test model sensors indicate that its MAM reflectances were uniform to $\pm$2.5%. When the solar simulator was operated at the 521 $Wm^{-2}sr^{-1}$ radiance level (1.2 Suns), the total-wave and shortwave sensors measured MAM-reflected shortwave radiances at the 120 $Wm^{-2}sr^{-1}$ level

The uncertainty requirements for the flight calibrations are presented in the lower portions of figures 1-13 and 1-16.

1.5. Input Data

The primary data stream is a 24-hour data file or set of archival science data packets containing CERES instrument science measurements and associated engineering data. The contents of a packet are listed in Appendix A, table A-2. A packet consists of instrument data acquired during a 6.6-second scan period when the instrument is operating in one of the two primary science modes. A packet also contains a time stamp and an application process identifier (APID) that identifies the data as archival science data from a specific CERES instrument. Calibration data packets are generated during solar calibrations, and the structure and content are identical to the science packets.

In addition to the CERES science and calibration data, the Instrument Subsystem must also process data sets consisting of packets of diagnostic data generated by the CERES instruments. The structure of these packets is similar to that for the science data packets, but the data content is different and the packets are identified by different application identifiers.

For every 24-hour period of CERES instrument data, a corresponding 24-hour file of spacecraft orbit and attitude data are required to calculate the Earth locations of the measurements and other pertinent Earth-Sun-spacecraft parameters.

The files containing the CERES instrument measurements and spacecraft orbit and attitude data are generated at the GSFC and transferred to the LaRC DAAC. Data in these files required to perform all CERES science data processing are accessed through software toolkit routines provided in the Science Data Processing (SDP) Toolkit.

1.6. Housekeeping Data Conversions to Engineering Units

The basic engineering data provided by the CERES instrument package are elevation and azimuth positions, voltage and temperature measurements, and instrument status information. The temperature and voltage measurements and the status data are essential in monitoring the health and safety of the instruments and in studying the instrument condition during emergencies.

Table 1-5. "C" Coefficients for CERES PFM(TRMM) Instrument

Equation:	C_0	C_1	C_2	C_3
1-22	$3.3922 \cdot 10^3$	$1.3208 \cdot 10^7$	$8.4931 \cdot 10^2$	N/A
1-23 (Tot.)	860.85	4.5525	N/A	N/A
1-23 (LW)	862.30	4.4925	N/A	N/A
1-23 (SW)	865.16	4.179167	N/A	N/A
1-24	$7.8431 \cdot 10^6$	$7.3365 \cdot 10^3$	$1.7341 \cdot 10^3$	273.15

Table 1-6. "K" Coefficients for CERES PFM(TRMM) Instrument

Sensor:	K_0	K_1	K_2	K_3	K_4
PRT.	14794.25	1.0	7.85955	$-5 \cdot 10^{-5}$	0
Control Htr. Tot.	275520.4	1.0	269.0211	$-2 \cdot 10^{-4}$	0
Control Htr. LW	275520.4	1.0	269.0211	$-2 \cdot 10^{-4}$	0
Control Htr. SW	275520.4	1.0	271.4712	$-2.018 \cdot 10^{-4}$	0
Thermistor Det.	27405.4	1.0	1.7024	$-1 \cdot 10^{-5}$	0
Thermistor SEA	273.7300	1.0	0.04291	$-8.264 \cdot 10^{-6}$	0
Thermistor GTM	273.7300	1.0	0.04291	$-8.264 \cdot 10^{-6}$	1200.
Thermistor S/C	0	12.2100	5000.	0.00244	0
Thermistor GSE	0	22.8934	9375	0.00244	0

The elevation and azimuth positions, along with the ephemeris and attitude data, determine the location of instrument measurements at the top of the atmosphere. The bias voltage, digital to analog (DAC) drift voltage, and heat-sink temperature are used in the calculation of filtered radiances. The blackbody temperatures and shortwave internal calibration source output voltage are needed in analyzing the calibration data. The instrument status words identify the instrument's operational state

The data conversion equations for transforming temperature measurements in counts to degrees Celsius are outlined by the CERES Science Team and by TRW. The following relationships are used to calculate the CERES PFM(TRMM) instrument, sensor heater control, and thermistor temperatures.

Detector Temperature:

$$T_{PRT} = C_0 - \sqrt{(C_1 - (C_2 \cdot K_T))} \tag{1-22}$$

Sensor Heater Control Temperature:

$$T_s = (K_T - C_0) / C_1 \tag{1-23}$$

Thermistor Temperature:

$$T_m = C_0/(C_1 + C_2 \cdot \log K_T + \log K_T^{\,3}) - C_3 \quad (1\text{-}24)$$

where K_T is given as

$$K_T = (K_0 + K_1 \cdot counts)/(K_2 - (K_3 \cdot counts)) - K_4 \quad (1\text{-}25)$$

The numerical constant values for the C_i and K_i constants required in the above equations for the CERES PFM(TRMM) instrument are given in tables 1-5 & 1-6, respectively. The corresponding constant values for the EOS flight model instruments will be defined at a later date.

1.7. Field-of-View Location

1.7.1. Overview

It is essential in interpreting the CERES radiance measurements to accurately locate the radiation

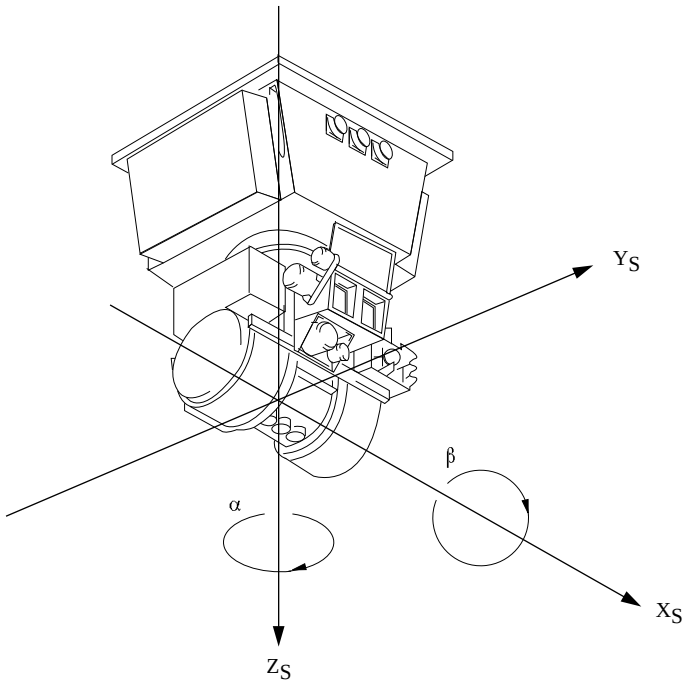

Figure 1-21. Relationship of rotating detectors to fixed axes of CERES instrument

source of each measurement on the surface of the Earth. Calculation of the Earth locations of the measurements requires pointing knowledge of the detectors referenced to the instrument coordinate system, spacecraft position and attitude data, and a geometric model of the Earth.

The geolocation calculations are performed in two main steps. Calculations in the first step are performed using CERES-unique equations and data. This step calculates pointing angles (in degrees) of the detectors in the CERES instrument fixed-axes coordinate system by converting the raw pointing data contained in the science data packets. The pointing angles are then used to calculate unit pointing vectors of the detectors in the spacecraft coordinate system. The second step calculates the Earth locations, or

fields of view, associated with the radiance measurements, using science data processing (SDP) toolkit routines provided to the NASA Langley Research Center (LaRC) distributed active archive center (DAAC) by the ECS Project. The toolkit calculates the points where the detector pointing vectors, which lie along the line of sight of the detectors, intersect the surface of a geometric Earth model or the surface of some other specified model.

1.7.2. Calculation of Detector Pointing Vectors

Figure 1-21 illustrates the relationship of the rotating detectors to the fixed-axes coordinates of the instrument [X_s, Y_s, Z_s]. The detectors have two rotational degrees of freedom relative to the fixed-axes coordinate system. The detectors rotate in azimuth (alpha) about the Z_s axis and in elevation (Beta) about an axis normal to the azimuth-rotation plane. The figure shows the detectors at an azimuth angle of 180 degrees and an elevation angle of 90 degrees (nadir).

$$\begin{bmatrix} X_S \\ Y_S \\ Z_S \end{bmatrix} = \begin{bmatrix} \cos\alpha & -\sin\alpha\cos\beta & -\sin\alpha\sin\beta \\ \sin\alpha & \cos\beta\cos\alpha & \sin\alpha\cos\alpha \\ 0 & -\sin\beta & \cos\beta \end{bmatrix} \begin{bmatrix} X_i \\ Y_i \\ Z_i \end{bmatrix} \tag{1-26}$$

using values of the measured azimuth and elevation angles (Alpha and Phi) contained in the science data packets. The vectors, [X_i, Y_i, Z_i] are unit vectors which define the initial pointing direction of the detectors [$\alpha = 0$, $\beta = 0$]. During integration of a CERES instrument with a spacecraft (TRMM, EOS AM, or EOS PM) the fixed axes of the instrument will be coaligned with the fixed axes of the spacecraft. If the alignment is perfect and if the detectors are aligned perfectly with the fixed axes of the instrument, the initial pointing vectors will have values of [0, -1, 0]. This alignment points the detectors along the negative direction of the spacecraft Y axis. Misalignments between the detectors and the fixed axes of the instrument and between the instrument and spacecraft fixed-axes systems will be accounted for in equation 1-26 by modifying the components of the initial unit pointing vector.

1.7.3. Calculation of Detector Fields Of View

Earth locations of the ERBE radiance measurements were calculated by the equations derived in (Hoffman, *et al*, 1987). Earth locations of the CERES radiance measurements and other pertinent Earth-spacecraft-Sun parameters are calculated using the science data processing (SDP) toolkit provided by the ECS project. Using the SDP Toolkit to calculate the FOV's and other geometric parameters helps insure compatibility in Earth-spacecraft-Sun geometry when comparing CERES instrument data with data from other instruments on the TRMM and EOS spacecraft.

A pixel-FOV toolkit routine calculates the points that the detector pointing vectors intersect the surface of the Earth or other specified geometric model [figure 1-22]. This toolkit routine performs the complete set of coordinate transformations corresponding to those described in (Hoffman, *et. at* 1987) using values of the detector pointing vectors calculated in step 1 and spacecraft position and attitude.

The CERES Data Management system DMS accesses the Pixel-FOV routine at the beginning of a 6.6-second scan period and specifies the spacecraft and Earth model to be used in the calculations. Input data to this routine includes an array of the 660 values of the detector unit pointing vectors in a scan period, time at the beginning of the scan, derived from the time stamp in the packet header, and an array of offset times which relate the radiance measurement times to the packet time.

The Pixel-FOV toolkit routine calculates values of longitude and geodetic latitude for each pointing vector that intersects the surface of the specified geometric model. It calculates values of longitude in a range from + π to - π and geodetic latitude in a range from + $\pi/2$ to - $\pi/2$. A toolkit coordinate transformation routine is used to convert values of geodetic latitude to geocentric latitude. Finally, values of geocentric longitude are converted to a range from 0 to 360 degrees and values of geocentric latitude

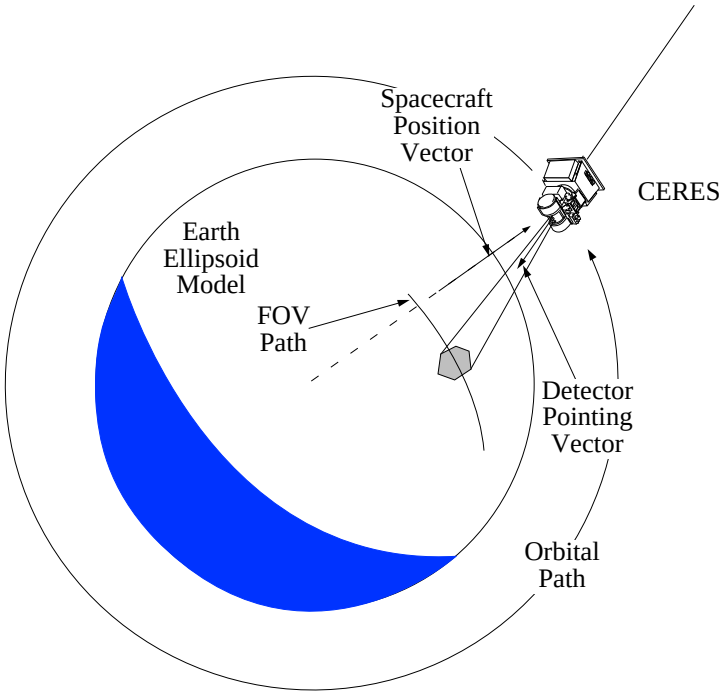

Figure 1-22. Geometry of the detector field-of-view and Earth ellipsoid intersection.

are converted to colatitude over a range of 0 to 180 degrees. These are the values of FOV longitude and colatitude that are output to the IES data product.

The CERES DMS makes maximum use of the ECS toolkit to calculate Earth-Sun-spacecraft parameters required as output data or to process science data. For example, toolkit routines are used to determine the position of the spacecraft and Sun in geocentric coordinates and to calculate zenith and azimuth angles measured from the radiance FOV locations to the spacecraft and the Sun. And finally, toolkit routines are used in all cases which require vector coordinate transformations.

1.8. Post Launch Calibration and Validation Data Quality Control Schemes

1.8.1. Monitoring Detector Housekeeping Parameters (Temperatures and Voltages)

Time histories of all flight housekeeping measurements in terms of minimum, mean, and maximum values will be graphically displayed daily.

1.8.2. Limit tests:

Flight edit routines will be used to justify/verify the set of converted data (detector housekeeping, attitude, spacecraft housekeeping, and radiometric). The tables for limits can be prepared accordingly.

1.8.3. Special Flight Algorithms

Will be used to detect possible abnormal space zero-radiance measurements.

1.8.4. Revision of Count Conversion Coefficients.

In the TRMM on-orbit activation plan, the sensor contamination doors will be closed during the first 30 days in orbit. During this period, the sensors will be calibrated every third day using the internal calibration module (ICM). On day 30 in orbit, the contamination doors will be opened. After the doors are

opened, the ICM and mirror attenuator mosaic (MAM) in-flight calibrations will be performed daily between day 30 and day 52 in orbit. After day 55, the calibrations will be conducted every 14 days. The EOS AM-1 and PM-1 on-orbit activation plans should closely follow the above-outlined TRMM plan.

For CERES total-wave, window, and shortwave sensors, the resulting time series plots will be analyzed to monitor the gain stability of these sensors (Lee *et al.* 1993b). In addition, the difference between the total-wave and longwave sensor nighttime radiance will be monitored on a daily basis to determine any drifts in the sensor coefficients.The sensors' flight gains and offsets will be evaluated using in-flight calibrations and validation studies. The preflight sensor gains and offsets will be used to initially convert the CERES sensor output signals into radiances. The in-flight calibrations will be used to detect drifts or abrupt shifts in the sensors' responses. Validation measurements of the Earth radiances will be used to verify sensor response changes, indicated by in-flight calibrations. The CERES science team will conduct detailed analyses of the first 6 months of in-flight calibrations and of the validations before the sensor gains or offsets are revised. Thereafter, the gains or offsets will be revised only if the sensors' responses degrade by more than 0.5 percent in the longwave region or 1 percent in the shortwave region.

1.8.5. Detector Zero-Radiance Offset Determinations

Flight sensor zero-radiance offset for all three sensors will be determined from observations of cold space [3K temperature radiance source], located between the Earth horizon and the spacecraft platform. In addition, preliminary offset variations with elevation angle will be determined in ground calibration facilities. In addition, in-flight, shortwave sensor offset variations will be determined from observations of the nighttime side of the Earth (shortwave sensors) and of cold space (all sensors). The nighttime Earth shortwave radiance is zero by definition. During each orbit, the nighttime Earth radiances for each shortwave sensor are used to define the sensor zero-radiance offsets as a function of elevation angle. During the next series of day side measurements, these offset determinations are used to adjust the cold space determined offsets as a function of elevation angle. In the case of the total-wave and window sensors, the variations of the offsets with elevation angle will be derived from measurements of space during the 180^{o} deep space spacecraft pitch/calibration attitude maneuver (CAM). For the Tropical Rainfall Measuring Mission (TRMM) spacecraft experiment, the CAM will be conducted on the 40th and 41st day after launch and thereafter annually. On each of these days, the CAM will be performed during 3 non-consecutive orbits. The frequency of each EOS platform CAM will be defined in the near future.

The TRMM CAM orbital geometry is illustrated in figure 1-23 where the spacecraft is placed in an inertially-fixed configuration in which the spacecraft Earth-nadir pointing axis is maintained 180 degrees away from the spacecraft-Sun direction. The CAM orbital geometry should permit [1] deep space to be observed for about 20 minutes; and [2] deep space to be observed at geometries in which Earth radiance measurements are conducted [in the hemisphere centered around the nominal spacecraft Nadir direction]. The TRMM CAM geometry provides the best thermal environment in which to determine zero-radiance sensor offsets. It should be noted that the moon cannot be used as a radiance target because the CERES radiometers' corresponding signals would be in the radiometers noise and close to the zero-radiance levels of the deep space.

The CERES instrument radiometric offsets, corresponding to a zero radiance source, are determined every 6.6 seconds measuring the radiances of cold space at viewing geometries between the spacecraft and the Earth's limb. These offsets are applied to Earth-viewing measurement geometries in which the radiances from the Earth can be sensed. For the typical Earth scene of 76 $Wm^{-2}sr^{-1}$, the level 1 instrument offsets may vary as much as 1% with measurement geometry. CAM radiometric observations of space will allow the uncertainty associated with the measurement geometry to decrease to 0.2%. There are no known engineering risks associated with CAM's. The CERES project and science team have considerable experience in applying CAM deep space radiometric measurements in the level 1 data processing algorithms.

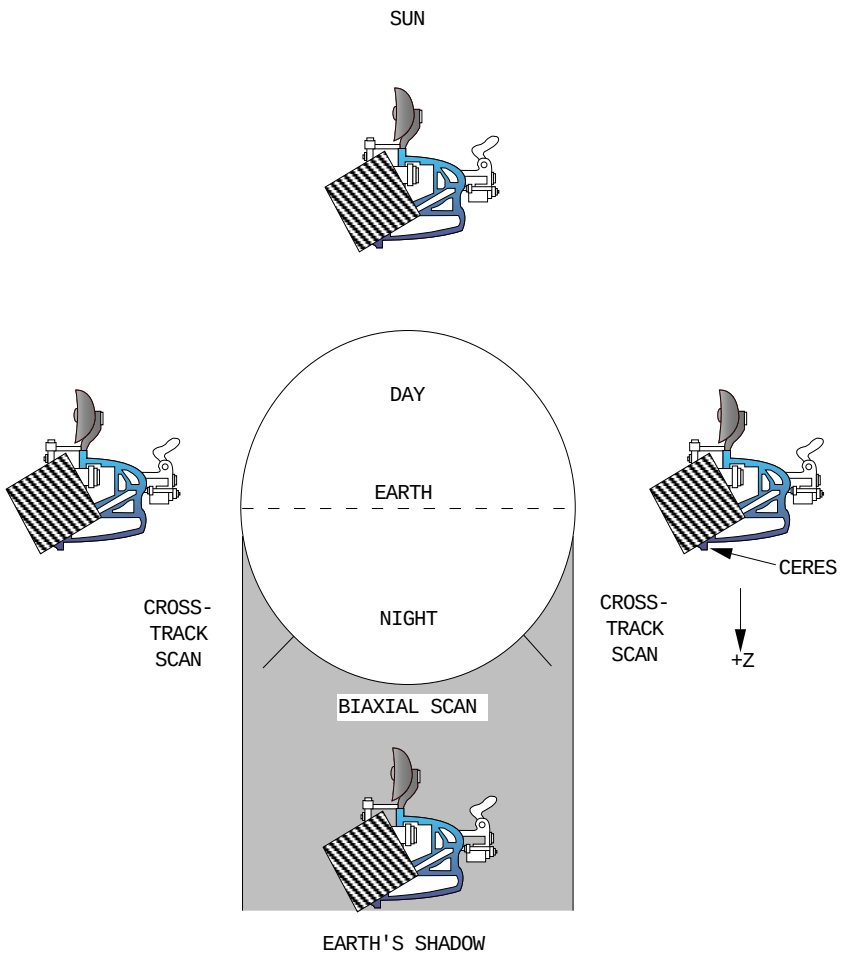

Figure 1-23. Orbital geometry for the determinations of CERES sensor zero-radiance offsets from the observation of cold space.

Basically, the sensors' measurements of cold space will be used to define the sensor flight zero-radiance offset. The nighttime Earth shortwave radiance is zero by definition. During each orbit, the nighttime Earth radiances for each shortwave sensor will be used to define the sensor zero-radiance offsets as a function of elevation angle. During the next series of day side measurements, these offset determinations will be used to adjust the cold space determined offsets as a function of elevation angle. In the case of the total-wave and window sensors, the variations of the offsets will be derived from measurements of space during the 180° deep space spacecraft pitch maneuver. The sensor offsets can also be determined from comparisons with different spacecraft calibrated/validation radiance measurements of the same geographical scenes using the techniques of Avis *et al.* (1994).

1.8.6. Geolocation and Validation Techniques

The TRMM and EOS sensor pointing requirements are presented in tables 1-2 and 1-3. Co-registration refers to pointing knowledge between the CERES sensor optical axis and the axes of visible and infrared imaging sensors such as the TRMM visible imaging radiometer sounder (VIRS) and EOS AM platform MODIS. The pointing knowledge for the CERES footprints will be checked using coastline crossings (Hoffmann *et al.* 1987). The crossings were used to verify the ERBE pointing knowledge with average geographical local errors less than 6.1 km from the Earth Radiation Budget Satellite orbital altitude of 610 km.

The geolocation process uses spacecraft ephemeris and attitude, Earth rotation and geoid, and instrument pointing data to calculate the latitude and longitude of the measurement location with estimated errors of the order of 1 km at nadir. A heuristic description of the process is given by Lee *et al. (1996b)*. The actual procedures used to implement the geolocation process are provided by the Earth observing system data and information system (EOSDIS) core system project in the science data production toolkit. The use of the science data production toolkit for geolocation is mandatory for EOS instruments. This mandate should eliminate some potential problems associated with correlation of satellite data from different instruments on EOS platforms.

Co-registration refers to pointing knowledge between the CERES sensor optical axis and the axes of visible and infrared imaging sensors such as the TRMM visible imaging radiometer sounder (VIRS) and EOS AM platform Moderate-Resolution Imaging spectrometer (MODIS). The pointing knowledge for the CERES footprints will be checked using coastline crossings.

End-to-end validation and accuracy assessment techniques for the geolocation process require detection and geolocation of independently geolocated Earth features for comparison. For CERES, as with its predecessor ERBE, a technique for detecting coastlines under certain conditions and comparing their geolocated position with coastline maps will be used. At night, using longwave radiance measurements, the coastline crossings were used to verify the ERBE pointing knowledge with average geographical local errors less than 6 km from the Earth Radiation Budget Satellite (ERBS) orbital altitude of 610 km. A brief overview of the CERES geolocation validation technique follows.

The ERBE longwave channel displayed a characteristic signature when the detector scanned certain high thermal contrast scenes such as desert adjacent to ocean. For a typical desert/ocean coastline, the ocean maintains a relatively constant diurnal temperature, the desert temperature fluctuates resulting in a diurnal reversal in the slope of the coastline signature. A set of threshold values based on empirical data were applied to the absolute signal levels to filter out cloudy scenes. To limit the amount of data searched, only data predicted to be within 25 km of the coastline was used. A cubic equation was found to fit the signature well and the inflection point was assumed to represent the exact location of the coastline. The latitude and longitude of the inflection point was determined by interpolating from the adjacent measurements. In figure 1-24, an example, in ERBE geolocation studies, is the coastline of Baja, California [22 - 32 North latitude, 243-252 East longitude] where coastline are measured radiometrically and compared to the geolocated map. In the studies, the coastlines of, Australia [16-22 South latitude, 115-124 East longitude], Libya [30-33 North latitude, 14-23 east longitude], and the Arabian Peninsula 16-24 North latitude, 52-61 East longitude] were used as validation targets, as well as the Baja coastline.

After the latitude and longitude errors are determined by comparison with the coastline map, the errors were transformed into cross track and along track errors for correlation with possible error sources. Additive cross-track and along-track bias parameters were introduced and adjusted to minimize the squared error. The bias parameters were determined for all cloud free coastlines under consideration over an extended time and displayed on a scatterplot to determine long term along-track and cross-track biases.

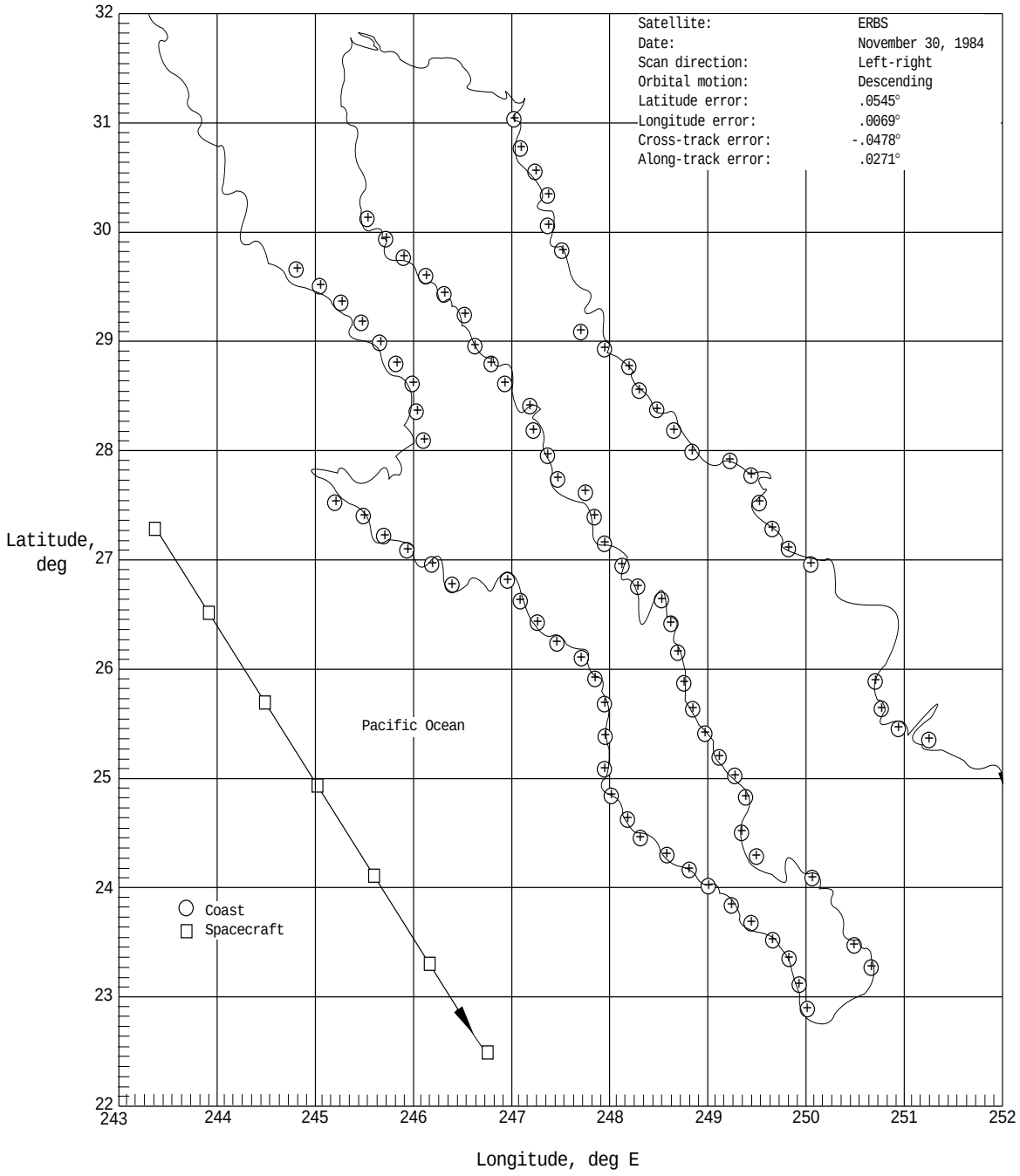

Figure 1-24. Plot of the Baja, California coastline overlaid with measured locations of detected coastlines. The Earth Radiation Budget Satellite (ERBS) spacecraft sub-satellite point is also indicated in the lower left portion of the plot.

Two conclusions drawn from coastline validation analysis for ERBE are that the geolocation process used was sufficiently accurate to accomplish the ERBE mission science objectives and that the coastlinedetection technique was sufficient for validating the geolocation process and evaluating long term end-to-end cross-track and along-track biases.

Enhancing the coastline detection technique for validating CERES geolocation processing will involve a few modifications to existing ERBE algorithms with potential for improvement. Most of the improvements are expected to be derived from utilization of CERES data products and SDP Toolkit routines that were not available during the ERBE mission, and bi-directional instrument scanning. For the ERBE geolocation analyses, the shortwave channel was not used for coastline validation since it is sensitive to large variations due to clouds and was not useful at night. By analyzing VIRS and MODIS imager data, the CERES Science Team will determine the presence or absence of clouds in the field of view of the CERES detectors. This determination for all footprints is called a cloud mask. The cloud mask will be used to insure that a chosen coastline is cloud free so coastline analysis can be performed. The ability to filter out cloudy scenes from consideration may also allow use of the shortwave channel on appropriate daytime scenes.

The viewing angles for the ERBE coastline detection processing were limited to 30 degrees from nadir to reduce the effect of atmospheric refraction. The SDP toolkit allows the use of an atmospheric refraction model so these effects can be easily accounted for resulting in both increased accuracy and range over which coastline data can be analyzed.

Since the CERES instrument performs a bidirectional scan there will be an opportunity to assess biases inherent in the technique due to scan direction, i.e. scanning from ocean to desert vs. desert to ocean. The instrument also uses a biaxial scanning mode to acquire data for deriving angular direction models. Data obtained in the biaxial mode will scan a coastline from many different directions during a single pass. Data of this type may further enhance the potential for recovering biases due to scan direction or allow refinement of the cubic model used to define the detected coastline point.

1.8.7. Consistency Checks Among CERES Sensors and other Spacecraft Sensors

1.8.7.1. Intercomparison Consistency Checks Among CERES Sensors On Single Spacecraft. The single spacecraft sensor consistency checks involve intercomparisons of (1) the three sensors' filtered Earth radiance measurements in the same instrument package (TRMM and EOS platforms) and of (2) the filtered Earth radiance output signals from the same type of sensor in two difference instrument packages (EOS platform). Differences in the Earth radiance measurements will define the level of consistency.

The first intercomparison check was used in evaluating the consistency of the three Earth Radiation Budget Satellite (ERBS) scanning thermistor bolometer sensors. The evaluation approach is described by Green and Avis (1996) and it is insensitive to the anisotropy of the target radiation field. For a particular geophysical scene like a desert, ocean, land, overcast cloud scene, etc., or the combination of all the scenes, the ratios of any two sensor outputs should be constant with time if the sensors' responses do not drift or shift. If changes in the ratios are observed, then, more detailed reviews of the calibration time series should be evaluated to determine the size and direction of possible response drifts or shifts in one or both of the ratioed sensors. In the consistency check, the ratios of sensor outputs will be monitored for all scenes. If changes in the ratios occur, then ratios will be collected and evaluated for different spectral scenes (overcast clouds, oceans, deserts, land, etc.) into to determine the spectral nature of the sensor changes.

In the second consistency check, on each EOS platforms, the stabilities of the same type of sensors can be evaluated. Operating both EOS instruments in the cross-track scan mode, many intercomparisons of the two shortwave, or total-wave, or window sensors Earth radiance measurements from the same geographical scene can be obtained. If both instruments are scanning in phase within + 0.1 second, 2 pairs of intercomparison radiance measurements for each type of sensor and for every scan elevation position will be obtained every 6.6-second scan. Operating one

instrument package in the cross-track scan mode and the other instrument in the rotating azimuth plane scan mode, 2 intercomparison radiance measurements from large (100 km) uniform scenes can be obtained at the nadir during a 6.6-second scan. At non-nadir elevation scan angles, the radiance Intercomparison cannot be conducted at the radiance level because the emitted and reflected Earth radiation fields vary with the azimuth elevation angles. For the non-nadir elevation angles, intercomparisons will not be conducted because angular distribution models[15] are required to account for the anisotropy of the target radiation fields and to convert the Earth radiances into unfiltered Earth irradiances.

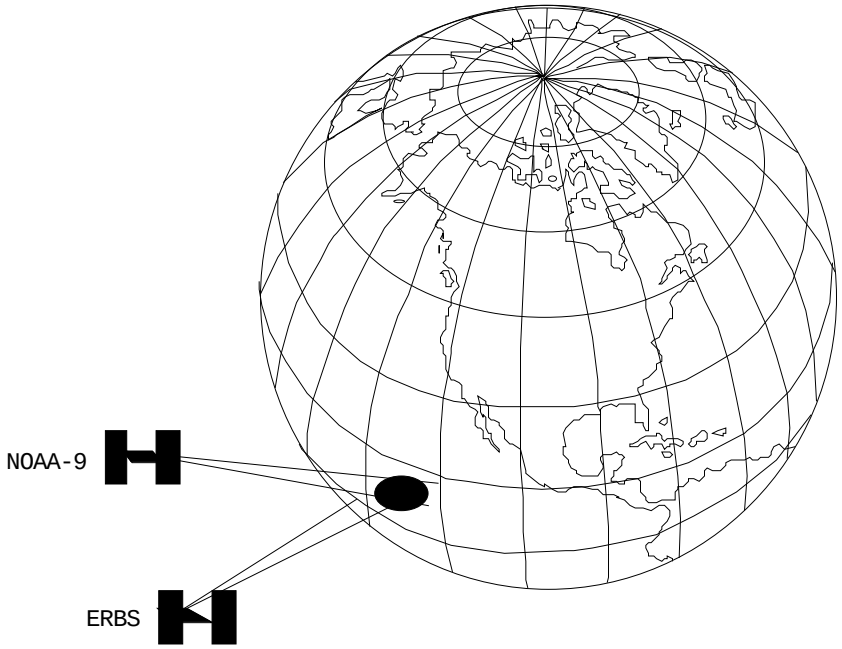

Figure 1-25. Geometry of Intercomparisons of similar sensors on multi-spacecraft platforms or with other sensors on different platform.

1.8.7.2. Multi-spacecraft Consistency Checks. Using multi-spacecraft platform CERES instruments (TRMM and EOS AM-1, or TRMM and EOS PM-1, or EOS AM-1 and EOS PM-1), filtered radiance products will be compared for the same type of sensor (shortwave, or total-wave, or window) in order to determine the consistencies among data products from the different CERES instrument packages. At least four times a day, at the intersection point between the two spacecraft ground tracks, the sensors from both platforms should measure nadir Earth radiances from the intersection point within 30 minutes (Bolden et al. 1993). In figure 1-25, the intersection point measurements from two different spacecraft platforms are illustrated. Two intersection points are night and the other two occur during the day. Since radiances are independent of the detector solid angle, then, the measurements from the two different platforms can be compared without correcting for the differences in attitude. For instrument level 1 validations, comparisons of radiance products at non-nadir scan elevation angles will not be performed because angular distribution models are required to account for the anisotropy in the Earth emitted and reflected radiation fields.

1.8.7.3.Consistency Checks Between CERES Sensors And Other Sensors. Since 1984, the ERBS spacecraft wide and medium fields of view radiometers measured broadband shortwave and longwave

irradiances. The ERBS radiometers are expected to be operational during the early lifetimes of the TRMM and EOS AM-1 missions. Therefore, Intercomparison between the global ERBS and CERES shortwave and longwave irradiances should link the CERES absolute radiometric scale to the ERBS scale. In addition, during the overlap period between the ERBS and CERES measurements, the intercomparisons should enable the detection of shifts or drifts in the CERES sensor responses using the stable ERBS irradiances as references. CERES spacecraft longwave Earth-emitted irradiances can be used to infer atmospheric temperatures (Cess 1990, Auer and Kao 1991) using the Stefan-Boltzman relationship. Therefore, intercomparisons among the broadband irradiances, global surface air station temperature, and NOAA spacecraft microwave sounding unit (MSU) mid-troposphere and lower stratosphere temperature soundings can be used [as a consistency check] to detect shifts or drifts in the CERES sensors.

1.9. Output Data

There are two output data products, the bidirectional scans (BDS) and the instrument Earth scan (IES). Appendix B lists these output products. Each BDS product is a time-ordered 24-hour bidirectional scan data product that is used in the production of the ERBE like products. The BDS product contains both the raw and converted values of radiometric, engineering, digital status, and location data. The IES product consists of 1-hour data of spatially organized footprints that are sent to the cloud subsystem. The IES products contain only the converted filtered radiance for the three channels with each footprint location data, along with associated viewing geometries and quality flags.

1.10. References

Astheimer, R. W. 1983: Thermistor Infrared Detectors. *Infrared Detectors: Proceedings of SPIE,* William L. Wolfe, ed., vol. 443, SPIE, pp. 95–109.

Avis, L. M.; Paden, J.; Lee, R. B. III; Pandey, D. K.; Stassi, J. C.; Wilson, R. S.; Tolson, C. J.; and Bolden, W. C. 1994: NOAA-9 Earth Radiation Budget Experiment (ERBE) Scanner Offsets Determination. NASA TM 109086.

Auer, L. H. and Kao, C. J. 1991: Further analysis of the global outgoing radiative flux observed by Nimbus, *J. Geophysical Research*, vol. 96, pp. 17,367-17,370.

Barkstrom, Bruce R. 1990: Earth Radiation Budget Measurements—Pre-ERBE, ERBE, and CERES. *Proc. of SPIE*, vol. 1299, pp. 52–60.

Barkstrom, Bruce R.; Harrison, Edwin F.; and Lee, Robert, B., III 1990: Earth Radiation Budget Experiment—Preliminary Seasonal Results. *EOS*, vol. 71, p. 297 and 304.

Bolden, W. C.; Lee III, R. B.; Paden, J.; Pandey, D. K.; and Wilson, R. S., 1993: A Validation Tool for the Earth Radiation Budget Experiment (ERBE) Nonscanner Data Product, *Proc. of SPIE*, vol. 1938, pp. 23-32.

Carman, Stephen L. 1983: Deep Concentric Grooves Enhance Blackbody Spectral and Spatial Uniformity. *Applications of Optical Metrology: Techniques and Measurements II—Proc. of SPIE,* John J. Lee, Jr., ed., vol. 416, pp. 178–186.

Cess, R. D., 1990: Interpretation of an 8-year record of Nimbus 7 wide-field-of-view infrared measurements, *J. Geophysical Research*, vol. 95, pp. 16,655-16,657.

Folkman, Mark A.; Jarecke, Peter J.; and Darnton, Lane A. 1991: Enhancements to the Radiometric Calibration Facility for the Clouds and the Earth's Radiant Energy System (CERES) Instruments. *Calibration of Passive Remote Observing Optical and Microwave Instrumentation—Proc. of SPIE,* Bruce W. Guenther, ed., SPIE, vol. 1493, pp. 255–266.

Folkman, Mark A.; Jarecke, Peter J.; Hedman, Ted R.; Yun, John S.; and Lee, Robert B., III 1993: Design of a Solar Diffuser for On-Orbit Calibration of the Clouds and the Earth's Radiant Energy System (CERES) Instruments. *Sensor Systems for the Early Earth Observing System Platforms—Proc. of SPIE*, William E. Barnes, ed., SPIE, vol. 1939, pp. 72–81.

Folkman, Mark; Jarecke, Peter; Hedman, Ted; Carman, Steve; Avis, Lee; Barkstrom, Bruce; Cooper, Jack; Kopia Leonard; Lawrence, Wes; Lee, Robert; and Smith, Lou 1994: Calibration of a Shortwave Reference Standard by Transfer From a Blackbody Standard Using a Cryogenic Active Cavity Radiometer. *IGRASS '94—Surface and Atmospheric Remote Sensing: Technologies, Data Analysis and Interpretation*, Volume IV, IEEE, pp. 2298–2300.

Foukal, Peter V.; Hoyt, C.; Kochling, H.; and Miller, P. 1990: Cryogenic Absolute Radiometers as Laboratory Irradiance Standards. *Remote Sens. Detect., & Pyrheliometers. Appl. Opt.*, vol. 29, pp. 988–993.

Frink, M. E.; Jarecke, P. J.; Folkman, M. A.; and Wright, R. E. 1993: Far-IR Spectral Measurements of the Clouds and the Earth's Radiant Energy System (CERES) Sensors Using a Fourier Transform Spectrometer and Pyro-Electric Reference Detector. *Sensor Systems for the Early Earth Observing System Platforms—Proc. of SPIE*, William E. Barnes, ed., SPIE, vol. 1939, pp. 82–91.

Gibson, Michael A.; Lee, Robert B., III; and Thomas, Susan 1992: Evaluation of the Earth Radiation Budget Experiment Shortwave Channel's Stability Using In-Flight Calibration Sources. *Instrumentation for Planetary and Terrestrial Atmospheric Remot*e, *Proc. of SPIE*, vol. 1745, pp. 108–216.

Green, R. N. and Avis, L. M. 1996: Validation of ERBS scanner radiances, *J. Atmospheric and Ocean Technology*, vol. 13, pp. 851-862.

Halyo, Nesim; Choi, Dan A., Jr.; and Samms, Richard W. 1987: *Development of Response Models for the Earth Radiation Budget Experiment (ERBE) Sensors. I—Dynamic Models and Computer Simulations for the ERBE Nonscanner, Scanner and Solar Monitor Sensors*. NASA CR-178292.

Halyo, Nesim; Pandey, Dhirendra K.; and Taylor, Deborah B. 1989: *Modeling and Characterization of the Earth Radiation Budget Experiment (ERBE) Nonscanner and Scanner Sensors*. NASA CR-181818.

Hesser, R. J.; and Carman, S. L. 1983: Integrating Sphere as a Precision Radiometer Calibration Source. *Proc. of SPIE*, vol. 416, pp. 111–118.

Hoffman, Lawrence H.; Weaver, William L.; and Kibler, James F. 1987: *Calculation and Accuracy of ERBE Scanner Measurement Locations*. NASA TP-2670.

Jarecke, P. J.; Folkman, M. A.; and Darnton, L. A. 1991: Radiometric Calibration Plan for the Clouds and the Earth's Radiant Energy System (CERES) Scanning Instruments. *Calibration of Passive Remote Observing Optical and Microwave Instrumentation—Proc. of SPIE*, Bruce W. Guenther, ed., vol. 1493, pp. 244–254.

Jarecke, P. J.; Folkman, M. A.; and Hedman, T. R. 1993: Clouds and the Earth's Radiant Energy System (CERES): Long-Wave Calibration Plan and Radiometric Test Model (RTM) Calibration Results. *Metrologia*., vol. 30, no. 4, p. 223.

Jarecke, Peter; Frink, Mark; Folkman, Mark; Carman, Steve; Baliga, Shankar; Doctor, Alan; Avis, Lee; Barkstrom, Bruce; Cooper, Jack; Kopia, Leonard; Lawrence, Wes; Lee, Robert; and Smith, Lou: End-to-End Spectral Response Characterization of the Clouds and the Earth's Radiant Energy System Sensors From 0.3 to 200 Microns. *IGRASS '94—Surface and Atmospheric Remote Sensing: Technologies, Data Analysis and Interpretation*, Volume IV, IEEE, pp. 2007–2009.

Kopia, Leonard P.; and Lee, Robert B., III 1992: Thermistor Bolometer Scanning Radiometer—Applications and Flight Experience. *Opt. Eng*., vol. 31, pp. 156–165.

Kyle, H. L. 1993: The Nimbus Earth Radiation Budget (ERB) Experiment—1975 to 1992. *Bull. Am. Meteorol. Soc.*, vol. 74, no. 5, p. 815.

Kyle, H. L.; Hickey, J. R.; Ardanuy, P. E.; Jacobowitz, H.; Arking, A.; Cambell, G. G.; House, F. B.; Maschhoff, R.; Smith, G. L.; Stowe, L. L.; and Vonder Haar, T. 1933: The Nimbus Earth Radiation Budget (ERB) Experiment: 1975 to 1992. *Bull. American Meteorol. Soc*., vol. 74, pp. 815–830/

Lee, Robert B., III; Barkstrom, Bruce R.; Avis, Lee M.; Halyo, Nesim; and Gibson, Michael A. 1989: Characterization of the Earth Radiation Budget Experiment (ERBE) Scanning Radiometers. *Proc of SPIE*, vol. 1109, pp. 186–194.

Lee, Robert B., III; Gibson, M. A.; Thomas, Susan; Meekins, Jeffrey L.; and Mahan, J. R. 1990: Earth Radiation Budget Experiment Scanner Radiometric Calibration Results. *Proc. of SPIE*, vol. 1299, pp. 80–91.

Lee, R. B., III; and Barkstrom, B. R. 1991: Characterization of the Earth Radiation Budget Experiment Radiometers. *Metrologia*, vol. 28, p. 183–187.

Lee, Robert B.; Avis, Lee M.; Gibson, M. Alan; and Kopia, Leonard P. 1992: Characterization of the Mirror Attenuator Mosaic: Solar Diffuser Plate. *Appl. Opt*., vol. 31, no. 31, pp. 6643–6652.

Lee, Robert B., III; Barkstrom, Bruce R.; Carman, Steve L.; Cooper, John E.; Folkman, Mark A.; Jarecke, Peter J.; Kopia, Leonard P.; and Wielicki, Bruce A. 1993a: *Sensor Systems for the Early Earth Observing System Platforms—Proc. of SPIE,* William E. Barnes, ed., SPIE, vol. 1939, pp. 61–71.

Lee, R. B., III; Avis, L. M.; and Gibson, M. A. 1993b: In-Flight Evaluations of Tungsten Calibration Lamps Using Shortwave Thermistor Bolometers and Active-Cavity. *Metrologia*., vol. 30, no. 4, p. 389.

Lee, R. B., III; Barkstrom, B. R.; Smith, G. L.; Cooper, J. E.; Kopia, L. P.; Lawrence, R. W.; Folkman, M. A.; Jarecke, P. J.; Thomas, S.; Pandey, D. K.; Gibson, M. A.; Degnan, K. T.; Weaver, W. L.; and Crommelynck, D. A. H. 1996a: The Clouds and the Earth's Radiant Energy System (CERES) Sensors and Preflight Calibration Plans, *J. Atmos. & Ocean. Technol*., vol. 13, pp. 300-313.

Lee, R. B., III; Childers, B. A.; Smith, G. L.; Paden, J.: Pandey, D. K.; and Thomas, S. 1996b: Clouds and the Earth's Radiant Energy System (CERES) Instrument Level 1 Science Data Validation Plan for Geolocated Radiances. *Proc. of SPIE*, vol. 2820, pp. 105-116.

Lee, R. B., III; Smith, G. L.; Barkstrom, B. A.; Priestley, K. J.; Thomas, S.; Paden, J.; Pandey, D. K.; Thornhill, K. L.; Bolden, W. C.; and Wilson, R. S., 1997: Ground calibrations of the Clouds and the Earth's Radiant Energy System (CERES) Tropical Rainfall Measuring Mission spacecraft thermistor bolometers, *Proc. of SPIE*, vol. 3117 (presented as paper 3117-37, San Diego, CA).

Paden, Jack; Smith, G. Louis; Lee, III, R. B.; Pandey, D. K.; and Thomas, Susan: Reality check: a point response function (PRF) comparison of theory to measurements for the Clouds and the Earth's Radiant energy System (CERES) Tropical Rainfall Mission (TRMM) instrument, *Proc. of SPIE*, vol. 3074 (presented as paper 3074-15, Orlando, Florida).

Ramanathan, V.; Barkstrom, Bruce R.; and Harrison, Edwin F. 1989: Climate and the Earth's Radiation Budget. *Phys. Today*, vol. 42, pp. 22–32.

Smith, G. L.; Green, R. N.; Raschke, E; Avis, L. M.; Suttle, J. T.; Wielicki, B. A.; and Davies, R.; 1986: Inversion methods for satellite studies of the earth's radiation budget: Development of algorithms for the ERBE mission, *Rev. Geophys.*, vol. **24**, pp. 407-42.

Smith, G. Louis 1994: Effects of Time Response on the Point Spread Function of a Scanning Radiometer. *Appl. Opt.*, vol. 33, no. 30, p. 7031.

Siegel, Robert; and Howell, John R. 1981: *Thermal Radiation Heat Transfer.* Hemisphere Publ., Corp and McGraw-Hill Book Company.

Wielicki, Bruce A.; and Barkstrom, Bruce R. 1991: Clouds and the Earth's Radiant Energy System (CERES)—An Earth Observing System Experiment. *Second Symposium on Global Change Studies×—Preprints*, Am. Meteorol. Soc., pp. 11–16.

Wielicki, Bruce A.; Barkstrom, B. R.: Harrison, E. F.; Lee, R. B.,III; Smith, G. L.; and Cooper, J. E. 1996: Clouds and the Earth's Radiant Energy System (CERES): An Earth Observing System Experiment. *Bulletin of American Meteorological Society*, vol. 77, 853-868.

Appendix A

Input Data Products

Geolocate and Calibrate Earth Radiances (Subsystem 1)

This appendix describes the data products which are used by the algorithms in this subsystem. The table below summarizes these products, listing the CERES and EOSDIS product codes or abbreviations, a short product name, the product type, the production frequency, and volume estimates for each individual product as well as a complete data month of production. The product types are defined as follows:

Archival products:	Assumed to be permanently stored by EOSDIS
Internal products:	Temporary storage by EOSDIS (days to years)
Ancillary products:	Non-CERES data needed to interpret measurements

The following pages describe each product. An introductory page provides an overall description of the product and specifies the temporal and spatial coverage. The table which follows the introductory page briefly describes every parameter contained in each product. Each product may be thought of as metadata followed by data records. The metadata (or header data) is not well-defined yet and is included mainly as a placeholder. The description of parameters which are present in each data record includes parameter number (a unique number for each distinct parameter), units, dynamic range, the number of elements per record, an estimate of the number of bits required to represent each parameter, and an element number (a unique number for each instance of every parameter). A summary at the bottom of each table shows the current estimated sizes of metadata, each data record, and the total data product. A more detailed description of each data product will be contained in a User's Guide to be published before the first CERES launch.

Table A-1. Input Products Summary

Product Code		Name	Type	Frequency	Size, MB	Monthly Size, MB
CERES	EOSDIS					
INSTR_PDS	CERX00a	Instrument Production Data Set	Archival	1/Day	93.4	2895.4

Instrument Production Data Set (INSTR_PDS)

The Instrument Production Data Set (INSTR_PDS) is the level 0 raw data from the CERES instrument as structured by the instrument itself, and is programmed by the instrument developer, TRW. All CERES instrument output is formatted into a CCSDS packet. CERES instrument packets contain the same data output formatting options, although some instrument data packets contain data unique to a particular spacecraft. There are seven basic pieces of information contained in a normal CERES data packet (i.e., science output format) are:

1. Packet Header - Same format for all instruments
2. Time (secondary header) - formats specified by platform's selected CCSDS option
3. Radiometric Detector Outputs
4. Instrument Elevation and Azimuth Position Data
5. Instrument Analog Engineering Data (e.g., Temperatures and Voltages)
6. Instrument Digital Engineering Data

There are five types of packets currently defined for the CERES instrument - Science, Diagnostic Memory, Diagnostic Processor, Diagnostic Gimbal, and Diagnostic Fixed Pattern. Each of these packet types correspond to a particular operation of the CERES instrument. Differences in packet content for each of these five types are defined in Table A-2.

For processing purposes, packets are grouped into Level 0 files which typically represent data collected from the CERES instrument over a 24 hour period. The types of Level 0 file formats for the Instrument Production Data Set are illustrated in Figure A-1.

Level: 0
Type: Archival
Frequency: 1/Day

Portion of Globe Covered
File: Satellite Swath
Record: N/A

Time Interval Covered
File: 1 Day
Record: Single 6.6 sec scans

Portion of Atmosphere Covered
File: N/A

Level 0 File Definitions

TRMM Level 0 File

File Header (48 to 52 Bytes)
Instrument Data Packets (Number of Packets x 7132 Bytes)
File Footer (QAC) (Total = Length of QAC Footer (4) +[Number of Entries x 5] Bytes)
File Footer (MDUL) (Total = Length of MDUL Footer (4) + [Number of Entries x 5] Bytes)

(Minimum number of QAC entries is always = 1)

QAC - List of packet IDs known to be corrupted or unusable;
MDUL - List of packet IDs missing;

EOS Level 0 File

File Header (TBD Bytes)
Instrument Data Packets (Number of Packets x TBD Bytes)

Figure A-1. TRMM and EOS level 0 file formats.

Table A-2. Instrument Production Data Set (INSTR_PDS)

Description	Parameter Number	Units	Range	Elements/ Record	Bits/ Elem	Elem Num
INSTR_PDS						
INSTR_PDS File Header (TRMM)						
Spacecraft ID		N/A	N/A	1	16	
Spacecraft Clock (first packet)		N/A	N/A	1	72	
Spare		N/A	N/A	1	8	
Spacecraft Clock (last packet)		N/A	N/A	1	72	
Spare		N/A	N/A	1	8	
Number of Packets in file		N/A	N/A	1	32	
Processing Options		N/A	N/A	1	8	
Data Type Flag		N/A	N/A	1	8	
Time of Receipt at Originating Node		N/A	N/A	1	56	
Spare		N/A	N/A	1	24	
Select Options		N/A	N/A	1	8	
Number of APIDs		N/A	N/A	1	8	
APIDs		N/A	N/A	1 to 3	16	
Spare		N/A	N/A	1	8	
Number of QAC lists in file		N/A	N/A	1	8	
Offset to QAC List		N/A	N/A	1	32	
INSTR_PDS File Header (EOS)		N/A	N/A		TBD	
Contents TBD						
INSTR_PDS Data is Array[13091] of:						
INSTR_PDS_Data_Packet						
INSTR_PDS_Data_Packet_Header is selection of						
INSTR_Packet_Hdr (TRMM)						
INSTR_Packet_Header_Data						
Version Number	1	N/A	N/A	1	3	1
Type	2	N/A	N/A	1	1	2
Secondary Header Flag	3	N/A	N/A	1	1	3
APID	4	N/A	N/A	1	11	4
Sequence Flags	5	N/A	N/A	1	2	5
Packet Sequence Count	6	N/A	N/A	1	14	6
Packet Length	7	N/A	N/A	1	16	7
INSTR_Packet_Secondary_Hdr (TRMM)						
Time Data	8	N/A	N/A	1	64	8
INSTR_Packet_Hdr (EOS)						
INSTR_Packet_Header_Data						
Version Number	1	N/A	N/A	1	3	1
Type	2	N/A	N/A	1	1	2
Secondary Header Flag	3	N/A	N/A	1	1	3
APID	4	N/A	N/A	1	11	4
Segment Flags	5	N/A	N/A	1	2	5
Source Sequence Count	6	N/A	N/A	1	14	6
Packet Length	7	N/A	N/A	1	16	7
EOS_Secondary_Hdr (EOS)						
Time Data	9	N/A	N/A	1	72	8
Quick Look Flag	10	N/A	N/A	1	8	9

Table A-2. Continued

Description	Parameter Number	Units	Range	Elements/ Record	Bits/ Elem	Elem Num
INSTR_Measurement_Data is selection of						
INSTR_Science_Data is Array[660] of:						
INSTR_Science_Record						
Azimuth Position Count	11	count	0.65535	660	16	13
Elevation Position Count	12	count	0.65535	660	16	673
Total Detector Output	13	count	0.4095	660	12	1333
SW Detector Output	14	count	0.4095	660	12	1993
Window Detector Output	15	count	0.4095	660	12	2653
Instrument Analog Data - see DRL64, Rev. D (TRW) for details	16	-	-	660	12	3313
INSTR_Diagnostic_Memory_Data is Array[660] of:						
INSTR_Memory_Record						
Azimuth Position Count	17	count	0.65535	660	16	3973
Elevation Position Count	18	count	0.65535	660	16	4633
DAP Memory Dump Data	19	N/A	0.65535	660	16	5293
ICP Memory Dump Data	20	N/A	0.65535	660	16	5953
Fill Data	21	N/A	0.15	660	4	6613
Instrument Analog Data - see DRL64, Rev. D (TRW) for details	22	-	-	660	12	7273
INSTR_Diagnostic_Gimbal_Operation_Data is Array[660] of:						
INSTR_Gimbal_Record						
Azimuth Position Count	23	count	0.65535	660	16	7933
Elevation Position Count	24	count	0.65535	660	16	8593
Elevation Error	25	count	0.55535	660	16	9253
Azimuth Error	26	count	0.65535	660	16	9913
Fill Data	27	N/A	0.15	660	4	10573
Instrument Analog Data - see DRL64, Rev. D (TRW) for details	28	-	-	660	12	11233
INSTR_Diagnostic_Processor_Operation_Data is Array[660] of:						
INSTR_Processor_Op_Record						
Azimuth Position Count	29	count	0.65535	660	16	11893
Elevation Position Count	30	count	0.65535	660	16	12553
DAP Timing	31	N/A	0.65535	660	16	13213
ICP Timing	32	N/A	0.65535	660	16	13873
Fill Data	33	N/A	0.15	660	4	14533
Instrument Analog Data - see DRL64, Rev. D (TRW) for details	34	-	-	660	12	15193
INSTR_Diagnostic_Fixed_Pattern_Data is Array[660] of:						
INSTR_Fixed_Record						
Fixed Pattern in Elevation Field	35	N/A	0.65535	660	16	15853
Fixed Pattern for Azimuth Field	36	N/A	0.65535	660	16	16513
Fixed Pattern for Total Channel Field	37	N/A	0.4095	660	12	17173
Fixed Pattern for Window Channel Field	38	N/A	0.4095	660	12	17833
Fixed Pattern for Shortwave Channel Field	39	N/A	0.4095	660	12	18493
Fixed Pattern for Analog Field	40	N/A	0.4095	660	12	19153
INSTR_Data						
INSTR_Digital_Status_Block is						
Instrument Digital Status - see DRL64, Rev D. (TRW) for details	41	-	-	1	2960	10
INSTR-EOS_Ancillary_Data is selection of						
INSTR_Ancillary_Data						
Ancillary Time Stamp	42	count	$0.1.84 \times 10^{19}$	1	64	19813
GPS/UTC Time Conversion	43	count	$0.4.29 \times 10^{9}$	1	32	19814

Table A-2. Concluded

Description	Parameter Number	Units	Range	Elements/ Record	Bits/ Elem	Elem Num
Solar Array Current	44	count	0.255	1	8	19815
Mag Coil Current X	45	count	0.255	1	8	19816
Mag Coil Current Y	46	count	0.255	1	8	19817
Mag Coil Current Z	47	count	0.255	1	8	19818
Satellite Position (X) Count	48	count	$0.4.29x10^9$	1	32	19819
Satellite Position (Y) Count	49	count	$0.4.29x10^9$	1	32	19820
Satellite Position (Z) Count	50	count	$0.4.29x10^9$	1	32	19821
Satellite Velocity (X) Count	51	count	$0.4.29x10^9$	1	32	19822
Satellite Velocity (Y) Count	52	count	$0.4.29x10^9$	1	32	19823
Satellite Velocity (Z) Count	53	count	$0.4.29x10^9$	1	32	19824
Satellite Attitude (Roll) Count	54	count	0.65535	1	16	19825
Satellite Attitude (Pitch) Count	55	count	0.65535	1	16	19826
Satellite Attitude (Yaw) Count	56	count	0.65535	1	16	19827
Satellite Attitude Rate (Roll) Count	57	count	0.65535	1	16	19828
Satellite Attitude Rate (Pitch) Count	58	count	0.65535	1	16	19829
Satellite Attitude Rate (Yaw) Count	59	count	0.65535	1	16	19830
Solar X Position	60	count	0.255	1	8	19831
Solar Y Position	61	count	0.255	1	8	19832
Solar Z Position	62	count	0.255	1	8	19833
Lunar X Position	63	count	0.255	1	8	19834
Lunar Y Position	64	count	0.255	1	8	19835
Lunar Z Position	65	count	0.255	1	8	19836
INSTR_Fill_Data						
TRMM	66	N/A	N/A	1	1104	19837
EOS	67	N/A	N/A	1	592	19838
INSTR_PDS File Footer (TRMM Only)						
INSTR_PDS_File_Footer is						
QAC List	N/A	N/A	N/A	1	32	1
QAC Entries	N/A	N/A	N/A	1 - q	16	2
MDUL	N/A	N/A	N/A	1	32	3
MDU	N/A	N/A	N/A	1 - m	16	4
Total Header Bits/File:	384..416					
Total Data Bits/Record:	57056					
Total Records/File:	13091					
Total Data Bits/File:	746920096					
Total Bits/File:	746920480.746920512	+ File Footer Size (TRMM Only)				

Appendix B - Output Data Products

Output Data Products

Geolocate and Calibrate Earth Radiances (Subsystem 1)

This appendix describes the data products which are produced by the algorithms in this subsystem. The table below summarizes these products, listing the CERES and EOSDIS product codes or abbreviations, a short product name, the product type, the production frequency, and volume estimates for each individual product as well as a complete data month of production. The product types are defined as follows:

Archival products:	Assumed to be permanently stored by EOSDIS
Internal products:	Temporary storage by EOSDIS (days to years)

The following pages describe each product. An introductory page provides an overall description of the product and specifies the temporal and spatial coverage. The table which follows the introductory page briefly describes every parameter which is contained in the product. Each product may be thought of as metadata followed by data records. The metadata (or header data) is not well-defined yet and is included mainly as a placeholder. The description of parameters which are present in each data record includes parameter number (a unique number for each distinct parameter), units, dynamic range, the number of elements per record, an estimate of the number of bits required to represent each parameter, and an element number (a unique number for each instance of every parameter). A summary at the bottom of each table shows the current estimated sizes of metadata, each data record, and the total data product. A more detailed description of each data product will be contained in a User's Guide to be published before the first CERES launch.

Table B-1. Output Products Summary

Product Code		Name	Type	Frequency	Size, MB	Monthly Size, MB
CERES	EOSDIS					
BDS	CER01	BiDirectional Scan	Archival	1/Day	710.92	22039
IES	CER09	Instrument Earth Scans	Internal	1/Hour	32.26	24001

BiDirectional Scan (BDS)

The BDS data product is an archival product containing level 1b CERES scanner data obtained for a 24 hour period. All science scan modes are included in the BDS, including the fixed and rotating azimuth scan modes that perform normal earth, internal calibration, and short scan elevation profiles. The BDS product includes samples taken for all 660 measurements (including space looks and internal calibration views).

The BDS includes the raw (unconverted) science and instrument data from the Level 0 input file (excluding Level 0 header and footer data) as well as the converted science and instrument data. The BDS also contains additional data not found in the Level 0 input file. This additional data is composed primarily of converted satellite position and velocity data, celestial data, and converted digital data.

All of the BDS data use Hierarchical Data Format (HDF) structures such as Vdata and Scientific Data Sets (SDSs). Metadata for the BDS is implemented using the ECS Toolkit metadata routines, which are based on HDF Annotations.

The general composition of a BDS in terms of HDF components is as follows:

1. Metadata	Annotations
2. Unconverted Science Data	SDS(s)
3. Unconverted Instrument Data	Vdata(s)
4. Converted Science Data	SDS(s)
5. Converted Instrument Data	Vdata(s)
6. Satellite/Celestial Data	Vdata(s)

A complete and more detailed listing of the data parameters for this product can be found in the subsequent figure(s) and tables of this section.

Level: 1b
Type: Archival
Frequency: 1/Day

Portion of Globe Covered
File: Satellite Swath
Record: N/A

Time Interval Covered
File: 24 hours
Record: Single 6.6 second packet

Portion of Atmosphere Covered
File: Satellite Altitude

BDS Metadata - TBD

BDS Scientific Data Sets

Every Scientific Data Set (SDS) in the BDS file, with exception of the SDS for Julian Times and the SDS for Unconverted Digital Data, represents a time ordered collection of data where each row in the SDS corresponds to a packet of data, and each column corresponds to a single sample within a packet.

(Note: n = the number of packets/scan lines processed)

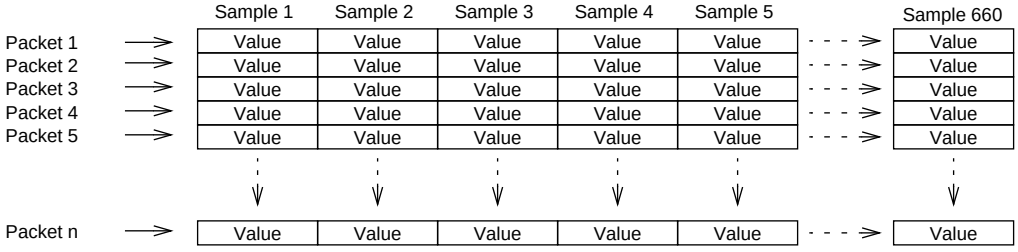

Table B-1 summarizes the contents of each SDS contained within the BDS file. For additional information regarding HDF Scientific Data Sets, consult the HDF User's Guide[1].

Table B-2. BDS SDS Summary

SDS Name	HDF Rank	Rows	Columns	Data Type	Range	Units	~Nominal Size (MB)*
Shortwave Detector Output	2	n	660	U16 Integer	0..4095	counts	16.45
Total Detector Output	2	n	660	U16 Integer	0..4095	counts	16.45
Window Detector Output	2	n	660	U16 Integer	0..4095	counts	16.45
Elevation Position Count	2	n	660	U16 Integer	0..4095	counts	16.45
Azimuth Position Count	2	n	660	U16 Integer	0..4095	counts	16.45
Raw Digital Status Measurement	2	n	185	U16 Integer	Table B-2	N/A	4.62
Shortwave Filtered Radiances	2	n	660	32 Bit Float	-10.0..510.0	$Wm^{-2}sr^{-1}$	32.96
Total Filtered Radiances	2	n	660	32 Bit Float	0.0..700.0	$Wm^{-2}sr^{-1}$	32.96
Window Filtered Radiances	2	n	660	32 Bit Float	0.0..50.0	$Wm^{-2}sr^{-1}$	32.96
Colatitude of FOV at TOA	2	n	660	64 Bit Float	0.0..180.0	degrees	65.92
Longitude of FOV at TOA	2	n	660	64 Bit Float	0.0..360.0	degrees	65.92
Viewing Zenith at TOA	2	n	660	64 Bit Float	0.0..90.0	degrees	65.92
Solar Zenith at TOA	2	n	660	64 Bit Float	0.0..180.0	degrees	65.92
Relative Azimuth at TOA	2	n	660	64 Bit Float	0.0..360.0	degrees	65.92
Converted Elevation Angles	2	n	660	64 Bit Float	0.0..180.0	degrees	65.92

[1] Version 4.0, February 1996 from NCSA

Table B-2. BDS SDS Summary (Continued)

SDS Name	HDF Rank	Rows	Columns	Data Type	Range	Units	~Nominal Size (MB)*
Converted Azimuth Angles	2	n	660	64 Bit Float	0.0..270.0	degrees	65.92
Quality Flags	2	n	660	U32 Integer	Table B-3	N/A	32.96
Julian Time Indices	2	n	2	64 Bit Float	N/A	N/A	0.20
SDS TOTAL SIZE							**680.35**

* - n = 13091

BDS Vdatas

HDF Vdatas contained in the BDS represent tables of records which typically contain instrument housekeeping data. As with the BDS Scientific Data Sets, each record in a Vdata is associated with a single packet. Associations between Vdatas and SDSs are mapped by matching row numbers and record numbers. For example, all data for packet no. 15 can be will contained in row 15 of all SDSs and record 15 of all Vdatas contained in the BDS[2]. Table B-2 contains summary information for all of the BDS Vdatas.

Table B-3. BDS Vdata Summary

Vdata Name	Total Records	Fields Per Record	Record Size (bytes)	Fields	~Nominal Size (MB)*
Temperature Counts	n	39	450	See Table B-5	5.62
Voltage and Torque Counts	n	24	180	See Table B-6	2.25
Position Counts	n	12	528	See Table B-7	6.70
Temperatures	n	35	708	See Table B-8	8.84
Voltages and Torques	n	23	348	See Table B-9	4.35
Satellite Positions	n	20	156	See Table B-10	1.95
Converted Digital Data	n	18	75	See Table B-11	0.94
VDATA TOTAL SIZE					30.65

* - n = 13091

Table B-4. Digital Data Word Definitions

Word	Parameter Name	Bits (MSB = 0)
0	Instrument Mode Sequence Number	0..4
	Instrument Previous Mode Sequence Number	5..9
	Mode Sequence Changed By	10..12
	Mode Sequence Has Changed	13..14
	Spare Bit	15
1	Sequence Command Index	0..4
	Sequence Execution Status	5..7
	Sequence Time to Next Command	8..15
2	Spare Word	0..15
3	Spare Word	0..15

[2]HDF row and record are actually 0 based, so the corresponding data for packet n would be contained in row n-1 of each SDS and record n-1 of each Vdata. For additional, information consult the HDF User's Guide.

Table B-4. Digital Data Word Definitions (Continued)

Word	Parameter Name	Bits (MSB = 0)
4	Spare Word	0..15
5	Spare Word	0..15
6	Spare Word	0..15
7	Instrument Command Counter	0..15
8	Instrument Command Main 1	0..15
9	Instrument Command Parameter 1	0..15
10	Instrument Command Sample Number 1	0..9
	Instrument Command Status 1	10..14
	Instrument Command Source 1	15
11	Instrument Command Main 2	0..15
12	Instrument Command Parameter 2	0..15
13	Instrument Command Sample Number 2	0..9
	Instrument Command Status 2	10..14
	Instrument Command Source 2	15
14	Instrument Command Main 3	0..15
15	Instrument Command Parameter 3	0..15
16	Instrument Command Sample Number 3	0..9
	Instrument Command Status 3	10..14
	Instrument Command Source 3	15
17	Instrument Command Main 4	0..15
18	Instrument Command Parameter 4	0..15
19	Instrument Command Sample Number 4	0..9
	Instrument Command Status 4	10..14
	Instrument Command Source 4	15
20	Instrument Command Main 5	0..15
21	Instrument Command Parameter 5	0..15
22	Instrument Command Sample Number 5	0..9
	Instrument Command Status 5	10..14
	Instrument Command Source 5	15
23	Instrument Command Main 6	0..15
24	Instrument Command Parameter 6	0..15
25	Instrument Command Sample Number 6	0..9
	Instrument Command Status 6	10..14
	Instrument Command Source 6	15
26	Instrument Command Main 7	0..15
27	Instrument Command Parameter 7	0..15
28	Instrument Command Sample Number 7	0..9
	Instrument Command Status 7	10..14
	Instrument Command Source 7	15
29	Instrument Command Main 8	0..15
30	Instrument Command Parameter 8	0..15
31	Instrument Command Sample Number 8	0..9
	Instrument Command Status 8	10..14
	Instrument Command Source 8	15
32	Instrument Error Counter	0..15
33	Instrument Error Sample Number 1	0..9
	Instrument Error Type 1	10..15
34	Instrument Error Sample Number 2	0..9
	Instrument Error Type 2	10..15
35	Instrument Error Sample Number 3	0..9
	Instrument Error Type 3	10..15

Table B-4. Digital Data Word Definitions (Continued)

Word	Parameter Name	Bits (MSB = 0)
36	Instrument Error Sample Number 4	0..9
	Instrument Error Type 4	10..15
37	Instrument Error Sample Number 5	0..9
	Instrument Error Type 5	10..15
38	Instrument Error Sample Number 6	0..9
	Instrument Error Type 6	10..15
39	Instrument Error Sample Number 7	0..9
	Instrument Error Type 7	10..15
40	Instrument Error Sample Number 8	0..9
	Instrument Error Type 8	10..15
41	Spare Word	0..15
42	Spare Word	0..15
43	Spare Word	0..15
44	Spare Word	0..15
45	Spare Word	0..15
46	Total Bridge Balance Control Status	0..2
	Total Bridge Balance DAC Update Status Value	3
	Total Bridge Balance Reset Counter	4..8
	Spare Bits	9..15
47	Total Spacelook Average	0..11
	Spare Bits	12..15
48	Total Bridge Balance DAC Coarse Value	0..11
	Spare Bits	12..15
49	Total Bridge Balance DAC Fine Value	0..11
	Spare Bits	12..15
50	SW Bridge Balance Control Status	0..2
	SW Bridge Balance DAC Update Status Value	3
	SW Bridge Balance Reset Counter	4..8
	Spare Bits	9..15
51	SW Spacelook Average	0..11
	Spare Bits	12..15
52	SW Bridge Balance DAC Coarse Value	0..11
	Spare Bits	12..15
53	SW Bridge Balance DAC Fine Value	0..11
	Spare Bits	12..15
54	LW Bridge Balance Control Status	0..2
	LW Bridge DAC Update Status Value	3
	LW Bridge Balance Reset Counter	4..8
	Spare Bits	9..15
55	LW Spacelook Average	0..11
	Spare Bits	12..15
56	LW Bridge Balance DAC Coarse Value	0..11
	Spare Bits	12..15
57	LW Bridge Balance DAC Fine Value	0..11
	Spare Bits	12..15
58	Bridge Balance Spacelook Start Sample Number	0..9
	Spare Bits	10..15
59	Bridge Balance Spacelook End Sample Number	0..9
	Spare Bits	10..15
60	Bridge Balance DAC Update Sample Number	0..9
	Spare Bits	10..15

Table B-4. Digital Data Word Definitions (Continued)

Word	Parameter Name	Bits (MSB = 0)
61	Bridge Balance Window High Value	0..11
	Spare Bits	12..15
62	Bridge Balance Window Low Value	0..11
	Spare Bits	12..15
63	Bridge Balance Window Setpoint Value	0..11
	Spare Bits	12..15
64	Total Detector Temperature Setpoint	0..11
	Total Detector Temperature Control Status	12
	Spare Bits	13..15
65	SW Detector Temperature Setpoint	0..11
	SW Detector Temperature Control Status	12
	Spare Bits	13..15
66	LW Detector Temperature Setpoint	0..11
	LW Detector Temperature Control Status	12
	Spare Bits	13..15
67	Blackbody Temperature Setpoint	0..11
	Blackbody Temperature Control Status	12
	Spare Bits	13..15
68	SWICS Intensity Level	0..1
	Spare Bits	2..15
69	Spare Word	0..15
70	Elevation Scan Mode	0..4
	Elevation On Deck Scan Mode	5..9
	Elevation Scan Status	10..12
	Elevation Motor Drive	13
	Elevation Encoder LED Intensity	14
	Elevation Stall	15
71	Elevation Offset Correction	0..15
72	Elevation Stall Error Threshold	0..15
73	Elevation Stall Count Threshold	0..9
	Spare Bits	10..15
74	Elevation Position Error Sample 1	0..15
75	Elevation Position Error Sample 2	0..15
76	Elevation Position Error Sample 3	0..15
77	Main Cover Command	0..3
	Main Cover Motion Status	4..7
	Main Cover Position Status	8..11
	Main Cover Sensor Active	12..13
	Spare Bits	14..15
78	Main Cover Commanded Position	0..11
	Spare Bits	12..15
79	Main Cover Accumulated Lag Error Sensor 1	0..7
	Spare Bits	8..15
80	Main Cover Accumulated Lag Error Sensor 2	0..7
	Spare Bits	8..15
81	Main Cover Fixed Step Count	0..15
82	Main Cover Defined Closed Position	0..11
	Spare Bits	12..15
83	Main Cover Defined Open Position	0..11
	Spare Bits	12..15
84	Main Cover Defined Closed Margin	0..11
	Spare Bits	12..15

Table B-4. Digital Data Word Definitions (Continued)

Word	Parameter Name	Bits (MSB = 0)
85	Main Cover Defined Open Margin	0..11
	Spare Bits	12..15
86	MAM Cover Command	0..3
	MAM Cover Motion Status	4..7
	MAM Cover Position Status	8..11
	MAM Cover Sensor Active	12..13
	Spare Bits	14..15
87	MAM Cover Commanded Position	0..11
	Spare Bits	12..15
88	Spare Word	0..15
89	Spare Word	0..15
90	MAM Cover Fixed Step Count	0..15
91	MAM Cover Defined Closed Position	0..11
	Spare Bits	12..15
92	MAM Cover Defined Open Position	0..11
	Spare Bits	12..15
93	MAM Cover Defined Closed Margin	0..11
	Spare Bits	12..15
94	MAM Cover Defined Open Margin	0..11
	Spare Bits	12..15
95	DAP Watchdog Boot Status	0
	DAP Watchdog Enable Status	1
	DAP PROM Power Status	2
	DAP Sample Clock Interrupt Occured	3..4
	Spare Bits	5..15
96	DA{ Scan Period Counter	0..15
97	DAP Memory Dump Start Address Offset	0..15
98	DAP Memory Dump Start Address Segment	0..15
99	DAP Memory Dump End Address Offset	0..15
100	DAP Memory Dump End Address Segment	0..15
101	DAP Packet Start Address Offset	0..15
102	DAP Packet Start Address Segment	0..15
103	DAP Address Changes Indicator	0..15
104	DAP Minimum Execution Time	0..15
105	DAP Minimum Sample Number	0..10
	Spare Bits	11..15
106	DAP Maximum Execution Time	0..15
107	DAP Maximum Sample Number	0..10
	Spare Bits	11..15
108	DAP RAM Code Checksum	0..15
109	DAP ROM Code Checksum	0..15
110	Spare Word	0..15
111	Spare Word	0..15
112	Spare Word	0..15
113	Spare Word	0..15
114	Spare Word	0..15

Table B-4. Digital Data Word Definitions (Continued)

Word	Parameter Name	Bits (MSB = 0)
115	Azimuth Mode	0..4
	Azimuth Motion Status	5
	Azimuth Direction Status	6
	Azimuth Position Status	7..10
	Azimuth Motor Drive Status	11
	Azimuth Encoder LED Status	12
	Azimuth Stall	13
	Spare Bits	14..15
116	Azimuth Defined Crosstrack Position	0..15
117	Azimuth Defined Fixed Position A	0..15
118	Azimuth Defined Fixed Position B	0..15
119	Azimuth Defined Fixed Solar Calibration Position	0..15
120	Azimuth Defined Fixed Cage Position	0..15
121	Azimuth Defined Fixed Position Spare 1	0..15
122	Azimuth Defined Fixed Position Spare 2	0..15
123	Azimuth Defined Fixed Position Spare 3	0..15
124	Azimuth Defined Normal Slew Rate	0..15
125	Azimuth Defined Asynchronous Scan Rate	0..15
126	Azimuth Defined Synchronous Scan Rate	0..15
127	Azimuth Offset Correction	0..15
128	Azimuth Stall Error Threshold	0..15
129	Azimuth Stall Count Threshold	0..9
	Spare Bits	10..15
130	Brake Command Status	0..3
	Brake Motion Status	4..7
	Brake Position Status	8..11
	Spare Bits	12..15
131	Brake Commanded Position	0..11
	Spare Bits	12..15
132	Brake Current Position	0..11
	Spare Bits	12..15
133	Brake Position SUBMUX Channel	0..7
	Spare Bits	8..15
134	Brake Step Count	0..15
135	Brake Defined Released Position	0..11
	Spare Bits	12..15
136	Brake Defined Applied Position	0..11
	Spare Bits	12..15
137	Brake Defined Cage Position	0..11
	Spare Bits	12..15
138	Brake Defined Released Margin	0..11
	Spare Bits	12..15
139	Brake Defined Applied Margin	0..11
	Spare Bits	12..15
140	Brake Defined Cage Margin	0..11
	Spare Bits	12..15
141	Azimuth Position Error Value	0..15
142	Safehold Input A Status	0
	Safehold Input B Status	1
	Safehold Response A Status	2..3
	Safehold Response B Status	4..5
	Spare Bits	6..15

Table B-4. Digital Data Word Definitions (Continued)

Word	Parameter Name	Bits (MSB = 0)
143	ICP Watchdog Boot Status	0
	ICP Watchdog Enable Status	1
	ICP PROM Power Status	2
	ICP Sample Clock Interrupt Occured	3..4
	DMA Communication Status	5..7
	Spare Bits	8..15
144	ICP Scan Period Counter	0..15
145	ICP Memory Dump Start Address Offset	0..15
146	ICP Memory Dump Start Address Segment	0..15
147	ICP Memory Dump End Address Offset	0..15
148	ICP Memory Dump End Address Segment	0..15
149	ICP Packet Start Address Offset	0..15
150	ICP Packet Start Address Segment	0..15
151	ICP Address Changed Indicator	0..15
152	ICP Minimum Execution Time	0..15
153	ICP Minimum Sample Number	0..10
	Spare Bits	11..15
154	ICP Maximum Execution Time	0..15
155	ICP Maximum Sample Number	0..10
	Spare Bits	11..15
156	ICP RAM Code Checksum	0..15
157	ICP ROM Code Checksum	0..15
158	Spare Word	0..15
159	Spare Word	0..15
160	Spare Word	0..15
161	Spare Word	0..15
162	Spare Word	0..15
163	SPS 1 State	0
	SPS 2 State	1
	SPS 1 Response	2
	SPS 2 Response	3
	Solar Warning	4..5
	Scan Timeout Response	6
	Scan Timeout Counting	7..8
	Scan Timeout Occurred	9..10
	Spare Bits	11..15
164	Solar Warning Event Sample Number	0..15
165	Solar Warning Event Scan Period	0..15
166	Scan Timeout Scan Period	0..15
167	SPS 1 Narrow FOV Signal	0..11
	Spare Bits	12..15
168	SPS 1 Wide FOV Signal	0..11
	Spare Bits	12..15
169	SPS 1 Threshold Noise	0..11
	Spare Bits	12..15
170	SPS 1 Threshold Scale Numerator	0..5
	Spare Bits	6..15
171	SPS 1 Solar Detection State	0
	Spare Bits	1..15
172	SPS 1 Solar Detection Count	0..9
	Spare Bits	10..15

Table B-4. Digital Data Word Definitions (Continued)

Word	Parameter Name	Bits (MSB = 0)
173	SPS 1 Solar Detection Count Threshold	0..9
	Spare Bits	10..15
174	SPS 1 Solar Detection Max Count	0..9
	Spare Bits	10..15
175	SPS 2 Narrow FOV Signal	0..11
	Spare Bits	12..15
176	SPS 2 Wide FOV Signal	0..11
	Spare Bits	12..15
177	SPS 2 Threshold Noise	0..11
	Spare Bits	12..15
178	SPS 2 Threshold Scale Numerator	0..5
	Spare Bits	6..15
179	SPS 2 Solar Detection State	0
	Spare Bits	1..15
180	SPS 2 Solar Detection Count	0..9
	Spare Bits	10..15
181	SPS 2 Solar Detection Count Threshold	0..9
	Spare Bits	10..15
182	SPS 2 Solar Detection Max Count	0..9
	Spare Bits	10..15
183	Solar Avoidance Initial Scan Count	0..9
	Spare Bits	10..15
184	Solar Avoidance Current Scan Count	0..9
	Spare Bits	10..15

Table B-5. BDS Quality Flag Definition

Bits (MSB = 0)	Flag Parameter	Definition
0..3	Azimuth Position Status	0000 = At GoTo Position 0001 = At Stopped 0010 = At Initial Position 0011 = At Scan Position 0100 = In Motion All Others = Undefined
4..7	Elevation Scan Mode	0000 = Normal Earth Scan 0001 = Short Earth Scan 0010 = MAM Scan Profile 0011 = NADIR Scan Profile 0100 = Stowed Profile All Others = Undefined
8..8	Shortwave Radiance	0 = Good, 1 = Bad
9..9	Window Radiance	0 = Good, 1 = Bad
10..10	Total Radiance	0 = Good, 1 = Bad
11..12	Spaceclamp Algorithm	00 = No Clamp 01 = Dual Scan Clamp 10 = Single Scan Clamp 11 = Undefined
13..14	Science Scan Mode	0 = Crosstrack, 1 = Biaxial

Table B-5. BDS Quality Flag Definition (Continued)

Bits (MSB = 0)	Flag Parameter	Definition
15..15	Spare	
16..19	Geolocation Flag	0000 = Good 0001 = Failed Instrument Checks 0010 = Failed Spacecraft Checks 0011 = Failed Algorithm Checks All Others = Undefined
20..31	Spares	

Table B-6. Temperature Counts Record

Field No.	Field Name / Parameter	Data Type	Units	Range	No. of Components
1	Total Channel Heater DAC Value	U16 Integer	N/A	N/A	12
2	SW Channel Heater DAC Value	U16 Integer	N/A	N/A	12
3	LW Channel Heater DAC Value	U16 Integer	N/A	N/A	12
4	Blackbody Heater DAC Value	U16 Integer	N/A	N/A	12
5	Total Detector Control Temperature	U16 Integer	counts	0..4095	12
6	Total Detector Monitor Temperature	U16 Integer	counts	0..4095	12
7	SW Detector Control Temperature	U16 Integer	counts	0..4095	12
8	SW Detector Monitor Temperature	U16 Integer	counts	0..4095	12
9	LW Detector Control Temperature	U16 Integer	counts	0..4095	12
10	LW Detector Monitor Temperature	U16 Integer	counts	0..4095	12
11	Total Blackbody Temperature	U16 Integer	counts	0..4095	12
12	LW Blackbody Temperature	U16 Integer	counts	0..4095	12
13	Elevation Spindle Temperature (Motor)	U16 Integer	counts	0..4095	3
14	Elevation Spindle Temperature (Cable Wrap)	U16 Integer	counts	0..4095	3
15	Elevation Bearing Temperature (Motor)	U16 Integer	counts	0..4095	3
16	Elevation Bearing Temperature (Cable Wrap)	U16 Integer	counts	0..4095	3
17	SWICS Photodiode Temperature	U16 Integer	counts	0..4095	3
18	Sensor Module Temperature	U16 Integer	counts	0..4095	3
19	Sensor Electronics Temperature	U16 Integer	counts	0..4095	3
20	Main Cover Motor Temperature	U16 Integer	counts	0..4095	3
21	MAM Total Baffle Temperature 1	U16 Integer	counts	0..4095	3
22	MAM Total Baffle Temperature 2	U16 Integer	counts	0..4095	3
23	MAM Assembly SW Temperature	U16 Integer	counts	0..4095	3
24	MAM Assembly Total Temperature	U16 Integer	counts	0..4095	3
25	DAA Radiator Temperature	U16 Integer	counts	0..4095	3
26	DAA Processor Electronics Temperature	U16 Integer	counts	0..4095	3
27	DAA ADC Electronics Temperature	U16 Integer	counts	0..4095	3
28	ECA Radiator Temperature	U16 Integer	counts	0..4095	3
29	ECA Electronics Temperature	U16 Integer	counts	0..4095	3
30	ACA Electronics Temperature	U16 Integer	counts	0..4095	3
31	Azimuth Lower Bearing Temperature	U16 Integer	counts	0..4095	3
32	Azimuth Upper Bearing Temperature	U16 Integer	counts	0..4095	3
33	ICA Radiator Temperature	U16 Integer	counts	0..4095	3
34	ICA Processor Electronics Temperature	U16 Integer	counts	0..4095	3
35	ICA ADC Electronics Temperature	U16 Integer	counts	0..4095	3

Table B-6. Temperature Counts Record (Continued)

Field No.	Field Name / Parameter	Data Type	Units	Range	No. of Components
36	PCA Radiator Temperature	U16 Integer	counts	0..4095	3
37	PCA Electronics Temperature	U16 Integer	counts	0..4095	3
38	Pedestal Temperature 1 (Brake Housing)	U16 Integer	counts	0..4095	3
39	Pedestal Temperature 2 (Isolator)	U16 Integer	counts	0..4095	3

Table B-7. Voltage and Torque Counts Record

Field No.	Field Name / Parameter	Data Type	Units	Range	No. of Components
1	Detector +120V Bias	U16 Integer	counts	0..4095	3
2	Detector -120V Bias	U16 Integer	counts	0..4095	3
3	SWICS Photodiode Output	U16 Integer	counts	0..4095	3
4	SWICS Lamp Current	U16 Integer	counts	0..4095	3
5	ICA +5V Digital	U16 Integer	counts	0..4095	3
6	ICA +15V to ECA/ACA	U16 Integer	counts	0..4095	3
7	ICA -15V to ECA/ACA	U16 Integer	counts	0..4095	3
8	ICA + 5V Analog	U16 Integer	counts	0..4095	3
9	ICA +10V Bias	U16 Integer	counts	0..4095	3
10	ICA +15V Internal	U16 Integer	counts	0..4095	3
11	ICA -15V Internal	U16 Integer	counts	0..4095	3
12	DAA Ground Reference 1	U16 Integer	counts	0..4095	3
13	DAA Ground Reference 2	U16 Integer	counts	0..4095	3
14	DAA -10V Reference	U16 Integer	counts	0..4095	3
15	DAA +130V	U16 Integer	counts	0..4095	3
16	DAA -130V	U16 Integer	counts	0..4095	3
17	DAA +12V	U16 Integer	counts	0..4095	3
18	DAA -12V	U16 Integer	counts	0..4095	3
19	DAA +15V	U16 Integer	counts	0..4095	3
20	DAA -15V	U16 Integer	counts	0..4095	3
21	DAA +5V	U16 Integer	counts	0..4095	3
22	DAA +10V Reference	U16 Integer	counts	0..4095	3
23	ECA Torque Output	U16 Integer	counts	0..4095	12
24	ACA Torque Output	U16 Integer	counts	0..4095	12

Table B-8. Position Counts Record

Field No.	Field Name / Parameter	Data Type	Units	Range	No. of Components
1	ACA Encoder Clear Track A	U16 Integer	counts	0..4095	3
2	ACA Encoder Clear Track B	U16 Integer	counts	0..4095	3
3	ECA Encoder Clear Track A	U16 Integer	counts	0..4095	3
4	ECA Encoder Clear Track B	U16 Integer	counts	0..4095	3
5	Main Cover Position 1	U16 Integer	counts	0..4095	3
6	Main Cover Position 2	U16 Integer	counts	0..4095	3
7	MAM Cover Position	U16 Integer	counts	0..4095	3
8	Azimuth Brake Position	U16 Integer	counts	0..4095	3
9	SPS 1 Narrow FOV	U16 Integer	counts	0..4095	60
10	SPS 1 Wide FOV	U16 Integer	counts	0..4095	60
11	SPS 2 Narrow FOV	U16 Integer	counts	0..4095	60
12	SPS 2 Wide FOV	U16 Integer	counts	0..4095	60

Table B-9. Converted Temperatures Record

Field No.	Field Name / Parameter	Data Type	Units	Range	No. of Components
1	Total Detector Control Temperature	32 Bit Float	^{o}C	36.0..40.0	12
2	Total Detector Monitor Temperature	32 Bit Float	^{o}C	36.0..40.0	12
3	SW Detector Control Temperature	32 Bit Float	^{o}C	36.0..40.0	12
4	SW Detector Monitor Temperature	32 Bit Float	^{o}C	36.0..40.0	12
5	LW Detector Control Temperature	32 Bit Float	^{o}C	36.0..40.0	12
6	LW Detector Monitor Temperature	32 Bit Float	^{o}C	36.0..40.0	12
7	Total Blackbody Temperature	32 Bit Float	^{o}C	-15.0..60.0	12
8	LW Blackbody Temperature	32 Bit Float	^{o}C	-15.0..60.0	12
9	Elevation Spindle Temperature (Motor)	32 Bit Float	^{o}C	-30.0..70.0	3
10	Elevation Spindle Temperature (Cable Wrap)	32 Bit Float	^{o}C	-30.0..70.0	3
11	Elevation Bearing Temperature (Motor)	32 Bit Float	^{o}C	-30.0..70.0	3
12	Elevation Bearing Temperature (Cable Wrap)	32 Bit Float	^{o}C	-30.0..70.0	3
13	SWICS Photodiode Temperature	32 Bit Float	^{o}C	-30.0..70.0	3
14	Sensor Module Temperature	32 Bit Float	^{o}C	-30.0..70.0	3
15	Sensor Electronics Temperature	32 Bit Float	^{o}C	-30.0..70.0	3
16	Main Cover Motor Temperature	32 Bit Float	^{o}C	-30.0..70.0	3
17	MAM Total Baffle Temperature 1	32 Bit Float	^{o}C	-30.0..70.0	3
18	MAM Total Baffle Temperature 2	32 Bit Float	^{o}C	-30.0..70.0	3
19	MAM Assembly SW Temperature	32 Bit Float	^{o}C	-30.0..70.0	3
20	MAM Assembly Total Temperature	32 Bit Float	^{o}C	-30.0..70.0	3
21	DAA Radiator Temperature	32 Bit Float	^{o}C	-30.0..70.0	3
22	DAA Processor Electronics Temperature	32 Bit Float	^{o}C	-30.0..70.0	3
23	DAA ADC Electronics Temperature	32 Bit Float	^{o}C	-30.0..70.0	3
24	ECA Radiator Temperature	32 Bit Float	^{o}C	-30.0..70.0	3
25	ECA Electronics Temperature	32 Bit Float	^{o}C	-30.0..70.0	3
26	ACA Electronics Temperature	32 Bit Float	^{o}C	-30.0..70.0	3
27	Azimuth Lower Bearing Temperature	32 Bit Float	^{o}C	-30.0..70.0	3
28	Azimuth Upper Bearing Temperature	32 Bit Float	^{o}C	-30.0..70.0	3
29	ICA Radiator Temperature	32 Bit Float	^{o}C	-30.0..70.0	3
30	ICA Processor Electronics Temperature	32 Bit Float	^{o}C	-30.0..70.0	3
31	ICA ADC Electronics Temperature	32 Bit Float	^{o}C	-30.0..70.0	3
32	PCA Radiator Temperature	32 Bit Float	^{o}C	-30.0..70.0	3
33	PCA Electronics Temperature	32 Bit Float	^{o}C	-30.0..70.0	3
34	Pedestal Temperature 1 (Brake Housing)	32 Bit Float	^{o}C	-30.0..70.0	3
35	Pedestal Temperature 2 (Isolator)	32 Bit Float	^{o}C	-30.0..70.0	3

Vdata Name: Voltages and Torques Number of Fields: 23

Number of Records: n Parameter(s): Table B-8

Table B-10. Converted Voltages and Torques Record

Field No.	Field Name / Parameter	Data Type	Units	Range	No. of Components
1	Sensor +120V Bias	32 Bit Float	volts	115.0..125.0	3
2	Sensor -120V Bias	32 Bit Float	volts	-125.0..-115.0	3
3	SWICS Lamp Current	32 Bit Float	mA	0.0..100.0	3
4	ICA +5V Digital	32 Bit Float	volts	0.0..8.0	3
5	ICA +15V to ECA/ICA	32 Bit Float	volts	0.0..20.0	3
6	ICA -15V to ECA/ICA	32 Bit Float	volts	-20.0..0.0	3
7	ICA +5V Analog	32 Bit Float	volts	0.0..20.0	3
8	ICA +10V Bias	32 Bit Float	volts	-20.0..0.0	3
9	ICA +15V Internal	32 Bit Float	volts	0.0..30.0	3
10	ICA -15V Internal	32 Bit Float	volts	-30.0..0.0	3
11	DAA Ground Reference 1	32 Bit Float	volts	0.0..10.0	3
12	DAA Ground Reference 2	32 Bit Float	volts	0.0..10.0	3
13	DAA -10V Reference	32 Bit Float	volts	-20.0..0.0	3
14	DAA +130V	32 Bit Float	volts	90.0..170.0	3
15	DAA -130V	32 Bit Float	volts	-224.0..-36.0	3
16	DAA +12V	32 Bit Float	volts	0.0..20.0	3
17	DAA -12V	32 Bit Float	volts	-20.0..0.0	3
18	DAA +15V	32 Bit Float	volts	0.0..20.0	3
19	DAA -15V	32 Bit Float	volts	-20.0..0.0	3
20	DAA +5V	32 Bit Float	volts	0.0..20.0	3
21	DAA +10V Reference	32 Bit Float	volts	-20.0..0.0	3
22	Elevation Torque Output	32 Bit Float	in-oz	-95.7..95.2	12
23	Azimuth Torque	32 Bit Float	in-oz	-266.7..265.2	12

Table B-11. Satellite Positions Record

Field No.	Field Names / Parameters	Data Type	Units	Range	No. of Components
1	Satellite Position X at record start	64 Bit Float	km	-8000..8000	1
2	Satellite Position Y at record start	64 Bit Float	km	-8000..8000	1
3	Satellite Position Z at record start	64 Bit Float	km	-8000..8000	1
4	Satellite Position X at record end	64 Bit Float	km	-8000..8000	1
5	Satellite Position Y at record end	64 Bit Float	km	-8000..8000	1
6	Satellite Position Z at record end	64 Bit Float	km	-8000..8000	1
7	Satellite Velocity X at record start	64 Bit Float	km sec^{-1}	-10.0..10.0	1
8	Satellite Velocity Y at record start	64 Bit Float	km sec^{-1}	-10.0..10.0	1
9	Satellite Velocity Z at record start	64 Bit Float	km sec^{-1}	-10.0..10.0	1
10	Satellite Velocity X at record end	64 Bit Float	km sec^{-1}	-10.0..10.0	1
11	Satellite Velocity Y at record end	64 Bit Float	km sec^{-1}	-10.0..10.0	1
12	Satellite Velocity Z at record end	64 Bit Float	km sec^{-1}	-10.0..10.0	1
13	Colatitude of satellite at record start	64 Bit Float	degrees	0.0..180.0	1
14	Longitude of satellite at record start	64 Bit Float	degrees	0.0..360.0	1
15	Colatitude of satellite at record end	64 Bit Float	degrees	0.0..180.0	1
16	Longitude of satellite at record end	64 Bit Float	degrees	0.0..360.0	1
17	Earth-Sun Distance	64 Bit Float	AU	0.98..1.02	1
18	Number of Orbits	U32 Integer	N/A	TBD	1
19	Colatitude of Sun at observation	64 Bit Float	degrees	0.0..180.0	1
20	Longitude of Sun ar observation	64 Bit Float	degrees	0.0..360.0	1

Table B-12. Converted Digital Data

Field No.	Field Names / Parameters	Data Type	Units	Range	No. of Components
1	Elevation Offset Correction	32 Bit Float	degrees		1
2	Azimuth Offset Correction	32 Bit Float	degrees		1
3	Azimuth Defined Crosstrack Position	32 Bit Float	degrees		1
4	Azimuth Defined Fixed Position A	32 Bit Float	degrees		1
5	Azimuth Defined Fixed Position B	32 Bit Float	degrees		1
6	Azimuth Defined Fixed Solar Cal Position	32 Bit Float	degrees		1
7	Azimuth Defined Fixed Cage Position	32 Bit Float	degrees		1
8	Azimuth Defined Fixed Position Spare 1	32 Bit Float	degrees		1
9	Azimuth Defined Fixed Position Spare 2	32 Bit Float	degrees		1
10	Azimuth Defined Fixed Position Spare 3	32 Bit Float	degrees		1
11	Azimuth Defined Normal Slew Rate	32 Bit Float	deg sec^{-1}		1
12	Azimuth Defined Asynchronous Scan Rate	32 Bit Float	deg sec^{-1}		1
13	Azimuth Defined Synchronous Scan Rate	32 Bit Float	deg sec^{-1}		1
14	DAP Minimum Execution Time	32 Bit Float	sec		1
15	DAP Maximum Execution Time	32 Bit Float	sec		1
16	ICP Minimum Execution Time	32 Bit Float	sec		1
17	ICP Maximum Execution Time	32 Bit Float	sec		1
18	Instrument ID Number	U8 Integer	N/A		1
19	Packet Data Indicator	U8 Integer	N/A		1
20	Packet Data Version	U8 Integer	N/A		1
21	Science Packet Quick Look Flag Status	U8 Integer	N/A		1
22	Packet Timecode Indicator	U8 Integer	N/A		1
23	Packet Counter	U16 Integer	N/A		1

Instrument Earth Scans (IES)

The IES data product contains the equivalent of one hour of data from a single CERES scan. The data records are spatially ordered along the orbital ground track, with each footprint position related to the spacecraft's suborbital point at the start of the hour. The spatial ordering of records within this product will ease the comparison of CERES data with cloud imager data in subsystem 4.4. The footprint record is the basic data structure for this data product. This record contains the following kinds of information:

1. Time of Observation
2. Geolocation data (at both the Top of Atmosphere (TOA) and at the Earth's surface)
3. Filtered radiances (at satellite altitude), with associated quality data
4. Spacecraft orbital data
5. Footprint viewing geometric data

The IES data product contain only measurements that view the Earth. For the TRMM mission, this means that approximately 225 Earth-viewing footprints (records) are stored on the IES for each 3.3 second half-scan. Because the Earth scan pattern of the CERES instrument in the biaxial scan mode is irregular, the exact number of pixels in each IES data product varies. This variation is caused by the asynchronous scan azimuth position at both the start and end of the hour. If the azimuth angle near the start (or end) of an hour is near the crosstrack position, then the number of footprints in the IES product is near the estimated value given below. If the azimuth angle is near the alongtrack position, some of the footprints are instead spatially located within the previous (or next) hour's IES. Thus, we have used an estimate of the number of 3.3 second half-scans per hour (approximately 1091) times the number of Earth-viewing measurements in

a half-scan (TRMM estimate is 225, EOS estimate is 195) to arrive at the IES product size. For TRMM, this is estimated as 245475 measurements per IES data product and for EOS the estimate is 212745 measurements. The larger of these two measures is used to determine product storage sizing.

Level: 1b
Type: Internal
Frequency: 1/Hour

Portion of Globe Covered
File: Satellite Swath
Record: One CERES footprint

Time Interval Covered
File: 1 Hour
Record: 100 Hz

Portion of Atmosphere Covered
File: Satellite Altitude

IES Metadata - TBD

IES Vdatas

The IES product currently contains two HDF Vdatas. The primary Vdata nominally contains an hourly collection of Footprint records sorted by time. The second Vdata serves as an sort index for the Footprint table, allowing Footprint records to be retrieved in a sorted manner by Along Track angle. The two IES Vdatas are summarized in Table B-12.

Table B-7. IES Vdata Summary

Vdata Name	Total Records	Fields Per Record	Record Size (bytes)	Fields	~Nominal Size (MB)*
Footprints	~260,000	30	136	See Table B-13	33.72
Along Track Sort Index	~260,000	2	8	See Table B-14	1.98
VDATA TOTAL SIZE					35.70

Table B-13. Footprint Record

Field No.	Field Name / Parameter	Data Type	Units	Range	No. of Components
1	Colatitude at TOA	32 Bit Float	degrees	0.0..180.0	1
2	Longitude at TOA	32 Bit Float	degrees	0.0..360.0	1
3	Colatitude at Surface	32 Bit Float	degrees	0.0..180.0	1
4	Longitude at Surface	32 Bit Float	degrees	0.0..360.0	1
5	Viewing Zenith Angle	32 Bit Float	degrees	0.0..90.0	1
6	Solar Zenith Angle	32 Bit Float	degrees	0.0..180.0	1
7	Relative Azimuth Angle	32 Bit Float	degrees	0.0..360.0	1
8	Azimuth Viewing Angle North	32 Bit Float	degrees	0.0..360.0	1
9	Crosstrack Angle	32 Bit Float	degrees	-90.0..90.0	1
10	Along Track Angle	32 Bit Float	degrees	0.0..360.0	1
11	Cone Angle	32 Bit Float	degrees	0.0..180.0	1
12	Clock Angle	32 Bit Float	degrees	0.0..180.0	1
13	Cone Angle Rate	32 Bit Float	deg sec^{-1}	-100.0..100.0	1
14	Clock Angle Rate	32 Bit Float	deg sec^{-1}	-10.0..10.0	1
15	Satellite Velocity X	64 Bit Float	km sec^{-1}	-10.0..10.0	1
16	Satellite Velocity Y	64 Bit Float	km sec^{-1}	-10.0..10.0	1
17	Satellite Velocity Z	64 Bit Float	km sec^{-1}	-10.0..10.0	1
18	Radius from Earth	64 Bit Float	km	6000.0..8000.0	1
19	Total Filtered Radiance	32 Bit Float	W m^{-2} sr^{-1}	0.0..700.0	1
20	SW Filtered Radiance	32 Bit Float	W m^{-2} sr^{-1}	-10.0..510.0	1
21	LW Filtered Radiance	32 Bit Float	W m^{-2} sr^{-1}	0.0..50.0	1
22	Colatitude of Satellite	32 Bit Float	degrees	0.0..180.0	1
23	Longitude of Satellite	32 Bit Float	degrees	0.0..360.0	1
24	Colatitude of Sun	32 Bit Float	degrees	0.0..180.0	1
25	Longitude of Sun	32 Bit Float	degrees	0.0..360.0	1
26	Earth-Sun Distance	32 Bit Float	AU	0.98..1.02	1
27	Sample Number	U16 Integer	N/A	1..660	1
28	Quality Flags	U32 Integer	N/A	N/A	1
29	Scan Number	U16 Integer	N/A	1..26000	1
30	Observation Time	64 Bit Float	Julian Frac	N/A	1

Table B-14. Along Track Angle Sort Index

Field No.	Field Name	Data Type	Units	Range	No. of Components
1	Footprint Index	U32 Integer	N/A	0..n	1
2	Along Track Angle	32 Bit Float	degrees	0.0..360.0	1

Appendix C

Nomenclature

Acronyms

ADEOS	Advanced Earth Observing System
ADM	Angular Distribution Model
AIRS	Atmospheric Infrared Sounder (EOS-AM)
AMSU	Advanced Microwave Sounding Unit (EOS-PM)
APD	Aerosol Profile Data
APID	Application Identifier
ARESE	ARM Enhanced Shortwave Experiment
ARM	Atmospheric Radiation Measurement
ASOS	Automated Surface Observing Sites
ASTER	Advanced Spaceborne Thermal Emission and Reflection Radiometer
ASTEX	Atlantic Stratocumulus Transition Experiment
ASTR	Atmospheric Structures
ATBD	Algorithm Theoretical Basis Document
AVG	Monthly Regional, Average Radiative Fluxes and Clouds (CERES Archival Data Product)
AVHRR	Advanced Very High Resolution Radiometer
BDS	Bidirectional Scan (CERES Archival Data Product)
BRIE	Best Regional Integral Estimate
BSRN	Baseline Surface Radiation Network
BTD	Brightness Temperature Difference(s)
CCD	Charge Coupled Device
CCSDS	Consultative Committee for Space Data Systems
CEPEX	Central Equatorial Pacific Experiment
CERES	Clouds and the Earth’s Radiant Energy System
CID	Cloud Imager Data
CLAVR	Clouds from AVHRR
CLS	Constrained Least Squares
COPRS	Cloud Optical Property Retrieval System
CPR	Cloud Profiling Radar
CRH	Clear Reflectance, Temperature History (CERES Archival Data Product)
CRS	Single Satellite CERES Footprint, Radiative Fluxes and Clouds (CERES Archival Data Product)
DAAC	Distributed Active Archive Center
DAC	Digital-Analog Converter
DAO	Data Assimilation Office

DB	Database
DFD	Data Flow Diagram
DLF	Downward Longwave Flux
DMSP	Defense Meteorological Satellite Program
EADM	ERBE-Like Albedo Directional Model (CERES Input Data Product)
ECA	Earth Central Angle
ECLIPS	Experimental Cloud Lidar Pilot Study
ECMWF	European Centre for Medium-Range Weather Forecasts
EDDB	ERBE-Like Daily Data Base (CERES Archival Data Product)
EID9	ERBE-Like Internal Data Product 9 (CERES Internal Data Product)
EOS	Earth Observing System
EOSDIS	Earth Observing System Data Information System
EOS-AM	EOS Morning Crossing Mission
EOS-PM	EOS Afternoon Crossing Mission
ENSO	El Niño/Southern Oscillation
ENVISAT	Environmental Satellite
EPHANC	Ephemeris and Ancillary (CERES Input Data Product)
ERB	Earth Radiation Budget
ERBE	Earth Radiation Budget Experiment
ERBS	Earth Radiation Budget Satellite
ESA	European Space Agency
ES4	ERBE-Like S4 Data Product (CERES Archival Data Product)
ES4G	ERBE-Like S4G Data Product (CERES Archival Data Product)
ES8	ERBE-Like S8 Data Product (CERES Archival Data Product)
ES9	ERBE-Like S9 Data Product (CERES Archival Data Product)
FLOP	Floating Point Operation
FIRE	First ISCCP Regional Experiment
FIRE II IFO	First ISCCP Regional Experiment II Intensive Field Observations
FOV	Field of View
FSW	Hourly Gridded Single Satellite Fluxes and Clouds (CERES Archival Data Product)
FTM	Functional Test Model
GAC	Global Area Coverage (AVHRR data mode)
GAP	Gridded Atmospheric Product (CERES Input Data Product)
GCIP	GEWEX Continental-Phase International Project
GCM	General Circulation Model
GEBA	Global Energy Balance Archive
GEO	ISSCP Radiances (CERES Input Data Product)
GEWEX	Global Energy and Water Cycle Experiment
GLAS	Geoscience Laser Altimetry System

GMS	Geostationary Meteorological Satellite
GOES	Geostationary Operational Environmental Satellite
HBTM	Hybrid Bispectral Threshold Method
HIRS	High-Resolution Infrared Radiation Sounder
HIS	High-Resolution Interferometer Sounder
ICM	Internal Calibration Module
ICRCCM	Intercomparison of Radiation Codes in Climate Models
ID	Identification
IEEE	Institute of Electrical and Electronics Engineers
IES	Instrument Earth Scans (CERES Internal Data Product)
IFO	Intensive Field Observation
INSAT	Indian Satellite
IOP	Intensive Observing Period
IR	Infrared
IRIS	Infrared Interferometer Spectrometer
ISCCP	International Satellite Cloud Climatology Project
ISS	Integrated Sounding System
IWP	Ice Water Path
LAC	Local Area Coverage (AVHRR data mode)
LaRC	Langley Research Center
LBC	Laser Beam Ceilometer
LBTM	Layer Bispectral Threshold Method
Lidar	Light Detection and Ranging
LITE	Lidar In-Space Technology Experiment
Lowtran 7	Low-Resolution Transmittance (Radiative Transfer Code)
LW	Longwave
LWP	Liquid Water Path
MAM	Mirror Attenuator Mosaic
MC	Mostly Cloudy
MCR	Microwave Cloud Radiometer
METEOSAT	Meteorological Operational Satellite (European)
METSAT	Meteorological Satellite
MFLOP	Million FLOP
MIMR	Multifrequency Imaging Microwave Radiometer
MISR	Multiangle Imaging Spectroradiometer
MLE	Maximum Likelihood Estimate
MOA	Meteorology Ozone and Aerosol
MODIS	Moderate-Resolution Imaging Spectroradiometer
MSMR	Multispectral, multiresolution

MTSA	Monthly Time and Space Averaging
MWH	Microwave Humidity
MWP	Microwave Water Path
NASA	National Aeronautics and Space Administration
NCAR	National Center for Atmospheric Research
NCEP	National Centers for Environmental Prediction
NESDIS	National Environmental Satellite, Data, and Information Service
NIR	Near Infrared
NMC	National Meteorological Center
NOAA	National Oceanic and Atmospheric Administration
NWP	Numerical Weather Prediction
OLR	Outgoing Longwave Radiation
OPD	Ozone Profile Data (CERES Input Data Product)
OV	Overcast
PC	Partly Cloudy
POLDER	Polarization of Directionality of Earth's Reflectances
PRT	Platinum Resistance Thermometer
PSF	Point Spread Function
PW	Precipitable Water
RAPS	Rotating Azimuth Plane Scan
RPM	Radiance Pairs Method
RTM	Radiometer Test Model
SAB	Sorting by Angular Bins
SAGE	Stratospheric Aerosol and Gas Experiment
SARB	Surface and Atmospheric Radiation Budget Working Group
SDCD	Solar Distance Correction and Declination
SFC	Hourly Gridded Single Satellite TOA and Surface Fluxes (CERES Archival Data Product)
SHEBA	Surface Heat Budget in the Arctic
SPECTRE	Spectral Radiance Experiment
SRB	Surface Radiation Budget
SRBAVG	Surface Radiation Budget Average (CERES Archival Data Product)
SSF	Single Satellite CERES Footprint TOA and Surface Fluxes, Clouds
SSMI	Special Sensor Microwave Imager
SST	Sea Surface Temperature
SURFMAP	Surface Properties and Maps (CERES Input Product)
SW	Shortwave
SWICS	Shortwave Internal Calibration Source
SYN	Synoptic Radiative Fluxes and Clouds (CERES Archival Data Product)

SZA	Solar Zenith Angle
THIR	Temperature/Humidity Infrared Radiometer (Nimbus)
TIROS	Television Infrared Observation Satellite
TISA	Time Interpolation and Spatial Averaging Working Group
TMI	TRMM Microwave Imager
TOA	Top of the Atmosphere
TOGA	Tropical Ocean Global Atmosphere
TOMS	Total Ozone Mapping Spectrometer
TOVS	TIROS Operational Vertical Sounder
TRMM	Tropical Rainfall Measuring Mission
TSA	Time-Space Averaging
UAV	Unmanned Aerospace Vehicle
UT	Universal Time
UTC	Universal Time Code
VAS	VISSR Atmospheric Sounder (GOES)
VIRS	Visible Infrared Scanner
VISSR	Visible and Infrared Spin Scan Radiometer
WCRP	World Climate Research Program
WG	Working Group
Win	Window
WN	Window
WMO	World Meteorological Organization
ZAVG	Monthly Zonal and Global Average Radiative Fluxes and Clouds (CERES Archival Data Product)

Symbols

A	atmospheric absorptance
$B_\lambda(T)$	Planck function
C	cloud fractional area coverage
CF_2Cl_2	dichlorofluorocarbon
$CFCl_3$	trichlorofluorocarbon
CH_4	methane
CO_2	carbon dioxide
D	total number of days in the month
D_e	cloud particle equivalent diameter (for ice clouds)
E_o	solar constant or solar irradiance
F	flux
f	fraction
G_a	atmospheric greenhouse effect

g	cloud asymmetry parameter
H_2O	water vapor
I	radiance
i	scene type
m_i	imaginary refractive index
$\hat{N}$	angular momentum vector
N_2O	nitrous oxide
O_3	ozone
P	point spread function
p	pressure
Q_a	absorption efficiency
Q_e	extinction efficiency
Q_s	scattering efficiency
R	anisotropic reflectance factor
r_E	radius of the Earth
r_e	effective cloud droplet radius (for water clouds)
r_h	column-averaged relative humidity
S_o	summed solar incident SW flux
S_o'	integrated solar incident SW flux
T	temperature
T_B	blackbody temperature
t	time or transmittance
W_{liq}	liquid water path
w	precipitable water
$\hat{x}_o$	satellite position at t_o
x, y, z	satellite position vector components
$\dot{x}, \dot{y}, \dot{z}$	satellite velocity vector components
z	altitude
z_{top}	altitude at top of atmosphere
α	albedo or cone angle
β	cross-scan angle
γ	Earth central angle
γ_{at}	along-track angle
γ_{ct}	cross-track angle
δ	along-scan angle
ε	emittance
Θ	colatitude of satellite
θ	viewing zenith angle
θ_o	solar zenith angle

λ	wavelength
μ	viewing zenith angle cosine
μ_o	solar zenith angle cosine
ν	wave number
ρ	bidirectional reflectance
τ	optical depth
$\tau_{aer}(p)$	spectral optical depth profiles of aerosols
$\tau_{H_2O\lambda}(p)$	spectral optical depth profiles of water vapor
$\tau_{O_3}(p)$	spectral optical depth profiles of ozone
Φ	longitude of satellite
ϕ	azimuth angle
$\tilde{\omega}_o$	single-scattering albedo

Subscripts:

c	cloud
cb	cloud base
ce	cloud effective
cld	cloud
cs	clear sky
ct	cloud top
ice	ice water
lc	lower cloud
liq	liquid water
s	surface
uc	upper cloud
λ	spectral wavelength

Units

AU	astronomical unit
cm	centimeter
cm-sec^{-1}	centimeter per second
count	count
day	day, Julian date
deg	degree
deg-sec^{-1}	degree per second
DU	Dobson unit
erg-sec^{-1}	erg per second
fraction	fraction (range of 0–1)
g	gram
g-cm^{-2}	gram per square centimeter

$g\text{-}g^{-1}$	gram per gram
$g\text{-}m^{-2}$	gram per square meter
h	hour
hPa	hectopascal
K	Kelvin
kg	kilogram
$kg\text{-}m^{-2}$	kilogram per square meter
km	kilometer
$km\text{-}sec^{-1}$	kilometer per second
m	meter
mm	millimeter
μm	micrometer, micron
N/A	not applicable, none, unitless, dimensionless
$ohm\text{-}cm^{-1}$	ohm per centimeter
percent	percent (range of 0–100)
rad	radian
$rad\text{-}sec^{-1}$	radian per second
sec	second
sr^{-1}	per steradian
W	watt
$W\text{-}m^{-2}$	watt per square meter
$W\text{-}m^{-2}sr^{-1}$	watt per square meter per steradian
$W\text{-}m^{-2}sr^{-1}\mu m^{-1}$	watt per square meter per steradian per micrometer

CERES VALIDATION SUMMARY

Subsystem 1.0 - CERES Geolocate and Calibrate Earth Radiances

Data Products

- **Earth radiances:**
  1) **Filtered broadband shortwave [0.3 - 5.0 μm]**
  2) **Total-wave [0.3 - >100 μm]**
  3) **Water vapor window [8 - 12 μm]**

Approach

- **Resolution/geometric sites used during the ERBE spacecraft missions**
- **Radiometric accuracy and precision in-flight calibration systems [demonstrated by ERBE] measurement accuracy via ground-to-orbit and precision via in-flight time series**
- **Radiometric precision/consistency checks among same and different types of CERES sensors using ERBE techniques**
- **Compare CERES radiances to earth validation targets calibrated with 5 years of ERBS data**
- **Three channel redundancy check for consistency**
- **Offsets validated using spacecraft pitch-up and monitored monthly against ERBS global limb-darkening**

CERES VALIDATION SUMMARY (CONTINUED)

Validation Activities

- **Prelaunch**

  1) All validation and consistency checks will be based upon CERES sensor ground calibration data sets

  2) Establish radiation statistics of earth validation targets. Longwave target is tropical ocean at night. Shortwave target is desert region in daytime. Learn technique by applying to ERBE NOAA-9 data.

- **Postlaunch**

  1) Collection of in-flight calibration measurements and calculated filtered Earth radiances on designated calibration days

  2) Compare CERES radiances to historical ERBS radiances via earth validation targets.

Archive

- **In-flight calibrations will be archived in BDS format at EOSDIS**

  Publications describing the sensor calibration and validation results as well as public science computing facility (SCF) files of the appropriate calibration and validation data.